THE
PHYSICAL REVIEW
A Journal of Experimental and Theoretical Physics
VOL. 46, NO. 2 JULY 15, 1934 SECOND SERIES

Diffuse Scattering of X-Rays from Sodium Fluoride. III. Using Sensibly Monochromatic Radiation

P. S. WILLIAMS, *Department of Physics, Washington University*

(Received April 23, 1934)

The Mo $K\alpha$ lines, together with a small amount of the continuous spectrum of half the wave-length, were isolated by crystal reflection and scattered from a crystal of NaF at room temperature. Ionization currents were measured by using an FP-54 pliotron and d.c. amplifier. Comparison was made with the scattering at 90° from paraffin, and S_{class} was determined between $x=0.1$ and $x=1.0$. It agrees fairly well with the S_{class} obtained by the author in a previous research using a band of wave-lengths. Comparison is made between the observed S_{class} and these computed by theory from wave-mechanics atomic structure factors, using the assumptions of zero-point-energy or no zero-point-energy. The discrepancy between experiment and theory, especially if the former assumption is correct, seems considerable enough to imply the need for some modification in the theory, probably in the incoherent scattering term.

I. INTRODUCTION

ACCORDING to the theory of the diffuse scattering of x-rays from simple cubic crystals[1, 2, 3, 4, 5] the scattering per electron in terms of the classical Thomson value is given by

$$S=S_1+S_2/R^3, \tag{1}$$

where

$$S_1=(f^2-F^2)/Z,$$

$$S_2=1-f'^2/Z^2.$$

By definition

$$S_{\text{class}}=S_1+S_2 \tag{2}$$

S_1 and S_2/R^3 represent the coherent and incoherent scattered intensities, respectively, and $R^3=[1+(h/mc\lambda)\text{ vers }\phi]^3$ is the Breit-Dirac factor.

The diffuse scattering from KCl, NaCl and NaF has been studied using a band of wave-lengths filtered through aluminum. Harvey,[6] however, has pointed out certain objections to this use of a band of wave-lengths, and has repeated the work on KCl using monochromatic radiation. Similar objections, but to a lesser degree, apply to the author's previous work[7] on NaF. In addition the imperfections of the available artificial crystal of NaF made difficult the avoidance of diffraction effects with a band of wave-lengths. Consequently, the present research was undertaken to attempt to overcome these difficulties.

[1] G. E. M. Jauncey, Phys. Rev. **37**, 1193 (1931).
[2] G. E. M. Jauncey and G. G. Harvey, Phys. Rev. **37**, 1203 (1931).
[3] G. E. M. Jauncey, Phys. Rev. **42**, 453 (1932).
[4] Y. H. Woo, Phys. Rev. **38**, 6 (1931).
[5] Y. H. Woo, Phys. Rev. **41**, 21 (1932).
[6] G. G. Harvey, Phys. Rev. **43**, 591 (1933).
[7] G. E. M. Jauncey and P. S. Williams, Phys. Rev. **41**, 127 (1932).

II. Experimental Method

Mo $K\alpha$ rays together with a small amount of 0.35A radiation from the continuous spectrum were reflected in the first and second orders, respectively, by a NaCl crystal from a molybdenum tube run at 20 m.a. and about 50 kv. The planes of reflection and scattering were the same. The reflected beam—the primary beam for the scattering work—passed through the scattering substance on the axis of the ionization spectrometer. Suitable screening slits were provided. The 13.7 cm brass ionization chamber contained methyl bromide at 1 atmosphere at 23°C; on it was built an evacuated metal housing containing an FP-54 pliotron and high resistance shunt of about 10^{11} ohm; a flexible metal conduit connected the pliotron assembly with a d.c. amplifier designed and built by DuBridge and Brown[8] in this laboratory. This was run at about 20,000 mm/volt, giving net deflections for NaF of the order of 5 cm, which corresponds to 2.5×10^{-14} amp.

Net deflections were obtained in all cases: base readings were taken with the scattering substance removed and an equivalent absorber placed in the primary beam, which automatically corrected for scattering from the air and one unscreened slit. At the scattering angle ϕ deflections for the NaF, $D_{\theta\phi}$, were noted for various values of θ (angle between crystal normal and primary beam) symmetrically chosen on both sides of $\theta=\phi/2$; these were interspersed with deflections D'_{90} for a paraffin slab replacing the NaF at $\theta=45°$, $\phi=90°$. Then the average deflection D_ϕ for NaF at ϕ was taken as the height at $\theta=\phi/2$ of the straight line passing through the groups of $D_{\theta\phi}$ when plotted against θ, as in previous researches,[9] and the ratio D_ϕ/D'_{90} formed. This was done several times for each ϕ chosen. The average values are given in Table I, and as circles in Fig. 1.

Table I.

ϕ	$x_{0.71}$	$x_{0.35}$	D_ϕ/D'_{90} Expt.	0.71A L_1	0.71A L_2	0.35A L_1	0.35A L_2
12.5°	.152	.305	.375	.72	.72	.031	.031
25	.305	.61	.57	.67	.66	.029	.029
29.5	.36	.72	.605	.64	.63	.029	.029
40	.48	.96	.67	.575	.55	.026	.026
45	.54	1.08	.555	.535	.505	.025	.025
50	.595	1.19	.535	.50	.47	.024	.024
60	.705	1.41	.49	.435	.40	.022	.022
70	.81	1.62	.385	.37	.33	.021	.021
80	.905	1.81	.375	.325	.28	.020	.019
90	.995	1.99	.285	.29	.24	.021	.019

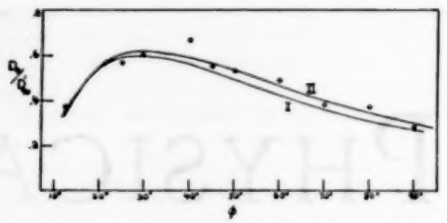

Fig. 1.

It was found that for a value of ϕ such that intense regular reflection took place at $\theta=\phi/2$, D_ϕ/D'_{90} came out ridiculously high (compared to values at adjacent ϕ's) no matter how far from $\phi/2$ were taken the θ's for the $D_{\theta\phi}$. This would be expected, of course, for any very imperfect crystal. Accordingly readings were taken only at such ϕ's that the Bragg peak at $\theta=\phi/2$ was small or non-existent. Even this apparently did not eliminate troubles with diffraction, for the spottiness of certain points is greater than the reproducibility of results would allow.

By replacing the scatterer with a second NaCl crystal either primary wave-length could be adequately isolated. The ratios $h=$(transmitted intensity)/(primary intensity) at normal incidence ($\theta=0$) were measured for the NaF crystal and the paraffin slab: for the crystal $h_{0.71}=0.220$, $h_{0.35}=0.76$; for the paraffin $h'_{0.71}=0.88$, $h'_{0.35}=0.94$.

The mass per unit area of the crystal was $(\rho t)=0.694$, that of the paraffin was $(\rho t)'=0.282$. The formula for the latter was taken as C_nH_{2n}—this is sufficiently valid here since $n>20$.

The ratio $e_{0.71}/e_{0.35}=36$ for the primary intensities was computed from the relative energies in the corresponding 100 Debye-Scherrer rings from a slab of powdered NaF on the spectrometer table.

[8] L. A. DuBridge and Hart Brown, Rev. Sci. Inst. **4**, 532 (1933).

[9] G. E. M. Jauncey and H. L. May, Phys. Rev. **23**, 128 (1924).

III. Interpretation of Results

The observed D_ϕ/D'_{90} at ϕ is related to S values by Eq. (10), reference 10, where here

$$B=h_{0.71}(e_{0.71}/e_{0.35})[K_0S_1+K_\phi T_\phi S_2/R_\phi{}^3]_{0.71} + h_{0.35}[K_0S_1+K_\phi T_\phi S_2/R_\phi{}^3]_{0.35} \quad (3)$$

and B' is exactly similar in form and refers to paraffin at 90°. However, $1+\cos^2\phi$ is replaced by $1+(\cos 14°\ 30')^2\cos^2\phi$ to account for the departure from non-polarization of the Mo $K\alpha$ induced by the reflection at the NaCl; this is sufficiently correct for the small 0.35A component. The h's in (3) are computed for $\theta=\phi/2$ from the measured values at $\theta=0$; these also (with $(\mu/\rho)\propto Z^3$) yield the T's. The K's are calculated from Compton's[11] tables of absorption coefficients. Everything in square brackets in Eq. (3) is taken at the indicated wave-length: for instance, the first S_1 is at $x=(\sin\phi/2)/(0.71)$, the second at $x=(\sin\phi/2)/(0.35)$, etc. For 0.71A, $S_1'=0.13$, $S_2'=0.94$; for 0.35A, $S_1'=0$, $S_2'=1$.[11a]

The equation cited, with Eq. (3), reduces finally to

$$D_\phi/D'_{90}=(L_1S_1+L_2S_2)_{0.71}+(L_1S_1+L_2S_2)_{0.35}, \quad (4)$$

where the L's are the numbers given with the corresponding x's in Table I, for the experimental ϕ's. Eq. (4) is strictly true only for infinitely small slits, but close enough in this case for the actual ϕ tolerance of $\pm 2°$.

By a trial and error process of postulating various S_{class} *vs.* x curves until the D_ϕ/D'_{90} *vs.* ϕ curve computed by Eq. (4) fits sufficiently the experimental points, S_{class} can be determined between $x=0.1$ and $x=1.0$. S_{class} values corresponding to $x>1$ enter only the relatively small 0.35A component of Eq. (4) and cannot be accurately fixed by this experiment; conversely, any reasonable assumption (say 1) for S_{class} in $1<x<2$ will serve for computations of D_ϕ/D'_{90} for $0<\phi<90°$.

Since $(L_1-L_2)_{0.71}$ becomes increasingly noticeable above $\phi=50°$, S_2/S_1 as well as S_{class} will affect Eq. (4). The shape of the S_2 curve was taken as determined by $(1-f''^2/Z^2)$, with theoretical f'' values as tabulated by Jauncey and Pennell.[10] The absolute value was fitted to Wollan's[12] experimental result $S_2/R^3S_1=3.15$ for NaF at $x=1.22$, $\lambda=0.71$A, giving k in $S_2=k(1-f''^2/Z^2)$, $S_1=S_{class}-S_2$.

IV. Discussion of Results

As a first approximation the S_{class} curve obtained in the previous research[7] (Column I, Table II) was divided into components as just described and put into Eq. (4), yielding curve I of Fig. 1. Curve II is given by the S_{class} curve finally selected as the net result of this experiment (Column II, Table II, and curve II, Fig. 2).

The observed S_{class} may be compared with values computed by Eq. (2) from wave mechanics

Table II.

	S_{class}			
x	Ref. 7 I	Present II	Wave mech.* III	Wave mech.** IV
.1	.12	.11	.32	.24
.2	.67	.66	.81	.59
.3	.85	.87	1.09	.92
.4	.93	.96	1.19	1.03
.5	.97	1.02	1.19	1.05
.6	.99	1.06	1.16	1.05
.7	.99	1.08	1.12	1.04
.8	1.00	1.10	1.10	1.03
.9	1.00	1.11	1.09	1.03
1.0	1.00	1.11	1.08	1.03

* With zero-point energy.
** Without zero-point energy.

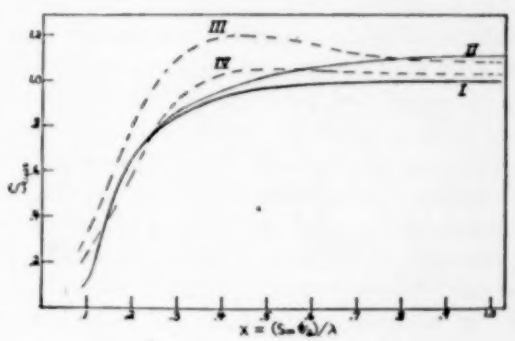

Fig. 2.

[10] G. E. M. Jauncey and Ford Pennell, Phys. Rev. **43**, 505 (1933).
[11] A. H. Compton, *X-Rays and Electrons*.
[11a] Using James and Brindley's f_0 values [reference 12] in (1) we have (at 90°, 0.71A) for a C atom, $S_1=0.17$, $S_2=0.92$ and for H atoms $S_1=0$, $S_2=1$. Neglecting interatomic interference and weighting these by 6 and 2, respectively, (from C_6H_{12}) the average S_1' and S_2' given are arrived at. At 90°, 0.35A a similar analysis holds.
[12] E. O. Wollan, Phys. Rev. **43**, 955 (1933).

atomic structure pictures. James and Brindley[13] give the electronic amplitude factors for Na^+ and F^- in terms of x and from these Jauncey and Pennell[10] have tabulated f and f'' values for both, and their averages. $S_1=(f^2-F^2)/Z$ may be written $(f^2/Z)(1-e^{-2M})$, where M is the Debye-Waller temperature factor; it involves the characteristic temperature 442°K[13a] of NaF and the assumptions of zero-point-energy or no zero-point-energy for the atomic nuclei. These two assumptions yield, respectively, for S_{class} curves III and IV of Fig. 2 (Columns III and IV, Table II).

The curves of Fig. 2 may be compared either by absolute value or by shape. The author does not consider the former comparison very fruitful, for the absolute value of each of the observed S_{class} curves depends directly on about six separate measurements and also on the opinion held as to the scattering from paraffin at 90°. In view of this the agreement within 10 percent of all the S_{class} curves at $x=1.0$ is adequate.

The difference in shape between the S_{class} curves I and II of this and the preceding research is in the direction to be expected from the opening remarks on diffraction effects and is very probably real. On theoretical grounds the existence of zero-point-energy is probable. The discrepancy in shape, however, between curves II and III is considerable, the former showing no trace of a maximum at $x=0.45$. Here also the absolute difference between the curves is large, if we accept their agreement at $x=1.0$. The disagreement in shape between II and IV, while not so large, is still noticeable.

The conclusion seems reasonable, then, that Eqs. (1) and (2) are not adequate, at any rate if zero-point-energy exists. The fair agreement obtained by Harvey[6] for KCl between measured and calculated f' values indicates that the modifications should come in S_2, since this is relatively much larger for NaF than for KCl. Further, Waller's[14] wave-mechanical development for S_2 includes an additional negative term; its calculation for the present paper was not convenient. It is unlikely that the amplitude factors used for III and IV are sufficiently in error to account for the observed discrepancy, although they may be slightly too high, since field interaction between atoms in the crystal lattice would contribute to greater atomic diffuseness. This tendency should be more pronounced for NaF than for KCl.

In conclusion the author wishes to express his appreciation to Professor G. E. M. Jauncey, under whom the work was done, for his advice and interest throughout.

[13] R. W. James and G. W. Brindley, Phil. Mag. **12**, 81 (1931).

[13a] Found by J. J. Shonka, Phys. Rev. **43**, 947 (1933). See also G. E. M. Jauncey and P. S. Williams, Phys. Rev. **44**, 794 (1933).

[14] I. Waller, Phil. Mag. **4**, 1228 (1927).

Proton Production in the Low Voltage Arc

E. S. LAMAR AND OVERTON LUHR, *Eastman Laboratories, Massachusetts Institute of Technology*

(Received May 15, 1934)

Further investigations with the proton source previously described have yielded considerable information about the processes involved in its operation. The tube has been redesigned with the object of obtaining large proton currents in a beam. Ions are drawn out of the arc through a hemispherical grid inserted in the cylindrical electrode. Part of the resulting converging beam passes through a hole in a second electrode which separates the arc chamber from a region maintained at a lower pressure by differential pumping. Total currents of over 0.5 milliampere at current densities of about 8.0 milliamperes per square cm were obtained on the low pressure side. The ratio of proton current to total current was as high as 98 percent with pressures in the discharge tube of 0.3 to 0.4 mm. In order to attain this percentage it was necessary to maintain certain minimum potentials on the cylinder and second electrode. At the same time the metal parts must be prevented from exceeding red heat since an adsorbed layer of hydrogen on the walls is necessary to prevent recombination of atomic hydrogen there. The proton currents obtainable are limited by the speed of the differential pumping and the degree of vacuum desired. The observed pressure ratios were improved by a factor of two when the arc was in operation owing to the increased temperature of the gas streaming through the hole.

INTRODUCTION

THE present widespread interest in the atomic nucleus has made desirable the development of a convenient proton source as one of the necessary tools for nuclear investigations. Large ion currents can be obtained from various types of electrical discharges in hydrogen. Mass-spectrograph studies show,[1, 2] however, that under most circumstances only about ten percent of the ions are protons. The remainder are either diatomic or triatomic ions depending upon the number of collisions with neutral molecules made by the primary diatomic ions before entering the mass-spectrograph. A very effective proton source was reported recently by Oliphant and Rutherford.[3] However, since the discharge tube described by them is large and requires high voltage and considerable power for its operation, it seemed desirable to see what could be done with other types of electrical discharges. As a most efficient source of ions, a low voltage arc of the type described by Langmuir and Jones[4] was employed. A preliminary report of this work has been published.[5]

[1] W. F. Bleakney, Phys. Rev. **35**, 1180 (1930).
[2] O. Luhr, Phys. Rev. **44**, 459 (1933).
[3] Oliphant and Rutherford, Proc. Roy. Soc. **A141**, 259 (1933).
[4] Langmuir and Jones, Science **52**, 380 (1924); Phys. Rev. **31**, 357 (1928).
[5] Lamar and Luhr, Phys. Rev. **44**, 947 (1933).

IDEALLY SIMPLE THEORY

Consider a hot filament cathode and a circular plate anode between which a low voltage arc is maintained in hydrogen gas. One might expect between five and ten percent of the ions in the arc, formed by direct impact of electrons with hydrogen molecules, to be protons and the remainder to be molecular ions. Imagine now this region of ionized gas enclosed by a third cylindrical electrode which is maintained negative with respect to the anode. Positive ions which drift into the space charge sheath enclosed by this electrode will be accelerated and will strike the cylinder with kinetic energy gained in the space charge sheath. Since the accommodation coefficient for hydrogen ions on the electrode is small, they will rebound as neutrals retaining a large fraction of the kinetic energy gained in the sheath. Because of collisions, these neutralized positive ions quickly reach equilibrium with the gas enclosed by the cylinder and cause an increase in the temperature of the gas above that of its surroundings. A thermal reaction should then take place in which molecular hydrogen dissociates with a reaction rate which depends upon the temperature of the gas. If this rate of production of atomic hydrogen greatly exceeds the rate of disappearance by diffusion to the walls, the enclosed gas will be largely atomic hydrogen and thus the ions produced by direct electron impact largely protons.

Apparatus and Experimental Procedure

A diagram of the discharge tube is shown in Fig. 1. The filament was a composite made by wrapping twelve mil tungsten with five mil nickel. The resulting (piano wire) was wound in a helix on a one-sixteenth inch mandrel. The filament was coated with a mixture of barium and strontium oxides, the nickel serving to increase the emitting area, and acting as a binder for the coating. The filament together with the flanged plate anode shown in the diagram comprised the two electrodes between which an arc was maintained in hydrogen. The

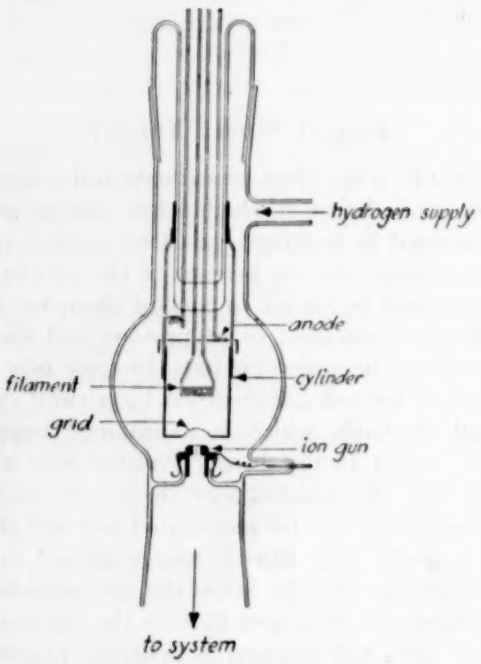

Fig. 1. Experimental tube.

resulting region of partly ionized gas was completely enclosed by a nickel cylinder 4.0 cm long and 3.0 cm in diameter. This cylindrical electrode was always maintained sufficiently negative with respect to the anode to prevent primary electrons from the filament from reaching it. At its lower end, the cylinder was fitted with a hemispherical grid about one cm in diameter, made of forty mesh nickel gauze. Of the ions which drifted into the space charge sheath covering the grid, about half were collected by the grid and the other half drawn from the arc. The grid tended to focus the ions drawn from the arc onto the surface of a fourth electrode or ion gun shown in the diagram. In an earlier tube the ion gun was placed directly in an opening in the cylinder, omitting the hemispherical grid, but this type of construction never yielded such high percentages of protons. The results indicate the desirability of reducing to a minimum all openings in the metal walls enclosing the discharge. The available evidence seems to show that the loss of atomic hydrogen from this region is largely by diffusion through such openings.

The ion gun was made of aluminum and the shape was as shown in the diagram. Several different ion guns having different sized openings in their upper faces were used in the course of the experiments. The ion gun fitted loosely in a glass tube whose upper end had been ground flat. A molybdenum spring held the ion gun against this flat grind, thus sealing the arc chamber from the region of high vacuum. Since the ion gun fitted loosely in the glass tube, any expansion of the metal due to heating introduced no mechanical strains in the glass.

A conical grind at the lower end of the tube made possible its attachment either to the mass-spectrograph or to any desired system of pumps and collecting electrodes. The upper end of the tube was also fitted with a conical grind to facilitate repairs or alterations of the metal parts.

When the tube was fastened to the mass-spectrograph the ion gun had in its upper face a hole 0.3 mm in diameter, countersunk from the back to reduce its thickness to a negligible value. Since the pumping system for the mass-spectrograph was not designed to take care of large quantities of gas, a larger hole in the ion gun would not permit the necessary low pressures to be maintained in the mass-spectrograph.

The filament was heated by alternating current, twenty-five watts being more than sufficient to maintain an arc current of one ampere measured at the cathode. The relative numbers of the different types of ions drawn from the arc were studied by means of the mass-spectrograph as functions of the negative voltages on cylinder and ion gun, pressure in the arc chamber, and previous history of the arc.

When the arc was first started, most of the ions measured were those of water vapor, CO and CO_2. After operating the arc for about an hour at low pressure and high arc drop so that the metal parts became bright red, these impurities were cleaned up.

After studying the nature of the ions with the mass-spectrograph, experiments were undertaken to determine the magnitude of the ion current which could be obtained from the arc with any degree of reliability. For these tests the tube was taken off the mass-spectrograph and put onto a system having a net pumping speed for air of about ten liters per second. A collecting electrode was placed several centimeters behind the ion gun. Several different types of ion guns were tried but the most satisfactory design was that shown in the figure. The hole in the face of the ion gun was 4.0 mm in diameter and 4.0 mm long. The hole was covered by a forty mesh grid to prevent distortion of the electric field at the face and thus to avoid undue spreading of the emerging ion beam. It was found advisable to round off the edges of the ion gun to prevent the concentration of electric field and thus the concentration of ions onto the edges of the gun.

Discussion of Results

The range of pressures in the discharge tube over which satisfactory proton yields were obtained was from 0.20 to 0.60 mm. In this range, the arc drop varied from about 25 to 50 volts. It was found possible to increase the arc drop by decreasing the heating current to the filament without undue damage to the filament. The higher arc drop gave greater ion currents to the cylinder. Results, in general, were found therefore to be more satisfactory with an arc drop between 40 and 50 volts than at lower voltages. All of the tests here reported were with an arc current of one ampere measured at the cathode. The current to the cylinder ranged from 0.23 to 0.32 ampere.

Fig. 2 shows two typical mass-spectrograph curves. The lower curve was taken under fairly ideal conditions and shows about 98 percent protons and the rest triatomic ions. The upper curve was taken under conditions not quite ideal in order to show the presence of diatomic ions. The peaks do not occur at the exact positions to be expected from the applied potentials because of collisions made by the ions before leaving the discharge chamber. The shift in the position of the maximum is greatest for the protons, and least for the triatomic ions.

For convenience the ordinates for the curves of Fig. 3 were computed from the heights of the peaks in curves of the type of Fig. 2 rather than from the areas under the curves since it was found that the error thus introduced was less than the error inherent in the experiments. Curve number 1 of Fig. 3 is a plot of the fraction of the ion current carried by protons as measured by the mass-spectrograph as a function of the negative potential of the cylinder with respect to the anode. The arc current was 1.0 ampere and the potential of the ion gun with respect to the anode was 300 volts. As can be seen from the curve, the proton percentage rose rapidly with increase in voltage of the cylinder, reaching a maximum at about 60 volts. Further increase in voltage resulted in a decrease in the percentage of protons. As a possible explanation for this decrease it was assumed that under the best conditions the recombination of atomic hydrogen on the cylinder was hindered by the presence of an adsorbed layer of hydrogen on the surface. Since an increase in voltage of the cylinder means an increase in power input, and thus in temperature of the cylinder, a temperature should be reached at which the adsorbed layer can no longer exist. Thus the rate of disappearance of atomic hydrogen to the walls should increase and the proton percentage should decrease if the cylinder voltage is raised above an optimum point.

In order to test the above hypothesis, the tube was water-cooled by wrapping with three-sixteenths inch rubber tubing. Unfortunately, a test on the exact same tube which yielded curve number 1 of Fig. 3 was not possible since a minor accident made it necessary to replace the filament before any test could be made after the discharge tube had been wrapped for cooling. When re-assembled, the filament was closer to the grid than previously and, further, it was learned later that the grid and ion gun were

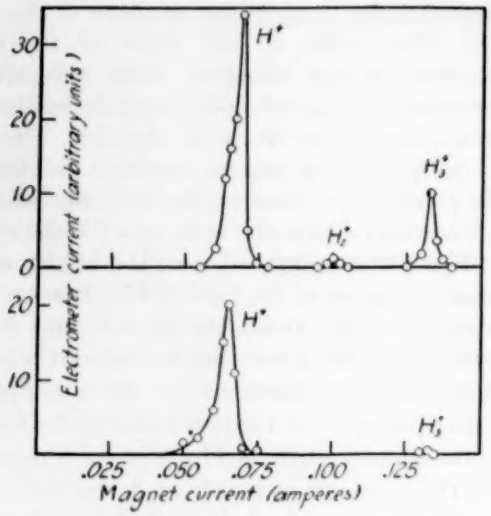

FIG. 2.

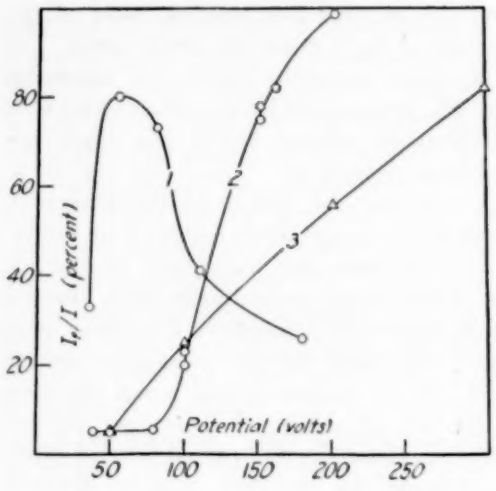

FIG. 3.

FIG. 2. Typical mass-spectrograph curves. (Tube water-cooled.) Upper curve: pressure = 0.230 mm; cylinder potential = 150 volts; ion gun potential = 300 volts; $H^+ = 75$ percent of total current. Lower curve: pressure = 0.380 mm; cylinder potential = 200 volts; ion gun potential = 300 volts; $H^+ = 98$ percent of total current.

FIG. 3. Ordinates give fraction in percent of measured current carried by protons. Abscissae, curves 1 and 2, negative voltage of cylinder with respect to anode. Abscissa, curve 3, ion gun voltage.

not in as perfect alignment as before. Curve number 2, of Fig. 3, is a plot of the proton percentage as a function of cylinder voltage for the water-cooled tube. It is to be noticed that although this curve starts up at a higher voltage than does curve number 1, possibly for the reason stated above, it continues on up to about 98 percent.

Curve number 3, Fig. 3, shows the proton percentage as a function of voltage on the ion gun for a cylinder potential of 162 volts for the water-cooled tube. For the tube whose grid was in good alignment with the ion gun, no change in proton percentage was observed when the potential of the ion gun was changed from 300 to 100 volts. Below 100 volts the proton percentage decreased with decreasing potential on the ion gun.

A possible explanation for the dependence of proton percentage on ion gun voltage is as follows: The rate of disappearance of atomic hydrogen from the inside of the cylinder by diffusion through the grid depends upon the atomic hydrogen concentration gradient at the grid. Collisions with gas molecules made by ions travelling toward the ion gun and by neutralized ions returning from the ion gun should be effective in producing atomic hydrogen in the region between grid and ion gun. As a result, the gradient at the grid, and thus the rate of loss of atomic hydrogen from inside the cylinder should be reduced. As soon as the voltage of the ion gun is so great that the diffusion of atomic hydrogen through the grid is small in comparison with the diffusion through other openings in the tube, the ion gun is no longer the controlling factor; thus further increase in its voltage does not increase the proton percentage.

The proton percentages, with the water-cooled tube seemed to be independent of pressure within the errors of measurement over the range of pressures in the arc chamber, from 0.23 to 0.4 mm. Above 0.4 mm, for the same voltages, the proton percentage was definitely higher than for the range given above, and for pressures below 0.23 mm, the proton percentage decreased rapidly until at 2×10^{-2} mm only about five percent protons were observed.

Two possible contributing causes for the decrease in proton percentage with decreasing pressure are as follows. When the mean free path for the neutralized positive ions rebounding

from the cylinder becomes comparable with the dimensions of the cylinder, the neutralized positives lose their energy in collisions with the cylinder rather than in collisions with the gas. The gas is therefore not raised to a temperature high enough to cause thermal dissociation. Also the cooling of the cylinder may not have been sufficient to keep its temperature at a value sufficiently low to permit the existence of an adsorbed layer of hydrogen at the lower pressures. Thus the rate of recombination of atomic hydrogen on the walls may have been high at low pressures.

Although they have not been tried, cooling fins of carbonized nickel spot-welded to the outside of the cylinder are suggested to replace the less convenient water-cooling employed in these experiments.

The maximum ion current obtainable from the arc depends upon the current density at the face of the ion gun, the pressure in the arc chamber, the speed of differential pumping, and the degree of vacuum desired on the high vacuum side of the ion gun. In these experiments the current density at the surface of the ion gun was about 8 milliamperes per square cm. The ion gun used in these experiments had in its surface an opening 4 mm in diameter and was covered by a mesh grid which reduced the open area by a factor of two. The total current through the ion gun was therefore about 0.5 milliampere.

Earlier experiments with holes of the order of 1 mm in diameter in the ion gun indicated considerable distortion of the electric field at the surface of the ion gun and thus wide spreading of the ion beam after leaving the arc chamber. With the introduction of the grid, however, it was possible to realize saturation current with only 200 volts between the ion gun and the collector on the high vacuum side. In other words, the ions were projected through the grid straight enough to prevent measurable loss to the walls in travelling the 4 mm length of the hole in the ion gun.

The pumping system employed in the second set of experiments had a net pumping speed for air of about 10 liters per second. When the arc was not in operation and hydrogen was being pumped through the 4 mm opening in the ion gun, the pressure ratio maintained between the arc chamber and the high vacuum side was about 20. This ratio increased by a factor of two when the arc was in normal operation. This increase in pressure ratio probably resulted in part from the fact that the gas diffusing through the opening in the ion gun was partly atomic, and in part from the decrease in gas density in the arc chamber resulting from the increased temperature of the gas.

As can be seen from the diagram, the entire apparatus is small, the voltages required can be obtained from storage batteries, and since the power requirements are small, these batteries need not be heavy duty, and thus need not require much space. It was hoped that the apparatus would yield high proton percentages at much lower pressures so that the problem of differential pumping for any high voltage installation would be less difficult. If the mechanism outlined above for the dissociation of hydrogen is the correct one, however, the apparatus should yield protons only at pressures such that the mean free path, for the high speed neutralized positive ions returning from the cylinder, is small in comparison with the dimensions of the apparatus. If one increases the dimensions, one must also increase the power input to maintain the same ion concentration. The present apparatus may of course be limited by recombination of atomic hydrogen on clean walls, and if so, more adequate cooling would insure the existence of an adsorbed hydrogen layer at lower pressures, and thus less recombination. Granted these two limitations, the other alternative is to increase the current density at the surface of the ion gun so as to reduce the size of the opening required for any desired ion current. Eight milliamperes per square centimeter were realized in these experiments and it may be hoped that by careful alignment of ion gun and grid, this current density might be somewhat increased.

The authors wish to express their indebtedness to Dr. K. T. Compton for his continued interest, advice and many valuable suggestions during the progress of these experiments. They wish also to thank various members of the staffs in the departments of Physics and Chemistry for many helpful discussions.

The *L* Absorption Discontinuities of Bismuth

LAURENCE H. CARR, *University of Chicago*

(Received May 3, 1934)

The problem of obtaining a thin enough absorber was solved by using the bismuth in solution. Bismuth nitrate dissolved in dilute nitric acid was held in one cell, while in another like cell was put only the dilute acid. The difference in the absorption of these two cells was then due entirely to the bismuth atoms, since the absorption of the $(NO_3)_3 \cdot 5H_2O$ group added with each Bi atom almost exactly balanced that of the water and acid displaced. The cells had been balanced by trial and error, until their absorption was the same, both when they were filled with water and when they were empty. The solution was analyzed to find the amount of bismuth, and the thickness of the cell was measured with a microscope, so that μ/ρ could be found. This was measured at twenty wave-lengths between 0.56 and 1.54A. By plotting these values, the equations of the four branches of the curve were obtained.

$$(\mu/\rho)(L_I) = 2.438\lambda^{3.5}; \quad (\mu/\rho)(L_{II}) = 2.548\lambda^{4}; \quad (\mu/\rho)(L_{III}) = 2.51\lambda^{3}; \quad (\mu/\rho)(M) = 1.860\lambda^{3.71}.$$

The magnitudes of the discontinuities, r, where r(I,II) is the ratio of μ/ρ on the short wave-length side of L_I to that on the long wave-length side, are r(I,II) 1.161; r(II,III) 1.572; r(III,M) 2.393) r(I,M) 4.37.

Apparatus

FOR these measurements an ordinary glass x-ray tube and a single crystal spectrometer were used. The wave-lengths that were studied were in all cases characteristic lines of the elements, and therefore the tube was constructed so that targets could easily be changed. The intensities of the beam were measured with an ionization chamber and a Compton electrometer. The slits were fixed at 0.2 mm width and were soldered to the ends of a tube 30 cm long so that after cellophane had been waxed over the ends the space between them could be evacuated and thus cut down the absorption of the beam.

Because the absorber was in solution, two cells of a certain thickness had to be built to hold it. To do this two plates of steel about 4 cm square were each ground to a thickness of 2.82 mm and a hole was cut in each that was about 1.5 cm square. Then sheets of mica were clamped to the front and back of each and holes were drilled so that the solution could be introduced into the enclosed space from the top. In order that there would be the same thickness of mica, in the windows of each cell, a piece of mica one inch by two inches was split to the desired thickness and then cut into two one-inch squares. One piece was then put on one cell and the other on the other cell. This process was then repeated for the remaining window of each cell. The cells were made water tight and the metal was protected from being attacked by the acid, by a thick layer of stopcock grease. The supports for these cells were placed between the second slit and the crystal, and in them were two pins that fitted in two reamed holes in the cells so that they were always replaced in exactly the same position.

Method

Following the method of Stephenson,[1] the absorber was held in solution. For success with this method there must be a large difference in the absorption of the dissolved substance and of the solvent. The reason for the two cells was that the intensity through the Bi solution could quickly be compared to the intensity coming through the acid alone. Therefore one cell was filled with $Bi(NO_3)_3 \cdot 5H_2O$ in a dilute nitric acid solution, and the other was filled with the same strength of acid solution. The reading through the former was the I, through the latter the I_0. Since the cells were quite easily removed, they were changed at the end of every reading which made the variations due to slight changes in the power output of the tube, average out very quickly.

Three methods were used to determine the thickness of the cell that contained the bismuth. In the first place it was built to be 2.82 mm thick. Secondly it was obtained by measuring the cell's absorption when filled with water and by using the known value for the absorption coefficient of

[1] R. J. Stephenson, Phys. Rev. **43**, 527 (1933).

water. This gave a value of 2.77 mm. The most accurate value, however, and the one on which the values of μ/ρ are based, were obtained with a very sharply focussed microscope that would measure vertical distances. It was focussed first on one sheet of mica in the cell and then on the other, this gave an average thickness of 2.78 mm. A solution of seventy-five grams of bismuth nitrate, containing an unknown amount of water of crystallization, in 500 cc of dilute nitric acid was made up and was analyzed through the courtesy of the chemistry department. It was found in this way that the solution contained 0.06238 gram of the element bismuth per cubic centimeter. For actual use this was diluted a certain amount at each wave-length so that the bismuth would absorb approximately half of the power going through the solution. Then the value of the mass absorption coefficient could be calculated from the equation $\mu/\rho=(1/\rho x)\log \times(I_0/I)$, where x is the average thickness of the cell and ρ is the number of grams of bismuth per cc.

One of the possible sources of error in this system was that the cells might not be of the same thickness. Before any readings were taken, therefore, they were checked and adjusted until the x-ray absorption of water in each of them was the same. There remained, however, the chance that they might change with time, so at the time of each set of readings at every wave-length they were rechecked with water in both cells, and the correction, if any, was applied to the readings taken at the time. These were found to be less than one percent at all but the very longest wave-lengths.

A second correcting factor considered was the absorption of the other atoms in the bismuth nitrate molecule, and the decreased absorbing power of the bismuth solution compared to the acid alone, due to the displacement of some of the water and some of the acid molecules by the bismuth molecules. These effects were calculated to be about one percent of the total absorption, but were in opposite directions, so that the net result was that the true absorption of the bismuth atoms was less than a quarter of one percent greater than that measured by this method. This was considered as below the accuracy of measurement, and therefore negligible.

Results

The average values of μ/ρ obtained are given in Table I. In Table II values of μ/ρ for bismuth as calculated with Jönsson's formula, and other values interpolated from Allen's data on lead, are compared with those obtained in this experiment.

In Fig. 1, $\log \mu/\rho$ is plotted against $\log \lambda$. The points enclosed in the brackets were not considered when plotting the curve, for they seemed to be unreliable. These points were taken at the Au $L\gamma_1$ line, which fell just 3 X.U. from the L_{III} limit. The trouble seemed to be that since the angular width of the slits was 10^{-4} radian, the wave-length range reflected from one position of the crystal was 6.2 X.U., and consequently some of the base line radiation was of high enough frequency to fall on the other side of the limit. This was particularly bad at this wave-length because the line was only about one-third the intensity of the background radiation, so that variations in it were very disturbing.

However, two other peculiar points were found that are not shown on this diagram. From the third order of the crystal the wave-length range reflected was 2 X.U., and consequently the Zr $K\alpha_1$ and $K\alpha_2$ lines could be resolved since they were 7 X.U. apart. It happened that the L_{II} limit fell between these two lines, and so the attempt was made to measure μ/ρ first on one side of the limit and then on the other, so as to get the magnitude of the discontinuity almost

Table I. *Average values of* μ/ρ.

μ/ρ	63.9	117.8	128.6	135.5	121.9	132.7	135.9	89.14	104.9	119.1
λ	0.558	0.708	0.745	0.753	0.764	0.781	0.784	0.792	0.838	0.873
μ/ρ	145.7	47.73	59.53	79.26	100.0	124.2	150.1	177.5	225.1	
λ	0.921	0.925	0.954	1.013	1.118	1.205	1.274	1.389	1.537	

TABLE II. *Comparison of values of μ/ρ.*

Source/λ	0.558	0.755	1.118	1.537
Jönsson	75	170	108	236
Allen	75	170	108	238
Author	64	136.5	100	225.1

Jönsson, Diss. Uppsala (1928).
S. J. M. Allen, Unpublished data prepared for Smithsonian Tables.

independently of the slopes of the curves on each side. The values obtained did not give a very good value of the size of the jump, and both points were much too low compared to the results in the first order of the crystal that are shown on the graph. Here again the trouble probably arose from the fact that some of the background radiation included with the line lay on one side of the limit and some lay on the other, so that it could not be corrected for.

Except for these two, all of the points obtained fitted reasonably well the four straight lines drawn in Fig. 1. Since all of these are straight lines they can be described by the equation

$$\mu/\rho = C\lambda^n,$$

where C and n vary from branch to branch of the curve. This gives

$$(\mu/\rho)L_I = 2.438\lambda^{2.5}, \quad (\mu/\rho)L_{II} = 2.548\lambda^4,$$

$$(\mu/\rho)L_{III} = 2.251\lambda^3, \quad (\mu/\rho)M = 1.860\lambda^{2.715},$$

as the equations of the four branches.

Since the absorption due to scattering is negligibly small at such long wave-lengths and in an absorber of such high atomic number as was used in this experiment, the discontinuity of the fluorescence coefficient can be taken as the ratio of μ/ρ on the short wave-length side of the limit to μ/ρ on the long side, which we shall call r. The log r for each jump is just the length of each discontinuity in Fig. 1, which gives

$$\log r(\mathrm{I,II}) = 0.065; \quad \log r(\mathrm{II,III}) = 0.1965;$$

$$\log r(\mathrm{III},M) = 0.379;$$

$$\log r(\mathrm{I},M) = \log r(\mathrm{I,II}) + \log r(\mathrm{II,III}) + \log r(\mathrm{III},M) = 0.6405;$$

$$\log r(\mathrm{II},M) = \log r(\mathrm{II,III}) + \log r(\mathrm{III},M) = 0.5755.$$

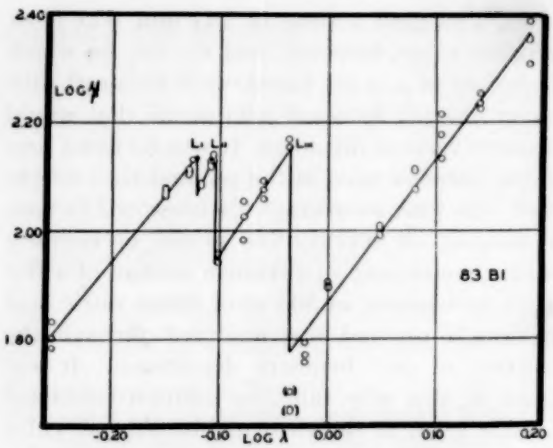

FIG. 1. Plot of log (μ/ρ) as a function of log λ.

In Table III are given the values of r obtained, together with those of several other observers on some of the neighboring elements. The ratio $E(L_I)/E(M_I)$ gives a value for the total jump $r(I,M)$ of 4.15 as compared with 4.37 obtained in this experiment.

TABLE III. *Values of the ratio r between the value of μ/ρ on the short wave-length side of the limit to that on the long wave-length side.*

Element	r(I,II)	r(II,III)	r(III,M)	r(I,M)	r(II,M)	Author
78 Pt	1.247	1.371	2.477	4.23	3.41	Backhurst
	1.13	1.58	2.68	4.79	4.23	Wolf
79 Au	1.2	1.4	2.5	4.2	3.5	Dauvillier
	1.26	1.36	2.52	4.25	3.37	Backhurst
	1.16	1.36	2.47	3.78	3.28	Küstner
	1.10	1.62	2.70	4.81	4.36	Wolf
	1.164	1.393	2.480	4.02	3.46	Uber and Patten
80 Hg	1.18	1.39	2.45	4.02	3.40	Uber
81 Tl	1.15	1.33	2.36	3.64	3.15	Küstner
82 Pb	1.12	1.40	2.38	3.70	3.21	Küstner
83 Bi	1.161	1.572	2.393	4.37	3.76	The author

Dauvillier, Comptes Rendus **178**, 719 (1924).
Backhurst, Phil. Mag. **7**, 353 (1929).
Küstner, Phys. Zeits. **33**, 46 (1932).
Uber and Patten, Phys. Rev. **42**, 229 (1932).
Uber, Phys. Rev. **38**, 217 (1931).
Wolf, Ann. d. Physik (5) **16**, 973 (1933).

The relative amount of absorbing done by the three L levels at any wave-length can be found from Fig. 1 by projecting the other three branches of the curve on to that wave-length. This will divide the vertical line into three parts. The ratios of the anti-logarithms of these three parts is equal to the relative absorption of the three

levels. This ratio was found to be 19 : 40.2 : 43.1 at the L_I limit. This does not agree with the value 19 : 32 : 49 given by Patten[2] for the five elements Au(79) to Bi(83), and neither does it compare well with the ratio interpreted from Wolf's curve for gold; 19 : 70 : 72.

I gratefully acknowledge my obligation to Professor S. K. Allison for the suggestion of the problem and for his helpful suggestions throughout the course of the investigation.

[2] C. G. Patten, Phys. Rev. **45**, 131 (1934).

The Nuclear Spin of Deuterium

G. M. Murphy and Helen Johnston, *Department of Chemistry, Columbia University*

(Received May 28, 1934)

By the methods of photographic photometry, the alternating intensities in emission of the $\Delta v=0$ sequence of the Fulcher bands of deuterium have been investigated in order to determine the nuclear spin. The alternation of intensities was determined for the P, Q and R branches of each of the 5 bands studied. The average value of g_s/g_a obtained from 4 plates is 1.97 ± 0.03. This value agrees best with the theoretical ratio of 2 and a consequent nuclear spin of 1. Since the even rotational levels are more intense than the odd levels, the nucleus obeys Bose-Einstein statistics.

THE nuclear spin of rare isotopes such as H^2, N^{15}, O^{17}, O^{18} is of the utmost importance in any theory of the nucleus but because of the low abundance of such nuclear species, it will probably be rather difficult to obtain this information. This is not true, however, for deuterium since it is possible to separate it almost completely from the more abundant protium. Measurements of the alternation of intensities in the molecular spectrum of deuterium seemed to offer the simplest approach to the problem of the determination of its nuclear spin. We[1] have therefore made such measurements on the P, Q and R branches of 5 bands in the $\Delta v=0$ sequence of the Fulcher bands of deuterium as analyzed by Dieke and Blue.[2]

The nuclear spin of protium is well established as $\frac{1}{2}$. Relative intensity measurements have been made on the protium molecular spectrum by Kapuscinski and Eymers[3] and on the acetylene spectrum by Childs and Mecke.[4] Specific heat measurements at low temperature also give the nuclear spin.[5]

These methods are all applicable to deuterium and in addition we may mention the magnetic deflection method of Breit and Rabi[6] and the study of scattering as proposed by Sexl.[7] Hyperfine structure cannot be used.

Since it is known[8] that the lines in the molecular spectrum of deuterium alternate in intensity, it follows at once that the spin cannot be zero. By analogy with N^{14}, deuterium would probably have a spin of 1, and if its nucleus consists of one proton and one neutron[9] this would be consistent with a spin of $\frac{1}{2}$ for each. This result is also indicated by the conservation of spin momentum in nuclear disintegrations involving deutons[10] and by a study of the ortho-para deuterium conversion.[11] From the latter experiment, it is also concluded that the deuton obeys Bose-Einstein statistics.

[1] Murphy and Johnston, Phys. Rev. **45**, 550 (1934).
[2] Dieke and Blue, Nature **133**, 611 (1934).
[3] Kapuscinski and Eymers, Proc. Roy. Soc. **A122**, 58 (1929).
[4] Childs and Mecke, Zeits. f. Physik **64**, 162 (1930).
[5] Dennison, Proc. Roy. Soc. **A115**, 483 (1927).
[6] Breit and Rabi, Phys. Rev. **38**, 2082 (1931).
[7] Sexl, Naturwiss. **22**, 205 (1934).
[8] Lewis and Ashley, Phys. Rev. **43**, 837 (1933).
[9] Heisenberg, Zeits. f. Physik **77**, 1 (1932).
[10] Raether, Naturwiss. **22**, 151 (1934).
[11] Farkas, Farkas and Harteck, Proc. Roy. Soc. **A144**, 481 (1934).

Apparatus and Procedure

The bands were photographed in the second order of a 21-foot concave grating in a Paschen mounting, giving a dispersion of about 1.3A per mm. A Jena glass filter, OG–1, was placed before the slit to remove overlapping orders. Eastman spectroscopic plates type III–F and IV–F were used since the bands lie in the orange region of the spectrum. The discharge tube, which was 60 cm long and 8 mm in diameter was of the usual H-type with 2 aluminum electrodes, the potential applied being about 4100 volts and the current 0.75 ampere. The latter was kept constant to within 1 percent during an exposure by manipulating an adjustable rheostat in series with the tube. Two large electric fans blew air across the tube during an exposure in order to keep it cool. Before use a solution of silver nitrate had been allowed to evaporate on the glass of the tube. The coating thus formed gave a catalytic surface for recombination of hydrogen atoms and the discharge showed a satisfactory "white stage" with most of the intensity in the molecular spectrum. The gas used was prepared by the electrolysis of water containing more than 90 percent deuterium.

Density marks were put in the center of each plate by means of a tungsten filament lamp burning with constant current of 0.85 ampere and a set of neutral wire screens.[12] These were prepared as described by Murphy and Urey[13] but had been recently recalibrated.[14] A system of slits placed directly in front of the photographic plate permitted a complete set of calibration marks for each band.[14] The density marks on the plates were 0.5 mm wide and in order to compensate for any developer effects a slit 0.5 mm wide was used for the deuterium spectrum. These plates are referred to as plates 19 and 20. Under these conditions some of the lines were not resolved but these were not used in the intensity measurements as explained below. Two exposures (plates 21 and 22) were also made using a narrower slit (0.05 mm) for the molecular spectrum. With the wide slit, the time of exposure for the density marks and the spectrum was 2 minutes each. With the narrow slit, the exposure time for the molecular lines had to be increased to 20 minutes.

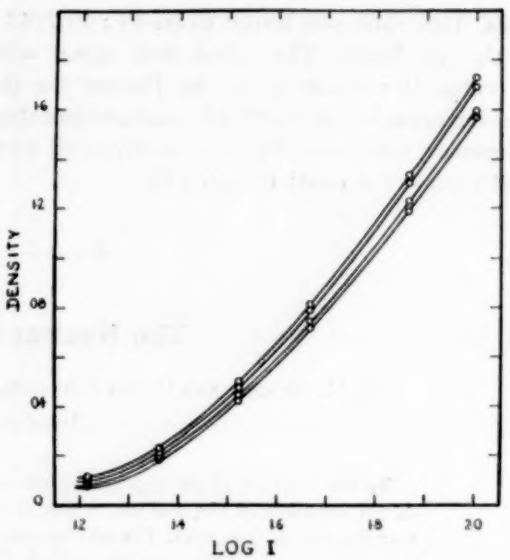

Fig. 1. Characteristic curves for plate 19.

The plates were carefully developed with Rodinal using all the necessary precautions for intensity measurements. Microphotometer curves were made with the Moll microphotometer and density curves plotted for each set of calibration marks. These curves were of the usual form and nearly parallel to each other as shown in Fig. 1. A typical microphotometer curve is given in Fig. 2. From the curves, log I for each line was determined by using a separate curve for each branch. The results for a typical plate are given in part in Table I.

Table I. *Logarithm of intensities of lines of the 2,2 band of deuterium.*

Branch	J	cm^{-1}	log I	Branch	J	cm^{-1}	log I
R	0	16,296.58	1.715	Q	4	16,232.64	1.892
	1	16,320.97	1.455		5	16,214.80	1.421
	2	16,341.73	1.718		6	16,193.59	1.483
	3	16,358.65	1.320	P	2	16,202.64	1.447
	4	16,371.71	1.432		3	16,164.94	1.373
	5	16,379.20	0.838		4	16,124.18	1.654
	6	16,384.58	1.006		5	16,080.43	1.359
Q	1	16,265.06	1.632		6	16,033.88	1.467
	2	16,257.80	1.997		7	15,984.70	0.952
	3	16,246.98	1.690		8	15,932.99	1.128

[12] Harrison, J.O.S.A. and R.S.I. **18**, 492 (1929).
[13] Murphy and Urey, Phys. Rev. **41**, 141 (1932).
[14] Joffe, Phys. Rev. **45**, 468 (1934).

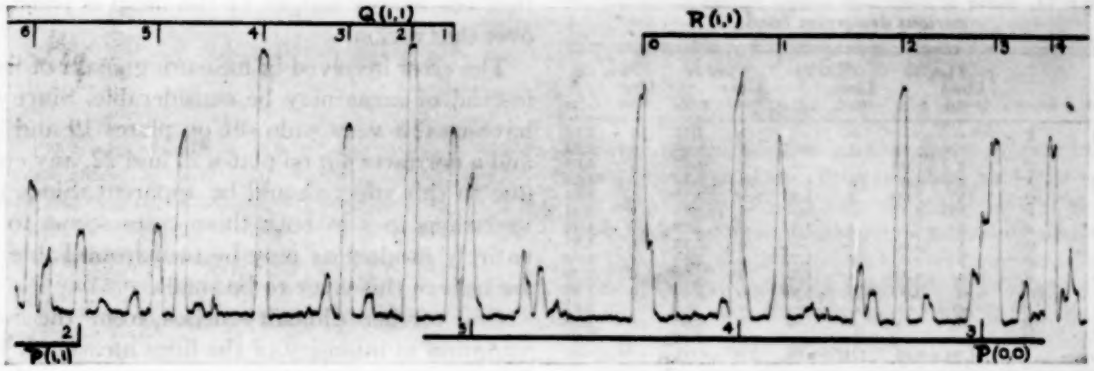

FIG. 2. Microphotometer curve showing portions of (0,0) and (1,1) bands from plate 19.

CALCULATION OF RESULTS

If the conditions of the discharge correspond to thermal equilibrium at an absolute temperature, T, the measured intensity of a line in emission is given by

$$I = Cgwe^{-E/kT}, \tag{1}$$

where E is the rotational energy of the molecule, w is the intensity factor and proportional to the statistical weight of the initial level neglecting any nuclear effects due to spin or statistics, k is Boltzmann's constant and g is the statistical weight due to nuclear spin. C is proportional to the fourth power of the wave number of the line and since the variation of the latter is small over the small range occupied by a band, C remains practically constant for each band.[15] The intensity factor, w has been computed by Hönl and London.[16] The hydrogen bands which were investigated represent a $^3\Pi \rightarrow {}^3\Sigma$ transition but since the spin separations in both states are so small, the bands may be treated as $^1\Pi \rightarrow {}^1\Sigma$ bands. Under these conditions the intensity factors are $J-1$, $2J+1$ and $J+2$ for P, Q and R branches, respectively, where J is the rotational quantum number for the initial level.

In the hydrogen molecule it is known that levels with even values of J are symmetric in the nuclei and those with odd J are antisymmetric.[17] The nuclear spin i is then given by

$$g_s/g_a = (i+1)/i \tag{2}$$

if the nucleus obeys Bose-Einstein statistics and

$$g_s/g_a = i/(i+1) \tag{3}$$

if it obeys Fermi-Dirac statistics.

If $E = BJ(J+1)$, it follows from Eq. (1) that

$$\ln (I/w) = \ln Cg - BJ(J+1)/kT \tag{4}$$

and if $\ln (I/w)$ is plotted against $J(J+1)$ for even and odd J, two parallel straight lines are obtained. The slope gives $-B/kT$ and the intercept on the $\ln (I/w)$ axis gives $\ln Cg$. This has been done for a typical case in Fig. 3. In this way we may determine g_s and g_a and hence the nuclear spin according to Eqs. (2) or (3).

The results for each branch have been plotted like Fig. 3 and in some cases it was found that certain lines were too intense and so did not fall on the parallel lines with the other points. In each case of this sort, it could be shown that these lines were blends due to the wide slit used and they were omitted in determining the nuclear spin as indicated in Table II. In obtaining

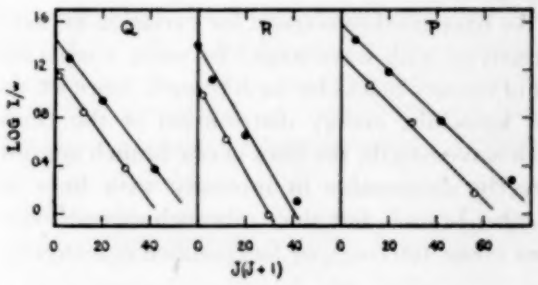

FIG. 3. Plot of log (I/w) against $J(J+1)$ for Q, P and R branches of the (2,2) band from plate 22. ○, odd values of J; ●, even values of J.

[15] Mulliken, Rev. Mod. Phys. **3**, 100 (1931).
[16] Hönl and London, Zeits. f. Physik **33**, 803 (1925).
[17] Heisenberg, Zeits. f. Physik **41**, 239 (1927); Hund, Zeits. f. Physik **42**, 93 (1927).

TABLE II. *Ratio of statistical weight factors calculated for various deuterium bands.*

Band	Branch	Plate 19 Lines used	Plate 19 g_s/g_a	Plate 20 Lines used	Plate 20 g_s/g_a	Plate 21 Lines used	Plate 21 g_s/g_a	Plate 22 Lines used	Plate 22 g_s/g_a
(0,0)	*R*	—	—	—	—	4	2.17	4	2.17
	Q	5	2.13	5	2.17	5	1.68	6	2.24
	P	4	1.93	—	—	4	2.47	4	1.61
(1,1)	*R*	4	1.85	5	1.73	4	2.27	5	2.16
	Q	5	1.90	5	1.91	6	2.13	6	1.81
	P	5	2.12	—	—	4	2.18	4	2.21
(2,2)	*R*	5	2.34	4	2.37	5	1.89	7	1.96
	Q	4	1.65	—	—	6	2.28	6	1.82
	P	5	2.01	4	1.72	6	1.51	7	1.57
(3,3)	*R*	4	1.52	4	1.71	6	1.98	6	2.29
	Q	4	1.93	5	1.90	6	2.22	6	1.89
	P	—	—	—	—	—	—	7	1.57
(4,4)	*R*	—	—	—	—	5	1.95	5	1.54
	Q	—	—	—	—	6	2.15	5	1.73
Average		1.94 ± 0.05		1.93 ± 0.06		2.07 ± 0.05		1.94 ± 0.05	

Weighted average of 4 plates $g_s/g_a = 1.97 \pm 0.03$.

actual values for g a least squares calculation has been made in each case. The ratio g_s/g_a for each band and branch is given in Table II.

As noted above, the slope of the parallel lines equals $-B/kT$. In this way one could determine the effective rotational temperature of the discharge tube. However, the branches are so short that considerable error is involved in obtaining the slope of the lines. A small error in the slope introduces a very large error in the temperature and it has been found impossible to determine the effective temperature from the experimental data.

Discussion of Results

There are several possible sources of systematic error. We have tried to reduce developer effects by careful brush development and in plates 19 and 20 by using spectral lines of the same width as our calibration marks. The plates were of very fine grain and since the lines were quite far above the background of the plate on the microphotometer curves the error due to grain size is negligible.

We have tried to account for variation in plate sensitivity with wave-length by using a separate set of density marks for each branch. Since we do not know the energy distribution of the lamp with wave-length, the lines in one branch are not directly comparable in intensity with lines in another branch, but since a branch extends only over about 100 cm^{-1}, we feel justified in assuming that the energy output of the lamp is constant over that region.

The error involved in measuring peaks of lines instead of areas may be considerable. Since we have used a very wide slit on plates 19 and 20, and a narrower slit on plates 21 and 22, any error due to this effect should be apparent. Since the variations in g in both these cases seems to be entirely random as may be seen from Table II, we believe this error to be small.

One further difficulty arises from the wide variation in intensity of the lines measured. For lines in a single branch, the strong lines may be as much as 35 percent more intense than the weaker lines. This means that the strong lines fall on the upper part of the density curves and the weak lines on the lower part, which fact introduces considerable inaccuracy. The ideal situation would require that all lines be near the middle or straight part of the density curves but since there is such a wide variation of intensities in the lines of a branch there is no simple way of fulfilling this requirement.

Conclusion

In spite of the fact that some systematic errors might be present the results from the analysis of 4 plates seem to indicate a random distribution of errors. Since the average of all the results gives $g_s/g_a = 1.97 \pm 0.03$ it immediately follows that the nuclear spin of deuterium is 1 and since the symmetric levels are more intense than the antisymmetric levels the nucleus obeys Bose-Einstein statistics. The value given for g_s/g_a is the weighted mean of the results for the 4 plates, and the deviation given is the probable error. With a nuclear spin of $\frac{1}{2}$ or $\frac{3}{2}$, the intensity alternation would be 3 : 1 or 1.66 : 1 and these figures are far outside of the deviation found even if the probable error had been much larger.

We take great pleasure in thanking Professor H. C. Urey for the heavy water used in these experiments. We also wish to thank Professor G. H. Dieke who provided us with the wave-lengths of the lines whose intensities we have measured and Dr. R. L. Garman of New York University for the microphotometer curves.

A Study of the Initial Stages of Spark Discharges in Gases

HARRY J. WHITE, *University of California*

(Received April 10, 1934)

The electro-optical shutter is used to study spark breakdown in nitrogen, hydrogen, oxygen, carbon dioxide, helium and argon at atmospheric pressure and for gap lengths up to about 1 cm. Four distinct types of breakdown, as characterized by the appearance and growth of the luminous streamers, are recognizable in these gases. The velocities of the streamers emanating from the cathode in the cases of hydrogen and nitrogen have been measured and have been found to be about 10^7 cm per sec. which is of the order of magnitude of the calculated velocities of electrons in these gases under breakdown conditions. Pencil drawings representing the course of the breakdown in hydrogen, nitrogen, helium and argon are reproduced. Photographs of single sparks in early stages are shown for nitrogen, oxygen, air and carbon dioxide, the exposure time for some of these being as short as 5×10^{-9} sec. The experiments indicate that the major portion of the current passing during breakdown is carried by electrons, and that these, for the most part, come from the cathode rather than from ionization in the gas. The shortness of the spark lag, and the breakdown times of the sparks, show that the phenomenon is essentially due to the motion of electrons, and that the space charges which cause breakdown result from the large difference in the mobility velocities of electrons and positive ions. A theory is formulated to explain the appearance and growth of the streamers observed in certain gases, such as nitrogen.

INTRODUCTION

A GREAT deal of work has been done on spark breakdown in gases, but until the last few years very little has been known about the exact evolution of the spark. That the time required for breakdown is very brief has been shown by oscillograms due to Rogowski and Klemper.[1] The theoretical treatment of the spark mechanism has been largely due to Townsend and his school. Recently these theories have been modified by Loeb[2] and Schumann[3] to take account of the important effect of space charges which develop just before a breakdown occurs.

The occurrence of a spark is the manifestation of an unstable condition of the gas, and this instability is evidenced by the extreme rapidity of the breakdown. Until the last few years the shortness of the times involved, which are of the order of magnitude of 10^{-8} sec., has prevented any study of the exact evolution of the spark. The electro-optical shutter is an apparatus capable of acting with the required speed. It was originally devised by Abraham and Lemoine[4] in 1899 and has been used since then by Beams,[5] Lawrence and Dunnington,[6] Dunnington,[7] and others to study spark phenomena, but for several reasons failed to give results when used to study the very earliest stages of spark breakdown. These difficulties have been largely overcome by Dunnington[8] who has made a detailed analysis of the shutter action and has applied it to the study of the early stages of breakdown in air. Washburn[9] has given a more general solution of the differential equation governing the operation of the shutter and has applied it to the study of the breakdown of liquids.[10]

APPARATUS

A schematic diagram of the apparatus is shown in Fig. 1. The apparatus is essentially the same as that used by Dunnington[8] and reference should be made to his paper for a detailed description of it and its operation. The high voltage is supplied by a transformer and Kenotron with a condenser resistance filter. The spark

[1] Rogowski and Klemper, Archiv f. Elektrotechnik **24**, 129 (1930).
[2] Loeb, J. Frank. Inst. **210**, 15 (1930).
[3] Schumann, Zeits. f. tech. Physik **11**, 58 (1930).
[4] Abraham and Lemoine, Comptes Rendus **129**, 206 (1899).
[5] Beams, Phys. Rev. **28**, 475 (1926).
[6] Lawrence and Dunnington, Phys. Rev. **35**, 396 (1930).
[7] Dunnington, Phys. Rev. **38**, 1535 (1931).
[8] Dunnington, Phys. Rev. **38**, 1506 (1931).
[9] Washburn, Phys. Rev. **39**, 688 (1932).
[10] Washburn, Physics **4**, 29 (1933).

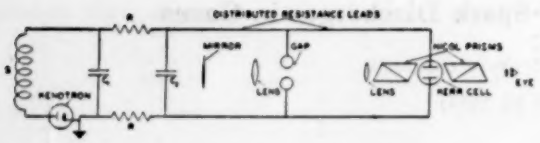

FIG. 1. Schematic diagram of the apparatus.

gap consists of two brass spheres 4 cm in diameter, mounted in a glass chamber which is part of a vacuum system. The gap length is made variable by screw feeds, and the spheres are readily removable for cleaning. The electro-optical shutter consists of the two crossed nicol prisms with the Kerr cell placed between them. A transmission line of variable length and resistance joins the spark gap to the Kerr cell. The optical system consists of two parts; the first a lens and eyepiece for viewing the gap directly through the shutter, the second a lens and plane mirror which forms a second image of the spark close to the original one. This latter system provides the means for varying the length of the light path to the shutter, the plane mirror being movable in a direction perpendicular to its plane. The cathode of the spark gap is illuminated by ultraviolet light from a quartz mercury arc, a large quartz prism being used to separate out the visible light.

The most important part of the apparatus is the Kerr cell[11] used in the electro-optical shutter, for the success of the research depends upon its proper functioning. The liquid used in the cell was nitrobenzene, this being chosen because of its relatively large Kerr constant. The sharpness of cut-off of a cell is very sensitive to small amounts of impurity in the Kerr substance, so that a cell which is to be used with a brilliant source, such as a spark, should contain only very pure liquid.

EXPERIMENTAL

In the experimental work several time concepts are used and these will be defined and described briefly.

[11] A description of the Kerr cell and of some improvements in its technique is being submitted for publication elsewhere.

$$\textit{Path time} = t_p = (L_w - L_1)/(3\times 10^{10}), \quad (1)$$

where L_w = length of the wire path from the gap to the Kerr cell in cm; L_1 = length of the direct light path from the gap to the Kerr cell in cm. The path time is simply a means of expressing the length of the wire path to the cell. As defined, it is the time the shutter would be open if the gap voltage dropped instantaneously and the Kerr cell had an infinitesimal capacity.

$$\textit{Light time} = t_L. \quad (2)$$

The light time is the time the shutter is open after the first visible light from the spark passes through it. This is susceptible to measurement by means of the movable mirror (Fig. 1). For a given value of t_p the mirror may, in some cases, be moved far enough away so that the reflected image entirely disappears, that is, the shutter closes before the light from the mirror reaches it. This extra or increased light path is then the time which the direct image of the spark has been in existence and is the value of t_L.

$$\textit{Effective time} = t_e. \quad (3)$$

This is the time the shutter is open after the voltage across the gap begins to drop rapidly. Its value can be measured by a method due to Dunnington.[8]

VISUAL STUDIES

The results of some visual studies of spark breakdown at atmospheric pressure in hydrogen, nitrogen, helium and argon are shown by the pencil drawings in Fig. 2. These must be considered as only approximate representations, especially in the case of helium. The lower lines represent the limit of the cathode sphere, and the upper lines that of the anode sphere. The values of t_L or t_p are given along the lower lines. It was not found possible to measure the value of t_L for argon and helium, hence only the values of t_p are given. The numbers along the upper lines indicate the gap lengths.

In hydrogen the breakdown begins at the cathode with a streamer which progresses across the gap with approximately uniform velocity,

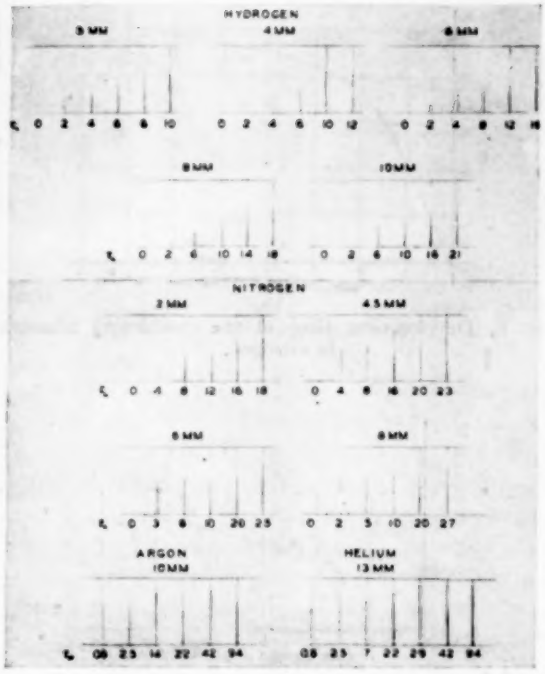

FIG. 2. Pencil drawings of the initial stages of sparks.

and joins a similar streamer from the anode at a point about three-fourths of the distance across the gap from the cathode. The spark is comparatively faint in this gas.

The breakdown in nitrogen may be one of two forms, depending on the gap length and pressure. For atmospheric pressure and gap lengths of less than about 3.5 mm, the breakdown is quite similar to that in hydrogen. For the longer gaps the breakdown starts in a region out in the gap as well as at the cathode, the two appearing simultaneously as nearly as can be determined. They grow together and the breakdown is completed in a manner similar to that for shorter gaps.

The earliest observable discharge in helium is a broad diffuse glow similar to a Geissler discharge and extending the length of the gap. An isolated streamer then appears in the gap and grows toward both the anode and the cathode. Later a spot forms at the surface of the cathode and a streamer appears at the anode. These different portions grow together and the breakdown region broadens and increases in intensity.

The breakdown in argon is similar to that in helium except that no glow discharge is observed and no anode streamer forms. Loeb has suggested that the glow would probably be present in this gas also if it were pure enough. The time required for the completion of the bright filament across the gap for both helium and argon is several times that for hydrogen and nitrogen. This quantity cannot be accurately determined but is larger than that indicated by t_p.

The velocity of the cathode streamers in hydrogen and nitrogen can be measured with considerable accuracy. This was done by observing the length of the streamer in the reflected image as a function of the increased light path for a series of values of t_p. A typical set of curves plotted from these data is shown for nitrogen with a 3 mm gap in Fig. 3. The value of t_p is indicated along each curve and the length of the streamer is expressed as a percentage of the distance across the gap. These curves are approximately parallel straight lines showing that the cathode streamer has, approximately, a uniform velocity. The time plotted is that taken by light in travelling the extra path to the mirror and back, thus an increase in this time means that

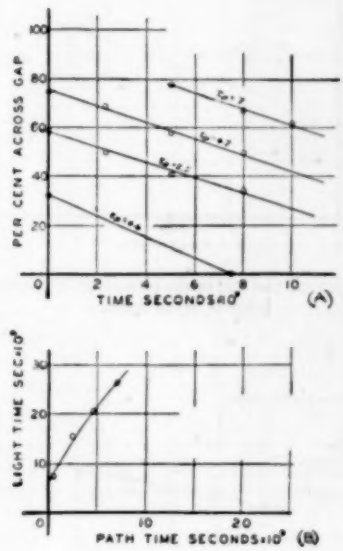

FIG. 3. (A) Growth of cathode pencil as a function of increased light path, nitrogen, 3 mm gap; (B) path time correction curve.

an earlier stage of breakdown is being observed.

The lower curve in Fig. 3 is designated as the "path time correction curve." It gives the value of t_L as a function of t_p and is obtained from the upper set of curves. The positions of these points serve as a partial check on the accuracy of the data, for they should lie on a continuous curve. A consideration of the electric circuit of which the Kerr cell is a part shows this curve to have the correct form.

The cathode streamer velocity was measured for several gap lengths in hydrogen and nitrogen and the results are shown in Figs. 4 and 5. For an 8 mm gap in hydrogen this velocity is 3.2×10^7 cm per sec. and the corresponding value in nitrogen is 1.4×10^7 cm per sec.

The time required for the bright filament to develop across the gap was also measured for these gases; the results are shown in Figs. 6 and 7. For an 8 mm gap in hydrogen this time is about 18×10^{-9} sec., while in nitrogen it is about 27×10^{-9} sec. The form of the curve obtained for nitrogen is similar to that obtained by Dunnington[8] for air. The knee of this curve corresponds to the appearance of the isolated streamer.

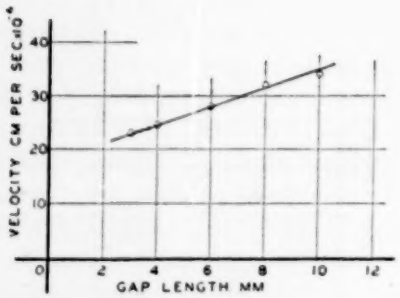

FIG. 4. Velocity of the cathode pencil as a function of gap length, hydrogen.

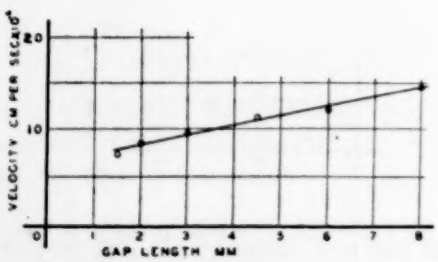

FIG. 5. Velocity of the cathode pencil as a function of gap length, nitrogen.

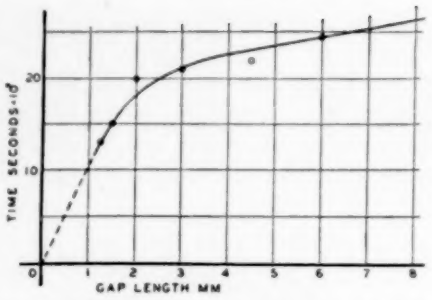

FIG. 6. Development time of the conducting filament in nitrogen.

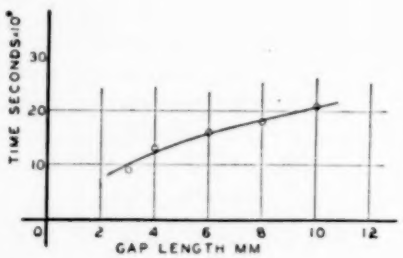

FIG. 7. Development time of the conducting filament in hydrogen.

The time interval between the beginning of the rapid drop in voltage across the gap and the appearance of light of visible intensity can be measured, being simply (t_e-t_L). Dunnington has measured the effective time t_e for certain gaps and pressures in air. He finds for a gap of 5 mm, atmospheric pressure, and $t_p=0.7\times10^{-9}$ sec., a value $t_e=8\times10^{-9}$ sec. The corresponding value of t_L is about 6×10^{-9} sec. These values show that visible light is emitted very soon after the voltage across the gap begins to drop rapidly, the time being, for this case, about 2×10^{-9} sec.

PHOTOGRAPHS

The photography of the early stages of spark breakdown presents considerable difficulty because of the extreme briefness of the exposure times, these being of the order of 10^{-8} sec. or less. The photographs in this paper were obtained by taking full advantage of the available light and using supersensitive panchromatic film with contrast developers.

In order to increase the intensity of the image, the photographic lens, previously placed behind

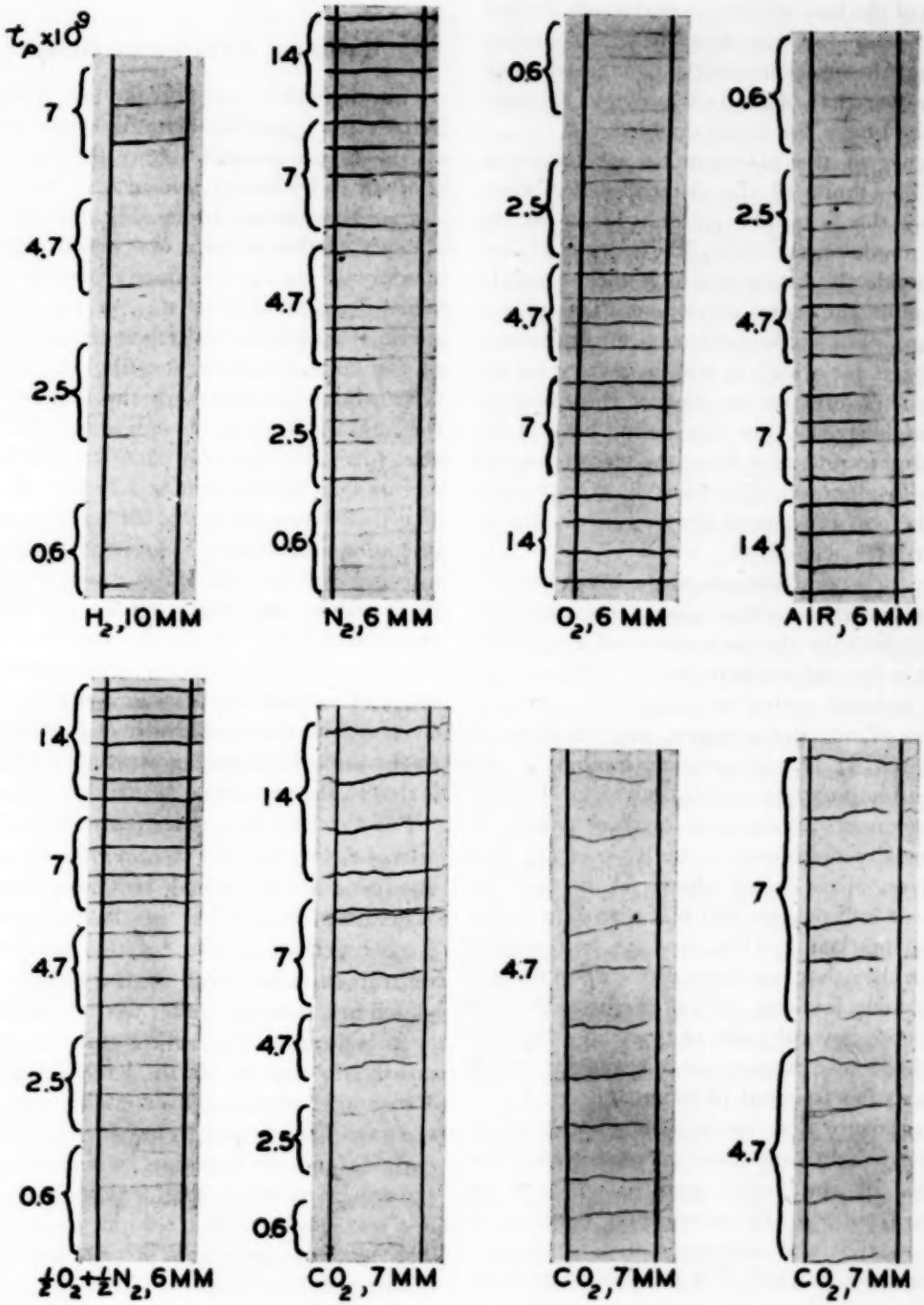

FIG. 8. Photographs of the initial stages of sparks.

the shutter, was placed in front of it as shown in Fig. 1. This greatly increases the effective aperture of the lens which was previously limited by the opening of the Kerr cell. Calculation shows that the image intensity is increased about 15 times over that of the best previous arrangements, the image size being doubled.

Examples of the photographs are shown in Fig. 8. The limits of the electrodes are represented by the lines, the cathode being on the left, the anode on the right. The values of t_p are given outside the brackets which enclose sparks taken under the same conditions. The photographs are all of single sparks, except in the case of hydrogen for which it was necessary to use multiple exposures on account of the faintness of the single sparks. The blackening beyond the lines is due to reflection from the electrodes and is to be disregarded. The faint haze extending across the gap in some of the pictures is due to the Kerr cell background.

There are several features of the breakdown to be noted in the various gases. The multiple filament effect, or the appearance of a multiple filament in the region where the cathode streamer and the isolated central streamer join, occurs in the cases of nitrogen, oxygen, and mixtures of these gases. It is especially noticeable in the mixture of half oxygen and half nitrogen. Double anode streamers appear also for these gases and are especially prominent in the case of air. The isolated region is clearly shown in air and the mixture of half oxygen and half nitrogen, in the brackets marked $t_p=0.6$, and is less clearly shown in the other two cases. For carbon dioxide the extremely tortuous path of the breakdown is to be noted. Several cases of branching towards the cathode also appear in this gas for which this is a rather frequent phenomenon.

The exposure time for a given photograph is equal to the light time t_L as can be seen from the definition of the latter quantity. t_L can be obtained from a set of curves such as shown in Fig. 4, so that the exposure times are known for those cases in which it is possible to measure t_L. As an example of the extreme shortness of the exposures, the exposure time for nitrogen with a 6 mm gap and a value of $t_p=0.6\times10^{-9}$ sec. is about 5×10^{-9} sec., while for the same gap length and $t_p=14\times10^{-9}$ sec., the exposure time is about 24×10^{-9} sec.

Types of Breakdown Observed

Four distinct types of breakdown, as characterized by the appearance and development of the streamers, are recognizable in the gases thus far studied. In hydrogen, and in nitrogen with gaps shorter than about 3.5 mm, the initial streamer appears at the cathode and grows towards the anode with an approximately uniform velocity. When it is about halfway across the gap, a streamer appears at the anode and grows towards the cathode streamer, meeting the latter at a point about one-fourth of the gap length from the anode. For an 8 mm gap, the cathode streamer velocity in nitrogen is 1.4×10^7 cm per sec. and in hydrogen it is 3.2×10^7 cm per sec. The calculated velocity of electrons[12] under breakdown conditions is 1.5×10^7 cm per sec. for nitrogen and 1.0×10^7 cm per sec. for hydrogen, these values depending on the average energy assumed for the electrons. The fact that the observed velocities of the streamers equals in order of magnitude the calculated velocities of electrons in the breakdown electric field, leads to the important conclusion that the breakdown is due to the motion of electrons.

For gap lengths greater than about 3.5 mm in nitrogen, two distinct streamers appear initially, one being at the cathode as above, the other in a detached region out in the gap. These two grow together, mainly by the advance of the central streamer, and the breakdown is completed in a manner similar to that for short gaps.

In helium, at the earliest time for which it is possible to observe, the discharge is a glow about 1 mm in diameter and extending the length of the gap. Then a spot forms at the surface of the cathode and an indistinct streamer appears in the gap, after which the breakdown is completed in a way similar to that for long gaps in nitrogen. The streamer velocities are smaller than those in nitrogen by a factor of about 3.

The distinguishing features of the breakdown in carbon dioxide are the tortuousness of the

[12] Langevin, Ann. Chim. Phys. **5**, 245 (1905).

streamers and the branching which occurs at the cathode. The position and growth of the streamers are otherwise similar to those occurring in the long gaps of nitrogen.

Discussion

The material presented in this paper is confined to the results of a study of the position and growth of the visible streamers which appear in the initial stages of spark breakdown. The complete understanding of a spark discharge involves a knowledge of the preceding or dark current stage, particularly of the distribution of ions in the gap just before the visible streamers appear. The fact that streamers are formed in localized regions shows that the phenomenon is primarily one of space charge effects. By correlating the emission of visible light with intense ionization, a knowledge of the streamers occurring in a spark breakdown shows in what region or regions the space charge fields are important.

Previous experimenters[1, 13] have shown that, in the case of static breakdown with the cathode illuminated with ultraviolet light, both the spark lag and the time of breakdown are of the order of 10^{-7} sec. Now the velocity of electrons, under breakdown conditions in gases, is so much greater than that of positive ions, that the latter may be considered as remaining practically stationary during such a short time interval. Thus the space charges which result in breakdown arise because of this great difference in velocity and are almost entirely built up by the motion of electrons. The large velocity of the initial streamers and the rapidity of breakdown show that the major portion of the charge transported during breakdown is carried by electrons. A simple calculation shows that these must come mostly from the cathode, for if any appreciable number of them came from ionization in the gap, the positive charge remaining after the removal of the electrons would raise some region of the gap to an impossibly high potential.

The results of this experiment together with those just mentioned, lead to a plausible explanation of breakdown as it occurs in a gas such as nitrogen. Suppose that a spark gap is at the sparking potential corresponding to a given set of conditions and that ultraviolet light is allowed to shine on the cathode beginning at a given instant. This initiates a stream of electrons moving to the anode with a velocity which is of the order of magnitude of 10^7 cm per sec. Each of these electrons produces ion pairs according to the Townsend equation, $n=\exp\int \alpha dx$, where α is the Townsend coefficient and x the distance moved in the direction of the field. There results an excess of positive charge in the gap immediately after the first burst of electrons reaches the anode, which, because of the exponential nature of the Townsend equation, lies for the most part very close to the anode. The presence of the excess positive charge disturbs the originally uniform field, decreasing it in a region close to the anode and increasing it in the rest of the gap.

Subsequent electrons produce more ions in the region of greater field and fewer in the region of lesser field, the net effect being to cause the region of large excess positive charge to advance towards the cathode. The most intense field lies directly in front of this advancing charge and its magnitude increases as it advances because the total amount of excess charge is being increased. If the ionization becomes sufficiently large and light of visible intensity is emitted, it will occur in this region, so that a streamer appears there first. The idea of an electron avalanche, and the resultant concentration of the field in the region of the cathode is due to von Hippel and Franck[14] and was developed quantitatively by Schumann.[15] A somewhat similar theory was proposed by Loeb[16] at about the same time.

The image, in the cathode, of the positive charge produces a field which becomes important as the head of this charge approaches the cathode. Owing to this, the field is still further increased in the region near the cathode. Thus for gap lengths short enough, the initial streamer is formed at this electrode, but increasing the gap length sufficiently, results in the formation of a

[13] Snoddy, Phys. Rev. **40**, 409 (1932).

[14] von Hippel and Franck, Zeits. f. Physik **57**, 696 (1929).
[15] Schumann, Zeits. f. tech. Physik **11**, 194 (1930).
[16] Loeb, Science **69**, 509 (1929).

detached streamer. Experimentally this is found to be true, but in addition, a streamer always appears at the cathode at about the same time that the central streamer appears, indicating that some other process is effective in building up positive space charge close to the cathode. This may be due to positive ion impact or to photoelectrons ejected from the cathode by radiation from the discharge.

Suppose that a short gap is being considered, so that initially the only streamer that appears is at the cathode. This streamer is semiconducting and the field is strongest at its tip, causing it to grow towards the anode. A previous discussion shows that most of the current is carried by electrons coming from the cathode. A considerable proportion of these leave the tip of the streamer and advance ahead of it, eventually annulling the positive space charge previously present, and building up a negative space charge which is concentrated near the anode. As a result, the field there in time becomes strong enough to cause a streamer to form.

For a long gap, a central streamer appears in addition to the one at the cathode. The field between these two is comparatively large, as shown by the above discussion, and the central streamer grows faster towards the cathode than towards the anode. Experimentally the ratio of these two velocities is found to be about three or four. After the two streamers join, the breakdown is completed in a manner similar to that for short gaps.

It follows from the above considerations that the spark lag is very nearly the time required for the space charge to build up a field of strength sufficient to cause a streamer to form, and is therefore dependent on the intensity of the ultraviolet illumination. For illumination of very high intensity, the lag will be of the order of magnitude of the time it takes electrons to traverse the gap, that is, about 10^{-7} sec.

Snoddy observed time lags of this magnitude when illuminating spark gaps with an intense ultraviolet light source. No doubt experimental investigations of the dependence of the spark lag on the intensity of illumination of the cathode will contribute to a more complete understanding of the breakdown process.

In conclusion, I wish to express my appreciation to Professor E. O. Lawrence, under whose direction this research is being carried on, for many helpful suggestions and discussions. I also wish to thank Dr. F. G. Dunnington for his help in the experimental work, and Professor L. B. Loeb and Dr. A. M. Cravath for their assistance in the interpretation of the results.

The Complex Neutron

HENRY MARGENAU, *Yale University*

(Received March 19, 1934)

The consequences of the assumption that the neutron be a combination of a proton and an electron, with a modified potential near the proton, are worked out on the basis of Schrödinger's and of Dirac's theory. Various features of such a model are discussed, and its unsatisfactory properties are exhibited. The significant results are stated under items B II, 1–6.

INTRODUCTION

THERE is at present no definite experimental evidence which could decide the question as to the nature of the neutron. In particular two alternative possibilities are open: (1) The neutron is an elementary particle the structure of which is as inexplicable on the basis of present theories as is that of the electron. (2) The neutron is complex and consists of a proton and an electron. The first alternative is annoying if true, for it adds another mystery to the already comprehensive list of difficulties, though perhaps a mystery in line with others; it should be adopted only if the second fails. The second alternative is capable of being examined theoretically with the use of the present quantum-mechanical formalism. It leads to some conclusions which are capable of verification or rejection. These conclusions I wish to consider in this note.

The results are not favorable for the second alternative, although their discussion seems instructive. I shall not, therefore, present here the details of the calculations, but describe them briefly and state the consequences.

Two difficulties inherent in every complex neutron model are well known; they are apparent without the more detailed studies which have here been made. The first is that such a model will not produce the correct angular momentum, which ought to be $\frac{1}{2}$ Bohr unit. If the composition of electronic angular momentum with that of the proton takes place according to the customary rules, the complex neutron must have a spin of 0 or 1 unit. We shall return to this point, which, as will be seen, is not entirely conclusive. Another difficulty, most clearly brought out in the recent work of Furry and Oppenheimer,[1] arises from the essential limitations of Dirac's theory which we shall disregard for the present.

A. METHOD OF CALCULATION

The fact is known that a Coulomb force, exerted by the proton on the electron, admits no stable solution of the Schrödinger or Dirac equation for energies smaller than that of the ground state of H.[2,3] Hence any attempt of producing a neutron according to present theories must involve a modification of the potential. The most natural hypothesis is that of a breakdown of the Coulomb potential near the proton. The present considerations are based on this assumption.

I have adopted the following method of calculation: Assuming at the start a certain value for the binding energy of the electron comparable to those found by experiment, we can integrate the wave equation numerically from ∞ inward along a Coulomb potential and with the specified eigenvalue. The ψ-function will not behave properly at the origin, and we inquire as to what change in the potential, applied at an arbitrary small radius r_0, will make ψ correct at the origin. In this form the problem is indefinite. We expect, however, that the results to be obtained are qualitatively independent of the actual form of the potential near $r=0$. Hence we assume that the potential for $r<r_0$ is constant, but in general different from $1/r_0$, so that the electron encounters at r_0 either a rectangular

[1] W. H. Furry and J. R. Oppenheimer, Phys. Rev. **45**, 245 (1934).
[2] J. L. Destouches, *Exposés de Phys. Théor.* III (1932).
[3] R. M. Langer and N. Rosen, Phys. Rev. **37**, 1579 (1931).

trough or a rectangular barrier, or experiences no change in potential at all. The discontinuity in potential at r_0 will be denoted by $\Delta\varphi$, a quantity to be determined by the condition on ψ at the origin. $\Delta\varphi$ will be a function of r_0.

If we use Schrödinger's equation, continuity both in ψ and in $\partial\psi/\partial r$ at r_0 must be required. A similar requirement is impossible and indeed unnecessary for the solutions of Dirac's equation; continuity of ψ is all that can be maintained. The method here is slightly more cumbersome. It involves the construction of a nonlinear equation in the derivatives of ψ which can be integrated numerically, and a subsequent integration of these derivatives across the point r_0 with the discontinuity replaced by a rapidly but continuously varying function. At the origin we impose the condition that the 4 functions: $(r\psi)_i \to 0$.[4]

B. Results

I. Schrödinger's equation

Since the mass defect of the neutron is always ascertained by arguments depending on the relativistic equivalence of mass and energy, an application of the Schrödinger equation to this problem is only of academic interest. For the sake of completeness, and for comparison with Part II, however, I shall state the results.

Assuming a binding energy of the neutron equal to ϵmc^2, or ϵ/α^2 in Hartree units (α = fine structure constant) the radial part of the solution in a Coulomb field has the form $R_0 = (c/r)\exp[-(2\epsilon)^{\frac{1}{2}}r/\alpha]$, which is approximately valid down to distances of the order of the classical electron radius. The condition of continuity at r_0 requires that φ_i, the potential inside, must be *greater* than $2\epsilon/\alpha^2$, so that, in general, a drop in the potential energy must occur to insure stability. Inside of r_0, the radial function then has the form $R_i = (c/r)\sin([2\varphi_i - 2\epsilon/\alpha^2]^{\frac{1}{2}}r)$, which joins r_0 in the proper way if $\varphi_i \sim \pi^2/8r_0^2$, r_0 being measured as multiple of the first Bohr radius. If r_0 is taken to be of the order of the "electron radius" α^2, the inside potential energy trough has a depth approximately 20,000 times the rest energy of an electron. Hence the kinetic energy of the electron inside r_0 would be enormous, which inference might also have been drawn from the uncertainty principle. This again indicates the inapplicability of the non-relativistic theory to the problem at hand.

There is, in this theory, no limitation upon ϵ. The charge distribution is roughly independent of the choice of r_0. As seen from the form of R, the charge density (multiplied by r^2) has a maximum at r_0 and extends with fair uniformity out to $r = \alpha/2(2\epsilon)^{\frac{1}{2}} \sim 10^{-11}$ cm. Only a very small part of the total electronic charge is inside r_0 and this, in fact, may be neglected as far as the scattering properties of this neutron model are concerned. For this reason its scattering radius should be independent of the choice of r_0. However, on computing the potential due to this combination of proton and electron, and thence its scattering radius, one finds that it acts upon nuclei approximately like a proton alone because the electronic charge is distributed so thinly. The scattering radius comes out about correctly, but varies too rapidly with the atomic number of the scattering nucleus.

II. Dirac's equation

(1) The solution of Dirac's equation for the state of lowest angular momentum has the form

$$\begin{aligned} \psi_1 &= (\tfrac{1}{3})^{\frac{1}{2}} if(r)Y_{10}(\vartheta, \varphi), \quad \psi_3 = g(r), \\ \psi_2 &= (\tfrac{2}{3})^{\frac{1}{2}} if(r)Y_{11}(\vartheta, \varphi), \quad \psi_4 = 0. \end{aligned} \tag{1}$$

The Y_{lm} are surface harmonics, normalized to 1. If we put

$$rf = P_1, \qquad rg = P_2, \tag{2}$$

Dirac's equation can be reduced to two second order equations for P_1 and P_2, both of which have the asymptotic form

$$P'' + \epsilon(\epsilon - 2)/\alpha^2 P = 0. \tag{3}$$

Here again ϵ is the binding energy (in units mc^2), related to the total energy of the electron by $E = (1-\epsilon)/\alpha^2$. Eq. (2) is independent of the special form of the potential, which vanishes at ∞. We see from (2) that P dies down exponentially at infinity only if $0 \leqq \epsilon \leqq 2$, otherwise it is sinusoidal. It can therefore be said generally

[4] This condition is more stringent than the usual one for S-states, but is necessary for the case of a potential constant near the origin.

that any stable neutron which consists of a proton and an electron obeying Dirac's equation must have a mass defect between 0 and twice the rest mass of an electron. Accordingly, the possible mass range of the neutron is from 1.0067 to 1.0077. A mass as low as that proposed by Lawrence[5] would constitute direct evidence against the applicability of Dirac's theory, or indeed the complex character of the neutron. The physical reason for this restriction is to be found in the fact that if $\epsilon > 2$ the electron, being at ∞ essentially free but in a negative kinetic energy state, would be repelled by the proton.

(2) In the subsequent calculations ϵ has been taken to be 1 for simplicity. The results obtained for this special case are qualitatively valid and typical for the entire range $0 < \epsilon < 2$. It is to be noted in the first place that $\Delta\varphi$ cannot be 0 for any choice of r_0. If we agree to consider values of $r_0 \gtrsim \alpha^2$, which alone are of physical interest for a reason discussed under 5, then there are for every r_0 two values of $\Delta\varphi$, one positive and one negative, which produce stability. Both are very large and of nearly equal magnitude. Such a neutron may result, therefore, from either a steep potential drop or a steep potential rise anywhere near the origin.

This dual possibility, which is characteristic of Dirac's theory, is intimately connected with the existence of states of negative kinetic energy. The case in which $\Delta\varphi < 0$ would correspond classically to a very strongly polarizable proton, the case $\Delta\varphi > 0$ to a highly impenetrable one, surrounded by a rigid potential wall. The electron would be passing back and forth through this obstacle, and at every passage the Klein paradox would take place.

One must not think of this combination as essentially the neutron discussed under I, but with relativity corrections. For if we make a similar calculation using the relativistic Schrödinger equation the answer is totally different, and in attempting to correct this answer by introducing Dirac's spin terms it is seen that their influence upon the energy is vastly predominant. Hence the models here investigated derive their stability not from the interaction of the electron's charge with the field of the proton, but from the fact that its quasi-electric moment is drawn near the proton into the very strong portion of the field. This interpretation is further corroborated by the fact that the charge distribution decreases rapidly at distances greater than r_0 and that, in the absence of a sudden change ($\Delta\varphi = 0$), no stability is possible. The magnitude of $\Delta\varphi$ is $\pi/\alpha r_0$. Hence the potential jump is about 400 mc² if $r_0 \sim \alpha^2$, 50,000 mc² if $r_0 \sim \alpha^3$.[6] In the former case, $|\Delta\varphi_+| - |\Delta\varphi_-| \sim 5$ mc², in the latter, this difference is ~ 400 mc².

In judging the plausibility of these models one must note, however, that stability requires very exact realization of these potential jumps. In the latter case, if $\Delta\varphi$ differed by much less than 1 percent from the calculated value a permanent combination could not be formed.

(3) The form of the P-functions (cf. Eq. (2)) depends, of course, essentially on the choice of r_0. They have been worked out as definite integrals over tabulated functions. Their form becomes very simple, however, if r_0 is taken to be quite small. Thus if we let $r_0 \gtrsim \alpha^3$ (in atomic units), and consider the model with the potential trough ($\Delta\varphi > 0$), we obtain the following set of approximate P-functions, valid to within a fractional error of the order α.

$r < r_0$	$r = r_0$	$r > r_0$
$P_1 = A(\frac{1}{2}\pi kr)^{\frac{1}{2}} J_{3/2}(kr)$	$P_1(r_0) = A$	$P_1 = A(r_0/r)e^{-r/\alpha}$
$P_2 = A \sin kr$	$P_2(r_0) = -\frac{1}{2}A\alpha$	$P_2 = -\frac{1}{2}A\alpha(r_0/r)e^{-r/\alpha}$

(4)

Here J is a Bessel function, $k \equiv (\pi + \alpha/2)/r_0$. The normalization factor has the value $A = (2r_0)^{-\frac{1}{2}}$. It is easily seen, by integrating $(P_1^2 + P_2^2)dr$, that half of the electron's charge is inside, half

[5] Livingston, Henderson and Lawrence, Phys. Rev. **44**, 781 (1933).

[6] These results are consistent with, and could have been derived from, general considerations regarding the localizability of electrons. Cf. L. Landau and R. Peierls, Zeits. f. Physik **69**, 56 (1931); W. R. Furry and J. R. Oppenheimer, Phys. Rev. **45**, 245 (1934).

of it outside of r_0. The charge distribution in the case $\Delta\varphi<0$ (potential wall) is similar and requires no separate discussion.

(4) The spin properties of the model (4) are of some interest. The average spin along any one direction is zero. For instance, if S_z is taken to be the diagonal matrix with elements $\frac{1}{2}$, $-\frac{1}{2}$, $\frac{1}{2}$, $-\frac{1}{2}$, the spin along Z is $\bar{S}_z=\Sigma^4_{\sigma=1}\int\psi_\sigma^*(S_z\psi)_\sigma d\tau$ $=\frac{1}{2}\int_0^\infty(P_2^2-\frac{1}{3}P_1^2)dr=0$. The same result holds for $\bar{S}_x$ and $\bar{S}_y$. The electron in this combination has no average spin. This is of course an entirely possible situation, for we know that the spin matrix does not commute with the energy operator. Hence the spin can be different at different distances from the origin and actually vanish on the average. In our case, the spin to the left of r_0 cancels that to the right.

On the other hand, the total angular momentum, $M+s$, is permutable with H, and the average value of this operator should therefore be $\frac{1}{2}(h/2\pi)$. This is the case since $\overline{M}_z=(h/2\pi i)\Sigma\int\psi_\sigma^*\partial\psi_\sigma/\partial\varphi d\tau=\frac{1}{2}(h/2\pi)$. $\overline{M}_y$ and $\overline{M}_x$ are both zero. Thus we are dealing with the somewhat peculiar case where the angular momentum of $\frac{1}{2}$ unit, which in the lowest H-state is carried almost entirely by the spin, is now borne by the M-operator. The electron spin has transformed itself into an orbital angular momentum. This statement has meaning inasmuch as we can assign separate operators to the two types of angular momentum.

One may be inclined to take this result as an indication that, when the electron is very intimately connected with an attractive center, something happens to its spin which is not adequately described by the Dirac theory. Nevertheless the orthodox rules force us to conclude that the total angular momentum of the neutron is either 0 or 1 Bohr unit. This, however, is not in complete contradiction to the facts. For the models here discussed correspond at best to a *free neutron*. The experimental evidence which supports the half-integral angular momentum refers to a particle embedded in nuclei, which cannot be expected to obey Dirac's equation, since this loses its validity in connection with a many-body problem. It is not impossible, therefore, that a neutron, upon entering nuclei, loses part of its spin (perhaps concomitant with the emission or absorption of a neutrino) because it ceases to obey a theory which preserves electronic angular momenta.

(5) Although the theory is incompetent to fix r_0, an upper limit for this quantity can be deduced by postulating that the modified potential near the origin, considered as a perturbation upon the H-states, shall produce an effect inferior to the fine structure splitting of the Balmer lines. Such an effect decreases indeed with r_0, and one is led in this way to assume that $r_0<10^{-12}$ cm.

(6) Knowing the ψ-functions for the neutron state (Eqs. (4)) it is easy to calculate the transition probability between the ground state of hydrogen and the neutron state, and thence the lifetime of normal hydrogen. In doing this, multipole transitions must be considered, since dipole transitions are impossible because of the spherical symmetry of both states. Thus the lifetime of H is found to have the small value 10^{-7} sec. This is perhaps the most serious defect of the complex neutron. It cannot be avoided by any reasonable choice of r_0, for it depends essentially on the asymptotic factor of P, i.e., $e^{-r/a}$, regarding which there is no choice.

It was hoped that this brief discussion of the features of the synthetic neutron might clarify its status. The result may fairly be said to be this: Unless one is willing to make very special assumptions there is little hope of accounting for the neutron's existence by the use of available theories. The mass of the neutron is not certain to fall into the range permitted by theory (cf. 1); the kinetic energy of the electron in this model is too great to be plausible (cf. 2); the lifetime of hydrogen is certainly very much greater than that allowed if a complex neutron could be formed (cf. 6).

Estimated Electron Affinities of the Light Elements

GEORGE GLOCKLER, *University of Minnesota*

(Received May 14, 1934)

The electron affinities of the light elements have been estimated by an empirical method of extrapolation. The ionization potentials (I) of isoelectronic systems are considered to be parabolic functions of the atomic number (Z). The Moseley curves $I^{\frac{1}{2}} : Z$ of the first ionization potential of the electronic systems containing from one to eighteen electrons have been completed. They are nearly straight lines except in their lower extremities where they show a bending towards the axis of atomic number Z. Wherever a check was possible it is found that the estimated electron affinities agree with experiment or with other calculation as obtained from wave mechanics or from thermochemical considerations by means of a Born-Haber cycle. The estimated electron affinities (in electron-volts) are: H (+0.7), He (−0.5), Li (+0.3), Be (−0.6), B (+0.1), C (+1.37), N (+0.04), O (+3.8), F (+3.9), Ne (−1.20), Na (+0.1), Mg (−0.9), Al (−0.2), Si (+0.6), P (+0.2), S (+2.1), Cl (+3.7), A (−1.0), Ni (+0.3), Cu (+1.2), Ag (+1.0), Hg (+1.8).

I. INTRODUCTION

THE total energy W of any atomic system can be expressed by equations of the form

$$W=\Sigma[(Z-s)/n]^2 \qquad (1)$$

where Z = charge on the nucleus, s = screening constant and n = effective quantum number.[1, 2] This relation can be used to calculate the ionization potential I of the outermost electron for any isoelectronic sequence. It is seen that the relation between ionization potential I and atomic number Z will be of the form of a parabola. These parabolas have been calculated from experimental data and they are used below to obtain the electron affinities of the atoms of the first two periods of the periodic table. These parabolas are considered a more satisfactory representation of the relations mentioned than the usual Moseley-curves ($I^{\frac{1}{2}} : Z$).

II. WAVE MECHANICS

Of the eighteen atoms mentioned, only the two and three electron systems have been treated on the principles of wave mechanics by Hylleraas, Eckart, Wilson and others.[3–5] The results of these calculations check satisfactorily but they involve enormous labor of calculation. It may therefore be permissible to suggest a very simple, empirical method of extrapolation, which will permit the calculation of electron affinities.

III. EMPIRICAL METHOD OF EXTRAPOLATION

It is suggested to establish the complete Moseley-curves for isoelectronic systems indicating in each case the removal of the first or outer electron. From the fact that the two and three electron systems show Moseley curves which have a bend near smaller atomic numbers it is evident that straight line extrapolation as indicated by Bartlett[6] and Braunbek[7] will not yield the most accurate values.

From the known experimental values[8] the best parabola is obtained (Fig. 1) showing the relation between ionization potential and atomic number:

$$I=(1/n^2)(aZ^2-bZ+c), \qquad (2)$$

$$dI/dZ=(1/n^2)(2aZ-b), \qquad (3)$$

$$d^2I/dZ^2=2a/n^2. \qquad (4)$$

The slope Eq. (3) were found to be straight lines which are parallel for the K, L and M shells as seen in Fig. 3. The values of the constant a (Eq. (2)) expected are $a=27.08$ (K); $a=\frac{1}{4}\times 13.54=3.39$ (L); $a=\frac{1}{9}\times 13.54=1.504$ (M) while the experimental quantities are nearly constant and

$$a=27.08\ (K);\quad a\doteq 3.6\ (L);\quad a\doteq 1.8\ (M).$$

[1] C. Zener, Phys. Rev. **36**, 51 (1930).
[2] J. C. Slater, Phys. Rev. **36**, 57 (1930).
[3] E. A. Hylleraas, Zeits. f. Physik **65**, 209 (1930).
[4] C. Eckart, Phys. Rev. **36**, 878 (1930).
[5] E. R. Wilson, J. Chem. Phys. **1**, 210 (1930).
[6] J. H. Bartlett, Nature **125**, 459 (1930).
[7] W. Braunbek, Zeits. f. Physik **63**, 20 (1930).
[8] R. F. Bacher and S. Goudsmit, *Atomic Energy States*, McGraw Hill Book Co., New York and London (1932).

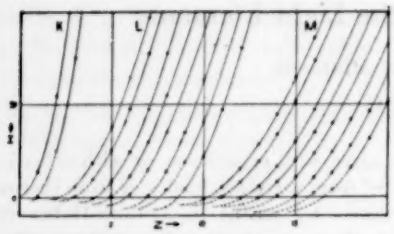

FIG. 1. Ionization potential of the outer electron for isoelectronic systems as parabolic function of the central charge.

The constants a, b and c of the empirical parabolas are given in Table I. Differences between theoretical and experimental values can be expressed as a quantum defect.

For some of the systems considered very little data are available and the slopes of the curves (Fig. 3) representing the 7, 9, 12, 14, 15, 16 and 17 electron system were obtained by interpolation. It is believed that the consistency of the whole scheme justifies this procedure.

TABLE I. *Ionization potentials of isoelectronic systems as parabolic functions of nuclear charge.*

Shell	No. of electrons	$I_1=aZ^2-bZ+c$ a	b	c	a/n^2
K	1	13.54	—	—	13.54
	2	13.54	16.87	4.06	
L	3	3.43	11.25	8.25	3.39
	4	3.43	15.10	14.77	
	5	3.57	23.28	35.43	
	6	3.58	28.23	51.87	
	7	3.67	34.6	76.85	
	8	3.77	43.04	116.6	
	9	3.75	48.95	155.4	
	10	4.0	58.47	206.1	
M	11	1.75	30.41	127.9	1.504
	12	1.8	33.87	154.9	
	13	1.7	35.59	181.3	
	14	1.7	37.62	201.6	
	15	1.7	39.70	223.2	
	16	1.85	47.20	291.9	
	17	2.0	55.14	372.3	
	18	2.0	58.00	411.5	

The eighteen parabolas enumerated in Table I fit the experimental ionization potentials very well wherever sufficient experimental data were found to make a test. The first three shells of electrons (K, L and M) were found to yield very satisfactory results by this method of treatment. However the atoms beginning with potassium do not add the next electron into the last M subshell. The situation is here more complicated but it appears that the electron affinity of argon is negative, i.e., A^- is unstable whether the electron would tend to enter the $3d(M)$ or the $4s(N)$ shell.

IV. ELECTRON AFFINITY

In the study of atomic structure as well as in the consideration of chemical processes the affinity of neutral atoms or molecules for electrons is a quantity of very great interest. A few direct determinations[9-11] have been made, optical methods have been attempted[12] and in the case of the hydrogen atom the only satisfactory knowledge which exists is the calculation of the electron affinity of hydrogen by Hylleraas.[13] Since both the experimental determination and the calculation of the electron affinity appear to present great difficulties, either of experimental manipulation or of intricate calculation it should be of some interest to use the above empirical extrapolation method for their evaluation. It is believed that it gives entirely satisfactory values of the electron affinity of the atoms which fit well into the whole scheme of our present knowledge of these quantities.

The method consists in the extrapolation of the known ionization potential of the stripped atoms of the same number of electrons as the negative ion. For example the two electron systems

$$H^- \rightarrow H + E^-$$
$$He \rightarrow He^+ + E^-$$
$$Li^+ \rightarrow Li^{++} + E^-$$
$$A^{+(Z-2)} \rightarrow A^{+(Z-1)} + E^-$$

are all isoelectronic structures and one parabola represents their first ionization potential or one Moseley curve (second curve of Fig. 2) pertains to them. From the eighteen parabola shown in Table I the electron affinities of the atoms have been estimated. The values are shown in Table II and in Fig. 4.

[9] J. E. Mayer, Zeits. f. Physik **61**, 798 (1930).
[10] L. Rolla and G. Piccardi, Atti acad. Lincei [6] **3**, 410 (1926).
[11] G. Piccardi, Atti. acad. Lincei [6] **3**, 413 (1926); **3**, 566 (1926).
[12] O. Oldenberg, Phys. Rev. **43**, 534 (1933).
[13] E. A. Hylleraas, Zeits. f. Physik **60**, 624 (1930).

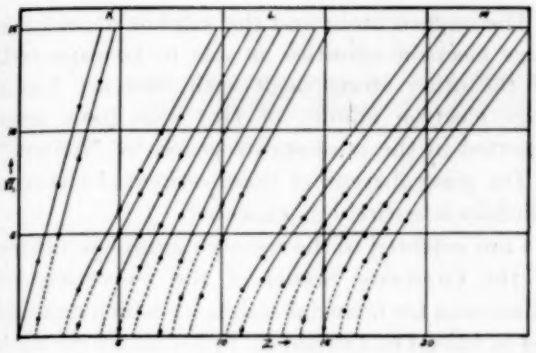

FIG. 2. Moseley curves of the ionization potentials of the outer electron of isoelectronic systems.

TABLE II. *Electron affinities of the light atoms.*

Atom	E. Aff.	Atom	E. Aff.
H	+0.76	Ne	−1.20
He	−0.53	Na	+0.08
Li	+0.34	Mg	−0.87
Be	−0.57	Al	−0.16
B	+0.12	Si	+0.60
C	+1.37	P	+0.15
N	+0.04	S	+2.06
O	+3.80	Cl	+3.70
F	+3.94	A	−(1.0)
Ni	+0.25	Ag	+0.95
Cu	+1.17	Hg	+1.79

V. GENERAL CONSIDERATIONS

It is seen that the electron affinities of the rare gases He, Ne and A are negative, i.e., the negative ions He^-, Ne^- and A^- are unstable. This is to be expected when it is recalled that the mobility of the negative carrier in these gases reaches very high values,[14] which can only mean that free electrons abound in these gases when very pure and they do not attach themselves to form negative ions. The negative rare gas ions do not occur in the mass-spectrograph. In only one case has He^- been reported.[15] The present considerations would throw doubt on the correctness of the interpretation of these mass-spectroscopic findings. The negative He^- ions may not be due to the neutral atom but may be due to excited helium which may well possess an affinity for electrons.

[14] A. M. Tyndall and C. F. Powell, Proc. Roy. Soc. **A129**, 162 (1930).

[15] Handbuch d. Physik, Vol 22/2 (2nd Ed.) page 93; Verlag von J. Springer, Berlin (1933).

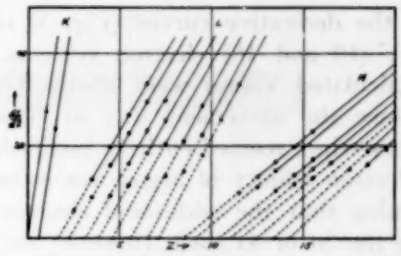

FIG. 3. First derivative of the ionization potential of the outer electron of isoelectronic systems as a function of the central charge.

The atoms beryllium and magnesium do not form Be^- and Mg^-. It is of interest to recall that the neutral alkaline earth atoms are in a $^1S_0$ state as are the rare gases and it is easy to believe that a further electron added would not attach readily since it would have to enter an outer shell.

The alkali metal atoms have a positive electron affinity and Li^- and Na^- are stable. The potassium ion K^- has been reported.[16]

The halogens fluorine and chlorine have a large electron affinity as has been shown by many workers and especially by J. Mayer.[9] His determination is so well established that his values have been used by us to determine the

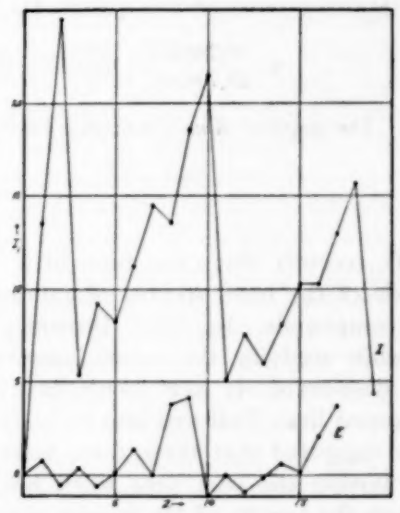

FIG. 4. Estimated electron affinities of light atoms E obtained from empirical extrapolation of the ionization potentials of analogous isoelectronic systems and experimental values of the ionization potentials I of the outer electron of the corresponding neutral atoms.

[16] R. W. Ditchburn and F. L. Arnot, Proc. Roy. Soc. **A123**, 516 (1929).

slope of the derivative curves (Fig. 3) of the respective (10 and 18) electron systems. Our earlier calculated values were about 0.8 e.v. lower. Since the agreement was so close the present procedure seemed entirely justified.

The electron affinity of argon was estimated by assuming that the additional electron was added to the *3d* or *4s* shell. However the long extrapolation involved will only permit the statement that A^- is most likely unstable. Negative ions have been reported in argon[17] but they may be due to an impurity or to excited atoms.

[17] H. A. Barton, Nature **114**, 826 (1927).

The oxygen atom and the sulphur atom have large electron affinities as was to be expected. Of the other atoms dealt with, mercury has a large electron affinity of Hg^- ions have been reported in the mass-spectrograph by Nielsen.[18]

The general trend of these estimated electron affinities is entirely as expected.

I am indebted to the research grant committee of the Graduate School of the University of Minnesota for financial assistance which enabled me to have Dr. Donald L. Fuller assist me with the calculations.

[18] W. M. Nielsen, Phys. Rev. **27**, 716 (1926); **31**, 1123 (1928); Proc. Nat. Acad. Sci. **16**, 721 (1930).

The Spectrum of Gallium Oxide

MARJORIE L. GUERNSEY, *Sloane Physics Laboratory, Yale University*

(Received May 23, 1934)

The spectrum of gallium oxide has been photographed with a 21-foot grating. A band system lying in the region 3800–4200A has been identified as a $^2\Sigma \rightarrow {}^2\Sigma$ transition and a vibrational quantum analysis is given. The band-heads are approximately located by the equation

$$\nu = \left.\begin{matrix}25{,}706.43\\25{,}709.04\end{matrix}\right\} + 763.63(v'+\tfrac{1}{2}) - 3.89(v'+\tfrac{1}{2})^2 - 767.69(v''+\tfrac{1}{2}) + 6.34(v''+\tfrac{1}{2})^2.$$

The spectrum of indium oxide is briefly discussed.

UNTIL recently there has been little study made of the band spectra of gallium and indium compounds. In 1916 Browning and Uhler,[1] while studying the atomic spectrum of gallium, discovered six new bands and eleven closely-spaced lines (believed also to be bands), and they suggested that these came from GaO or Ga_2. Within the past year work has been reported on the spectra of the halides of gallium and indium.[2, 3, 4] In a recent comprehensive study of these halide spectra Miescher and Wehrli[4] have discussed briefly the spectrum of GaO and have given vibrational quantum assignments to the bands observed. The analysis to be reported in this paper is based on spectrograms of this same system taken at higher dispersion. Measurements of the band-heads check those of Miescher and Wehrli and several additional bands have been noted. The more complete data now at hand indicate that the quantum assignments made by these workers are not entirely correct.

[1] P. E. Browning and H. S. Uhler, Am. J. Sci. **41**, 351 (1916).
[2] A. Petrikaln and J. Hochberg, Zeits. f. Physik **86**, 214 (1933).
[3] E. Miescher and M. Wehrli, Helv. Phys. Acta **6**, 256, 457 (1933).
[4] E. Miescher and M. Wehrli, Helv. Phys. Acta **7**, 357 (1934).

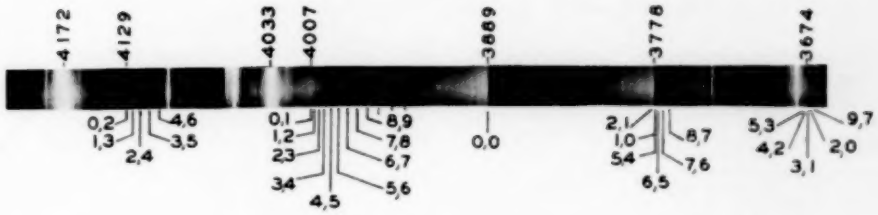

FIG. 1. Spectrogram of the GaO spectrum taken in the second order of a 21-foot grating.

EXPERIMENTAL PROCEDURE

Gallium metal was placed in the lower electrode of a copper arc which was run in air. The arc was operated at low currents (2 to 3 amperes) to reduce the continuous radiation to a minimum and prevent sputtering of the liquid metal. Photographs were taken in the first, second, and third orders of a 21-foot grating where the dispersion was approximately 5.2, 2.47, and 1.5 A/mm, respectively. The exposure times ranged from $\frac{1}{2}$ to $2\frac{1}{2}$ hours although the difficulties in operating the arc, due to oxidation of the metal, made the actual running times a great deal longer.

RESULTS

This band system lies near the atomic resonance lines of gallium and covers the region 3890–4130A. All of the bands degrade to the red and most of the heads are double, the average separation being 2.61 cm^{-1}. Fig. 1, a spectrogram taken in the second order of the 21-foot grating, shows the main portion of the spectrum and indicates how the bands are grouped in sequences, each of which is well separated from the next. The wave numbers, quantum assignments, and estimated intensities are given in Table I, and a matrix diagram of intensities in Table II. The positions of all the band-heads in this system are given approximately by the equation:

$$\nu_{\text{head}} = \left.\begin{matrix}25{,}706.43\\25{,}709.04\end{matrix}\right\} + 763.63(v'+\tfrac{1}{2}) - 3.89(v'+\tfrac{1}{2})^2 - 767.69(v''+\tfrac{1}{2}) + 6.34(v''+\tfrac{1}{2})^2.$$

This is undoubtedly a $^2\Sigma \rightarrow {}^2\Sigma$ system in which the R_2 and R_1 branches form the close double heads. The near equality of the ω_e values, which is characteristic of the other oxides in the third column of the periodic table, causes the bands to be grouped in long sequences which lie on a narrow Condon parabola. The $\Delta v = +1$ and $+2$ sequences have convergence points at low v'' values (1 and 3, respectively), and the bands of higher v'' values lie to the violet of this point, some of them coinciding with the first bands of the sequence. In each case the bands are crowded together giving the impression of a single band with several double heads. Because of low dispersion Browning and Uhler, and Miescher and Wehrli measured each of these sequences as a single band.

In the $\Delta v = 0$ sequence the convergence point occurs immediately so that the 1,1 band coincides with the 0,0 band. The intensity in this sequence drops off so rapidly that no bands beyond the 2,2 have been observed. The $\Delta v = -1$ and -2 sequences have a rather striking appearance because they begin immediately to diverge to the violet. This same phenomenon has been found in the spectra of CaF and SrF,[5] which are also isoelectronic molecules and probably have a structure somewhat similar to that of GaO. Miescher and Wehrli did not observe the first band in this sequence but did observe the second. However, they assumed that several bands, crowded together at the beginning of the sequence, had not been measured, and therefore they gave too high a quantum assignment to the remaining bands.

The writer has found evidence for a second band system in this spectrum lying in the region 4300–4900A, but the bands are faint, many of them being entirely obscured by the continuous background which it was found impossible to

[5] R. C. Johnson, Proc. Roy. Soc. **A122**, 189 (1929).

TABLE I. *Wave numbers, quantum assignments and intensities of lines of GaO.*

v', v''	ν (cm^{-1})	Int.	v', v''	ν (cm^{-1})	Int.
0,2	24,208.20 24,211.84	3	11,12	25,349.11	1
1,3	24,233.64 24,236.94	4	0,0 (1,1)	25,704.51	10
2,4	24,262.95 24,266.38	4	2,2	25,709.20 25,711.48	0
3,5	24,299.18 24,301.62	4	2,1 (3,2)	26,451.85 26,454.09	9
4,6	24,339.22 24,343.08	4	1,0 (4,3)	26,457.94 26,460.10	9
5,7	24,384.16 24,387.31	4	5,4	26,465.12 26,467.43	4
6,8	24,436.97	2	6,5	26,480.05 26,482.01	3
0,1	24,949.99 24,950.95	7	7,6	26,498.72 26,501.18	2
1,2	24,963.00 24,965.10	8	8,7	26,524.24	1
2,3	24,981.41 24,983.09	8	5,3 (6,4)	27,183.64 27,185.49	6
3,4	25,004.21 25,006.15	8	4,2 (7,5)	27,187.85 27,189.92	5
4,5	25,033.01 25,034.64	8	3,1 (8,6)	27,192.96 27,197.06	4
5,6	25,064.14 25,067.18	7	2,0	27,204.94 27,209.16	0
6,7	25,100.70 25,103.98	7	9,7	27,219.17	0
7,8	25,145.47	7	6,3	27,899.22	1
8,9	25,189.75	5	10,7	27,904.46 27,907.95	0
9,10	25,235.40	5	5,2	27,915.7	0
10,11	25,292.29	3	7,3	28,605.8	0

avoid. For this reason the present data are insufficient for a quantum analysis.

TABLE II. *Matrix diagram of the GaO bands. Intensities in ( ) represent bands that coincide with previous ones in the same sequence.*

v' \ v''	0	1	2	3	4	5	6	7	8	9	10	11	12
0	10	7	3										
1	9	(10)	8	4									
2	0	9	0	8	4								
3		4	(9)		8	4							
4			5	(9)		8	4						
5			0	6	4		7	4					
6				1	(6)	3		7	2				
7				0		(5)	2		7				
8							(4)	1		5			
9								0			5		
10								0				3	
11													1

Photographs have also been taken of the InO spectrum which consists mainly of a large group of bands lying between the two resonance lines of indium, 4102 and 4511A. The stronger bands degrade to the red but there are many which are shaded to the violet. This, together with the great irregularity in the distribution of the bands, suggests that there are two band systems overlapping in this region.

A prominent feature of this spectrum is the continuum which extends out from the resonance lines of indium to the high frequency side. Cases of such apparent broadening of resonance lines are known for the metals thallium, zinc, cadmium, mercury and magnesium,[6] as well as for the gas helium.[7] This continuum is undoubtedly due to semi-stable molecules of In_2. Further work is being done on this spectrum and it is hoped that a quantum analysis of InO may be possible in the near future.

The writer is indebted to Professor W. W. Watson for the suggestion of the problem, and the many discussions which have led to the quantum analysis presented here.

[6] H. Hamada, Phil. Mag. **12**, 50 (1931).
[7] J. J. Hopfield, Astrophys. J. **72**, 133 (1930).

The Infrared Absorption Spectrum of Formaldehyde. Part I

HARALD H. NIELSEN, *Mendenhall Laboratory of Physics, Ohio State University*

(Received May 25, 1934)

The infrared absorption spectrum of formaldehyde has been further investigated to beyond 11.0μ and bands were located at wave-lengths 5.7μ, 6.7μ, 7.5μ, 8.6μ and 9.6μ in addition to the regions originally reported by Salant and West and Patty and Nielsen near wave-lengths 3.5μ, 1.8μ, 1.4μ and 1.25μ. These regions of absorption were all studied under higher resolution and resolved into rotational components. *The 3.5μ region.* This region, originally studied by Patty and Nielsen, was remeasured and found to consist of two parallel type bands with an average spacing between lines equal to about 2.4 cm^{-1}, and a perpendicular type band with an average spacing of about 16.2 cm^{-1}. *The 5.7μ region.* This band was of the parallel type with its center at 5.73μ and with an average line spacing of about 2.4 cm^{-1}. *The 6.7μ region.* This band was also of the parallel type with its center at 6.65μ. Due to the bad overlapping of this region with the atmospheric water vapor bands, it was not attempted to resolve it into rotational structure. *The 7.5μ region.* The absorption near 7.5μ is due to a perpendicular vibration of the CH_2O molecule. The band shows considerable convergence, but when the spacings are averaged over an equal number of lines on either side of the center, it appears to be about 16.1 cm^{-1}. *The 8.6μ region.* The 8.6μ band is of the parallel type with its center at 8.58μ and shows an average separation between lines of about 2.4 cm^{-1}. It was possible also to measure this band as an emission band by heating the cell to somewhat higher temperatures. *The 9.6μ region.* This region was not thoroughly investigated, but a preliminary curve over this region made in emission indicates it to be of the perpendicular type with its center near 9.6μ.

I. INTRODUCTION

THE absorption by formaldehyde vapor was first investigated in the ultraviolet region by Henri and Schou.[1] This work has recently been repeated by Dieke and Kistiakowsky,[2] working under much improved experimental conditions. These investigators report complete resolution of a number of ultraviolet bands from which it is possible to determine values of the moments of inertia of the molecule in the ground state. The absorption by formaldehyde vapor in the infrared was first begun by Salant and West[3] who measured bands at 3.5μ, 1.8μ, 1.4μ and 1.25μ by means of a prism spectrograph. The region lying near 3.5μ was later investigated under higher resolving power by Patty and Nielsen,[4] with an echellette grating ruled with 3600 lines to the inch. This region revealed a complex absorption pattern which was interpreted to consist of three overlapping bands, two of which were of the parallel type and one of the perpendicular type. In addition to these a band of the parallel type, but much weaker, was found near 4.8μ. It also was partially resolved.

In all cases the parallel type bands were incompletely resolved, the lines appearing much like saw teeth. The spacings between lines were not uniform, however, ranging from 2.4 cm^{-1} to 4.0 cm^{-1}, the average being about 3.4 cm^{-1}. The perpendicular type band was identified by a series of broad prominent lines against an unresolved background. The spacings between these was estimated to be about 16 cm^{-1}, but due to the very bad overlapping with the parallel bands lying on both sides, this value could only be taken to be approximate. These two types of spacings should be sufficient to determine the molecular moments of inertia, but it was found that no good agreement was to be had with the values obtainable from Dieke and Kistiakowsky's work. This fact, in addition to the evidence of a non-uniformity of spacing of lines in the parallel type bands much too large to be accounted for by the asymmetry of the molecule, led one to suspect that the spacings observed by Patty and Nielsen were only apparent spacings arising out of incomplete resolution. It was therefore thought desirable, when an opportunity to continue the experiment presented itself, to remeasure these bands, if possible under still higher resolving power. A leave of absence presented this opportunity, and the spectrum has been measured on the spectrographs in the physics department at

[1] V. Henri and A. Schou, Zeits. f. Physik **49**, 774 (1928).
[2] G. H. Dieke and G. B. Kistiakowsky, Phys. Rev. **45**, 4 (1934).
[3] E. O. Salant and W. West, Phys. Rev. **33**, 640A (1929).
[4] J. R. Patty and H. H. Nielsen, Phys. Rev. **39**, 957 (1932).

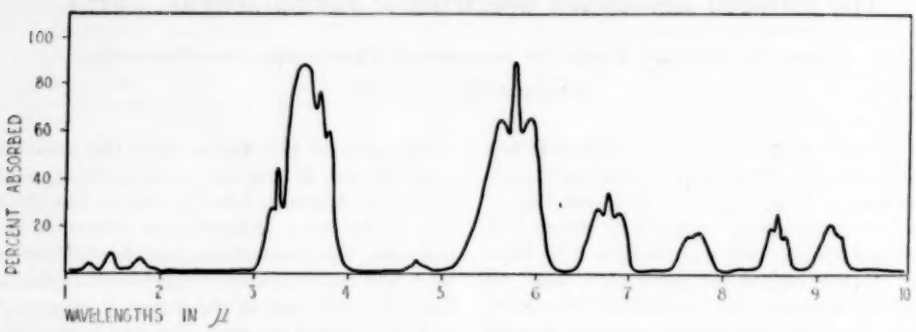

FIG. 1. Survey of absorption of formaldehyde with prism spectrograph in region from 1 to 11μ.

the University of Michigan, which were put at the writer's disposal.

In order that the spectrum might be studied much more extensively than before, an absorption cell was made, fitted with windows of rock-salt. The cell was made of a brass tube six inches long and could be heated by means of a coil extending the entire length of the cell. The inside of the tube contained flanges at some distance from the ends, to which the windows might be clamped by means of rings threaded to the inside of the tube. The windows were made air-tight at the joints by rubber gaskets. The formaldehyde vapor was generated by heating chemically pure trioxymethylene (paroformaldehyde). A container of brass attached to the side of the cell, heated by conduction from the cell itself, served as a reservoir for the paraformaldehyde. The cell and reservoir were thermally insulated by coatings of asbestos. It was found advantageous to operate the cell at a temperature of about 150°C.

Before beginning the measurements with the diffraction gratings, a preliminary prism exploration curve was made. This was done on a prism spectrograph of the Wadsworth type, designed by Sleator. The curve extends from 1.0μ to 11.0μ. This curve is reproduced in Fig. 1.

The grating spectrograph was one designed by Meyer and used by him and Barker and their collaborators in a great many investigations. It was equipped with three echellette gratings to diffract the various parts of the infrared spectrum. At 3.5μ, a grating ruled with 7200 lines per inch was available; from 5.0μ to 7.0μ, one with 4800 lines to the inch, and from 7.0μ to 11.0μ, one with 1200 rulings per inch was used in second order.

II. The Absorption Region from 3.3μ to 3.6μ

This is the region principally studied in the work of Patty and Nielsen, and has been remeasured with twice the dispersion and nearly four times the resolving power. In the major details it resembles quite accurately the absorption pattern reported in that work, there being three badly overlapping bands, two of which are of the parallel type, and a third of the perpendicular type.

The essential differences between these measurements and the earlier ones are details revealed by higher dispersion and resolution. The lines in the non-overlapping branches of the parallel type bands have been separated and the spacings near the center are now about 2.4 cm^{-1} instead of about 3.5 cm^{-1} as reported earlier. A certain irregularity in the short wave-length end of the 3.5μ band suggested that perhaps still another weak band was to be found near 3.2μ. This was borne out by a set of explorations in this region, but the cell was too short to obtain any definite results.

The perpendicular type band is identified as before by a group of rather prominent lines standing out against an unresolved background. Near the center of the band, where the overlapping with other bands is least, an alternation of intensities is evident; their ratios cannot, however, be determined exactly. An estimate of about 3 : 1 seems not implausible.

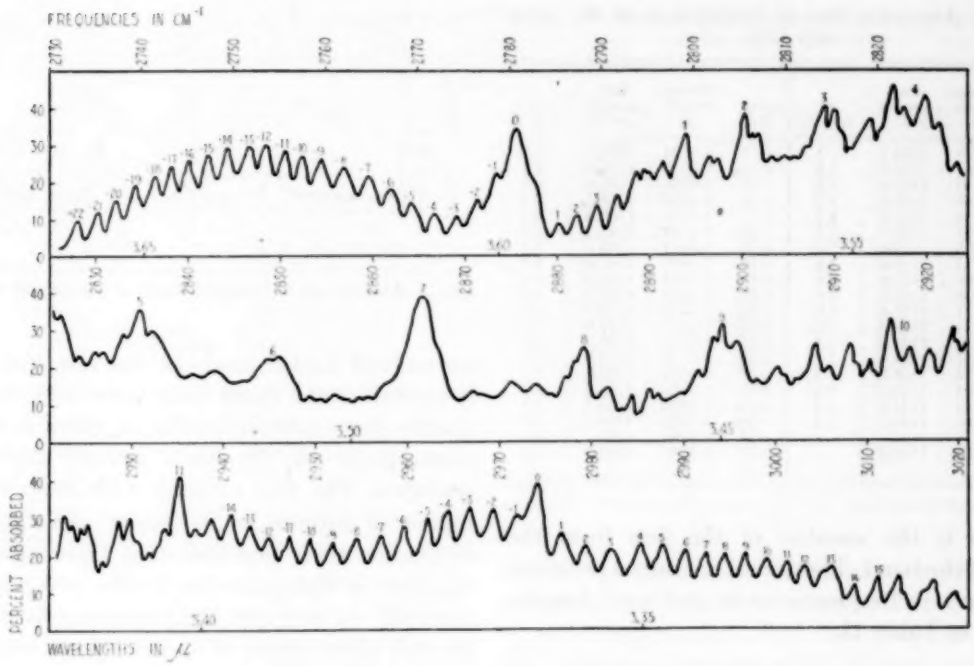

FIG. 2. Absorption of formaldehyde in region from 3.3 to 3.6μ.

In Fig. 2 is shown the new absorption curve for this region. The wave-lengths and frequency positions of lines in the parallel type bands and principal peaks in the perpendicular type band are tabulated in Table I.

TABLE I. *Wave-lengths and frequencies of principal absorption lines of formaldehyde in region 3.3 to 3.65μ.*

Line No.	Wave-length (μ)	Frequency (cm^{-1})	$\Delta\nu$ (cm^{-1})	Line No.	Wave-length (μ)	Frequency (cm^{-1})	$\Delta\nu$ (cm^{-1})
−21	3.6566	2734.8		−14	3.4002	2941.0	
−20	3.6539	2736.8	2.0	−13	3.3978	2943.0	2.0
−19	3.6512	2738.8	2.0	−12	3.3956	2945.0	2.0
−18	3.6486	2740.8	2.0	−11	3.3929	2947.3	2.3
−17	3.6459	2742.8	2.0	−10	3.3901	2949.8	2.5
−16	3.6433	2744.8	2.0	− 9	3.3873	2952.2	2.4
−15	3.7406	2746.8	2.0	− 8	3.3844	2954.7	2.5
−14	3.6380	2748.8	2.0	− 7	3.3817	2957.1	2.4
−13	3.6352	2750.9	2.1	− 6	3.3789	2959.5	2.4
−12	3.6324	2753.0	2.1	− 5	3.3761	2962.0	2.5
−11	3.6294	2755.3	2.3	− 4	3.3736	2964.2	2.2
−10	3.6265	2757.5	2.2	− 3	3.3713	2966.2	2.0
− 9	3.6236	2759.7	2.2	− 2	3.3679	2969.2	3.0
− 8	3.6206	2762.0	2.3	− 1	3.3652	2971.6	2.4
− 7	3.6176	2764.3	2.3	0	3.3625	2974.0	2.4
− 6	3.6145	2766.6	2.3	+ 1	3.3599	2976.3	2.3
− 5	3.6115	2768.9	2.3	2	3.3568	2979.0	2.7
− 4	3.6085	2771.2	2.3	3	3.3541	2981.4	2.4
− 3	3.6054	2773.6	2.4	4	3.3512	2984.0	2.6
− 2	3.6023	2776.0	2.4	5	3.3483	2986.6	2.6
− 1	3.5992	2778.4	2.4	6	3.3455	2989.1	2.5
0	3.5961	2780.8	2.4	7	3.3426	2991.7	2.6
+ 1	3.5907	2785.0	4.2	8	3.3400	2994.0	2.3
2	3.5881	2787.0	2.0	9	3.3374	2996.3	2.3
				10	3.3347	2998.8	2.5
+ 1	3.5727	2799.0		11	3.3322	3001.0	2.2
2	3.5638	2806.0	7.0	12	3.3296	3003.4	2.4
3	3.5524	2815.0	9.0	13	3.3267	3006.0	2.6
4	3.5411	2824.0	9.0	14	3.3240	3008.4	2.4
5	3.5280	2834.5	9.5	15	3.3213	3011.0	2.4
6	3.5100	2849.0	14.5				
7	3.4904	2865.0	16.0				
8	3.4692	2882.5	17.5				
9	3.4508	2897.9	15.4				
10	3.4290	2916.3	18.4				
11	3.4072	2935.0	18.7				

III. THE 5.7μ REGION

The absorption region near 5.7μ is a region of intense absorption and is a single band of the parallel type. As shown in Fig. 3, the *P* and *R* branches have been partially resolved showing a quite regular fine structure with some convergence toward higher frequencies. The average spacing of these lines is about 2.4 cm^{-1}. The positions of the lines seem well represented by the formula

$$\nu = 1744.1 + 2.44n - 0.0072n^2 + 0.000088n^3$$

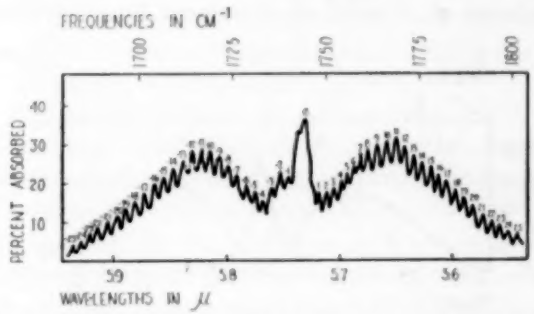

FIG. 3. Absorption of formaldehyde in the region near 5.7μ

TABLE II. *Absorption lines in formaldehyde in the region near 5.7μ.*

Line No.	Wave-length (μ)	Frequency (cm^{-1})	$\Delta\nu$ (cm^{-1})	Line No.	Wave-length (μ)	Frequency (cm^{-1})	$\Delta\nu$ (cm^{-1})
−17	5.8820	1700.1	..	+ 3	5.7104	1751.2	2.4
−16	5.8723	1702.9	2.8	+ 4	5.7026	1753.6	2.4
−15	5.8630	1705.6	2.7	+ 5	5.6948	1756.0	2.4
−14	5.8538	1708.3	2.7	+ 6	5.6870	1758.4	2.4
−13	5.8445	1711.0	2.7	+ 7	5.6792	1760.8	2.4
−12	5.8353	1713.7	2.7	+ 8	5.6715	1763.2	2.4
−11	5.8261	1716.4	2.7	+ 9	5.6641	1765.5	2.3
−10	5.8173	1719.0	2.6	+10	5.6567	1767.8	2.3
− 9	5.8086	1721.6	2.6	+11	5.6494	1770.1	2.3
− 8	5.7998	1724.2	2.6	+12	5.6421	1772.4	2.3
− 7	5.7911	1726.8	2.6	+13	5.6348	1774.7	2.3
− 6	5.7824	1729.4	2.6	+14	5.6275	1777.0	2.3
− 5	5.7740	1731.9	2.5	+15	5.6202	1779.3	2.3
− 4	5.7657	1734.4	2.5	+16	5.6129	1781.6	2.3
− 3	5.7574	1736.9	2.5	+17	5.6057	1783.9	2.3
− 2	5.7494	1739.3	2.4	+18	5.5988	1786.1	2.2
− 1	5.7415	1741.7	2.4	+19	5.5922	1788.2	2.1
0	5.7336	1744.1	2.4	+20	5.5857	1790.3	2.1
+ 1		....	..	+21	5.5782	1792.7	2.4
+ 2	5.7182	1748.8	..	+22	5.5713	1794.9	2.2

where n is the number of the line from the center of the band. The actual measured positions of the lines in frequency units and wave-lengths is given in Table II.

IV. THE 6.7μ REGION

This region of absorption coincides almost exactly with the intense absorption by water vapor near 6.27μ. The falsification arising from this background was so great that it seemed impractical really to attempt to resolve the band into fine structure. Hence, the spectrometer slits were widened, and only an envelope of the band was made. This envelope is shown in Fig. 4 and reveals it also to be of the parallel type with its center at 6.65μ. The maxima of the P and Q branches lie, respectively, near the frequency positions 1472 cm^{-1} and 1535 cm^{-1}.

V. THE 7.5μ REGION

This band is of the perpendicular type and consists of a series of prominent lines with an

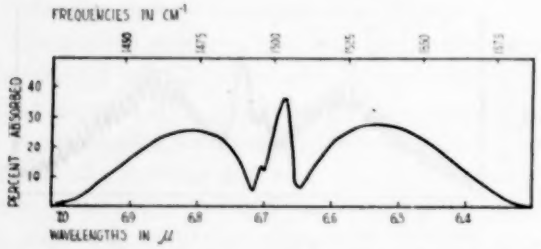

FIG. 4. Envelope of the 6.7μ band of formaldehyde.

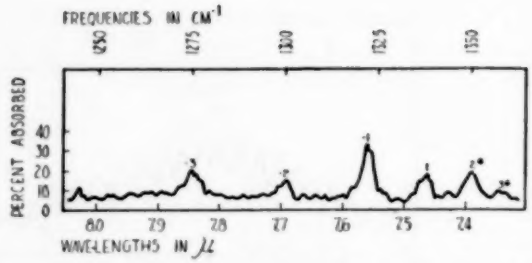

FIG. 5. Absorption of formaldehyde in the region near 7.5μ.

unresolved background. In the essential details it resembles the band lying near 3.5μ, but as is readily discernible from Fig. 5, there is a strong convergence of the lines toward higher frequencies. The two maxima with stars fell in a region of intense water vapor absorption. To determine their positions and their relative intensities in the spectrum, it was necessary very carefully to compare the transmission curve for the cell when empty of formaldehyde vapor with that for the cell when containing vapor. The two curves must be run immediately after each other before the background could change appreciably in intensity. In spite of this precaution, only estimates of the exact positions as well as their relative intensity could be made. In this band the alternation of intensities of the prominent lines is a prominent feature, their ratios being roughly 3 : 1. The positions of the lines in the band seem to be well expressed by the equation:

$$\nu = 1338.1 + 13.6n - 2.5n^2,$$

where n is a number arbitrarily assigned to the lines.

Table III gives the actually measured positions of the lines in terms of wave-lengths and frequencies.

TABLE III. *Wave-lengths of absorption lines in formaldehyde near 7.5μ.*

Line No.	Wave-length (μ)	Frequency in cm^{-1}	$\Delta\nu$(cm^{-1})
−4	8.0405	1243.7	
−3	7.8444	1274.8	31.1
−2	7.6870	1300.9	26.1
−1	7.5643	1322.0	21.1
0	7.4733	1338.1	16.1
1	7.4118	1349.2	11.1
+2	7.3784	1355.3	6.1
+3			

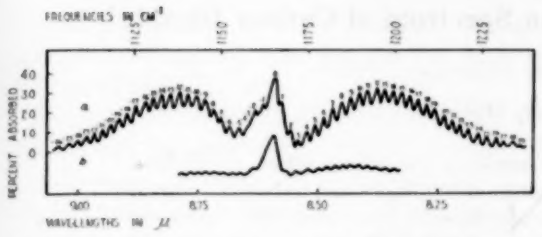

FIG. 6. Absorption of formaldehyde in the region near 8.6μ.

VI. THE 8.6μ REGION

This region has been examined and found to be of the parallel type band. It was measured in absorption in second order with a grating with 1200 lines ruled to the inch. This band also was resolved at least partially into a fine structure pattern (Fig. 6a) very similar to that at 5.8μ, there being here also some convergence toward higher frequencies, of the lines in the P and R branches. The average spacing between lines in frequencies found here agrees well with that in the 5.8μ region and is about 2.4 cm^{-1}. The lines are found to fit quite well to the equation:

$$\nu = 1165.64 + 2.403n - 0.00215n^2 - 0.00001n^3,$$

where as before n is the number of the line measured from the center.

It was found, also that with a somewhat hotter cell, this spectrum could be measured in emission (Fig. 6b). It was measured in first order with the same grating as before, but in spite of the much more incomplete resolution, it is still possible to correlate emission peaks with lines in absorption.

The data obtained are summarized in Table IV where the positions of the lines in terms of wavelengths and frequencies are tabulated.

VII. THE 9.6μ REGION

Lack of time prevented the measurement of this band in absorption. A set of emission measurements was, however, obtained extending from about 9.4μ to 9.7μ or covering what appears to be about two-thirds of the band. The measurements revealed about four or five quite prominent maxima against an unresolved background with apparently some convergence toward higher frequencies. This emission curve is not reproduced here since it is believed that the measurements extended over too narrow a region to give a picture complete enough not to be subject to misinterpretation. One can from its general character say, however, that his band appears to be of the perpendicular type with what apparently is its center at 9.6μ, having none of the characteristics of a parallel type. It is hoped to remeasure this band both in absorption and in emission in the very near future in order to ascertain its character definitely.

TABLE IV. *Wave-lengths of absorption lines of formaldehyde in the region near 8.6μ.*

Line No.	Wave-length (μ)	Frequency (cm^{-1})	$\Delta\nu$ (cm^{-1})	Line No.	Wave-length (μ)	Frequency (cm^{-1})	$\Delta\nu$ (cm^{-1})
−20	8.9542	1116.8		1	....	....	..
−19	8.9342	1119.3	2.5	2	8.5441	1170.4	..
−18	8.9142	1121.8	2.5	3	8.5266	1172.8	2.4
−17	8.8952	1124.2	2.4	4	8.5092	1175.2	2.4
−16	8.8755	1126.7	2.5	5	8.4918	1177.6	2.4
−15	8.8558	1129.2	2.5	6	8.4746	1180.0	2.4
−14	8.8370	1131.6	2.4	7	8.4581	1182.3	2.3
−13	8.8176	1134.1	2.5	8	8.4410	1184.7	2.4
−12	8.7982	1136.6	2.5	9	8.4239	1187.1	2.4
−11	8.7796	1139.0	2.3	10	8.4069	1189.5	2.4
−10	8.7604	1141.5	2.5	11	8.3907	1191.8	2.3
− 9	8.7420	1143.9	2.4	12	8.3738	1194.2	2.4
− 8	8.7237	1146.3	2.4	13	8.3570	1196.6	2.4
− 7	8.7055	1148.7	2.4	14	8.3410	1198.9	2.3
− 6	8.6873	1151.1	2.4	15	8.3250	1201.2	2.3
− 5	8.6685	1153.6	2.5	16	8.3091	1203.5	2.3
− 4	8.6505	1156.0	2.4	17	8.2932	1205.8	2.3
− 3	8.6326	1158.4	2.4	18	8.2775	1208.1	2.3
− 2	8.6147	1160.8	2.4	19	8.2617	1210.4	2.3
− 1	8.5955	1163.4	2.6	20	8.2461	1212.7	2.3
0	8.5793	1165.6	2.2				

VIII. CONCLUSION

A discussion of the data herein obtained will be given in Part II by Nordsieck and the writer. It will suffice to point out that with the much more extensive and self-consistent data obtained in this experiment, the apparent discrepancy, which earlier obscured the agreement of the information derived from infrared bands with that obtained from ultraviolet bands, have now been corrected and shown to have been due to incomplete resolution. The results of this investigation thus offer an excellent confirmation of the results of Dieke and Kistiakowsky.

The writer wishes to acknowledge his indebtedness to all his friends in the Michigan laboratory where these measurements were made. He wishes especially to express his gratefulness to Professor H. M. Randall who so kindly placed spectrographs and gratings at his disposal and who in every respect made him feel as one of the Michigan group.

Intensity Measurements in the Raman Spectrum of Carbon Dioxide*

ISABEL HANSON, *Duke University*

(Received April 26, 1934)

A simple photographic method of measuring intensities in the Raman effect was devised. The ratio of the intensities of the strong Raman doublet of CO_2 was found to be 0.572 instead of 0.667 as roughly estimated by Dickinson, Dillon and Rasetti. This value (0.572) although in apparent disagreement with the calculations of Dennison and Adel is in fair agreement with Placzek's recent work. An exposure of 24 days brought out three lines in addition to the four commonly observed. They may be identified with three of the lines predicted by Dennison and Adel.

RECENT theoretical work on the Raman effect in CO_2[1] has brought out the need for accurate intensity measurements of the strong Raman doublet under ordinary conditions. No very satisfactory method of measuring intensities in the Raman effect has been devised. On account of the long exposure times necessary in the Raman effect the reciprocity law would not be expected to hold.[2] For the measurements to be of greatest possible accuracy it is desirable that the experiment be conducted in such a way that errors due to the failure of the reciprocity law may be avoided. To avoid these errors the density marks for comparison must be exposed for the same length of time as the lines whose intensities are to be measured. When the exposure times are from 40 to 120 hours as is usually the case for gases, it is not practical to expose the plate to the Raman scattering and the comparison consecutively. A means was devised therefore of exposing the two simultaneously.

The gas was sealed at a pressure of 6 atmospheres in a quartz tube about 10″ long and ¾″ in inner diameter with walls thick enough to withstand 15 atmospheres pressure. The back end of the tube was bent and blackened with aquadag to prevent reflection and diaphragms were so placed in the tube that no light reflected from the walls of the tube could reach the spectrograph. The front end of the tube was ground and polished to form a plane window. Gas was taken from a commercial cylinder. It was introduced into the tube through a capillary sealed in the bent end of the tube to a pressure of 6 atmospheres. The tube was then immersed in liquid air, the gas frozen and the capillary sealed off.

Light was taken from a Hanovia Sc-2537 quartz mercury arc in spiral form surrounding the tube. The arc operated at a little above room temperature. The tube and arc were contained in a furnace. At higher temperatures the electrodes of the arc were water-cooled. The temperatures were measured with a thermocouple.

For comparison a Zeiss step filter of platinum sputtered on quartz in five layers of different transmissive powers was used. The transmissive power of each step for the 2537 mercury line was measured photoelectrically.

The slit of the Hilger E-1 quartz spectrograph which was used throughout was opened very wide and made as long as possible by removing the Hartmann diaphragm. The upper portion of the slit was narrowed with a piece of razor blade to a width such that the faint and strong Raman doublets of CO_2 were just resolved. The step filter was held over the slit with wax, the clear quartz area above the steps being placed over the narrowed part of the slit and the steps over the lower wider portion. The filter was illuminated by light from a small quartz mercury arc. This light was passed through a ground quartz plate to insure the uniformity of the beam and was made approximately monochromatic by passing through a monochromator. This uniform, approximately monochromatic (around 2537A) beam was reflected on to the slit by means of a silvered mirror. The light from the Raman tube

* Part of a thesis in partial fulfillment of the requirements for the degree of Doctor of Philosophy at Duke University, Durham, North Carolina.

[1] Dennison and Adel, Phys. Rev. **43**, 716 (1933).

[2] Harrison, J.O.S.A. and R.S.I. **19**, 267 (1929).

passed above this mirror, through the clear portion of the filter, and fell on the narrowed portion of the slit.

Although slow, Eastman 33 plates were used throughout because of their high contrast. Exposure times were from 35 to 115 hours.

The densities of blackening of the lines and comparison were measured with a Moll microphotometer.

At arc temperature the experimental error was around 2 percent but at high temperatures the error was greater, around 9 percent, because at higher temperatures the 2537 line in the Raman scattering was accompanied by a background which varied in intensity in the region of the Raman lines and it was difficult to determine the intensities of the lines from that of the background. The background was probably due to the presence of a small amount of gas not mercury vapor in the arc.

The results of the intensity measurements at arc temperature and at 200°C are contained in Table I.

TABLE I. *Intensity measurements.*

Temperature	R_3/R_2	R_1/R_2	$\frac{\text{No. mols. in 0101 state}}{\text{No. mols. in 0000 state}}$
50°C	0.572	0.225	0.104
200°C	0.608	0.521	0.262

R_1, R_2 and R_3 represent the intensity of the lines 1409, 1388 and 1285 cm^{-1}, respectively. The line 1409 cm^{-1} arises in the 0101 state and the other two in the 0000 state. The ratio of the number of molecules in the two states was calculated for the two temperatures from the Boltzmann formula. The weight of the 0101 state was taken as 2 and of the 0000 state as 1.[3]

It may be seen that under ordinary conditions the ratio of the intensities of the strong Raman doublet is 0.572 instead of 0.667 as estimated by Dickinson, Dillon and Rasetti.[4] Dennison and Adel[5] used the latter value in their calculation of Δ from the expression for the ratio of the intensities of the strong Raman doublet

$$(1-\Delta/2^{\frac{1}{2}}|b|)/(1+\Delta/2^{\frac{1}{2}}|b|)$$

in which b is a constant related to the separation of the strong Raman doublet and Δ is a constant related to the difference between ν_1 and $2\nu_2$ for CO_2. They obtained a preliminary value for $\Delta=20$ and found the most probable value to be 14.7 cm^{-1}. When the expression is set equal to 0.572 the value for Δ obtained is 28 which is in disagreement with the most probable value found by Dennison and Adel. In a letter from Dr. Dennison he calls my attention to a very recent paper by Placzek[6] in which the latter takes into account the polarizability of the molecule and finds the expression for the ratio of the intensities of the strong doublet in CO_2 to be more nearly

$$\left|\frac{(x-|\Delta|)^{\frac{1}{2}}\alpha_1 \mp (x+|\Delta|)^{\frac{1}{2}}\alpha_2}{(x+|\Delta|)^{\frac{1}{2}}\alpha_1 \pm (x-|\Delta|)^{\frac{1}{2}}\alpha_2}\right|^2,$$

where $x=2^{\frac{1}{2}}|b|$ and α_1 and α_2 are related to the first and second derivatives of the polarizability. This expression is not completely correct, further measurements on the polarization of the lines being necessary in order to obtain an exact expression, but Placzek estimates that α_1/α_2 should be approximately equal to ± 10. If Dennison and Adel's value for $b=72.9$ cm^{-1} and $\Delta=14.7$ cm^{-1} are substituted and the expression set equal to 0.572 we find $\alpha_1/\alpha_2=\pm 14.8$ which is in fair agreement with Placzek's estimate.

The intensity of the weak Raman doublet increases with the temperature as would be expected from the Boltzmann distribution.

An exposure of 24 days brought out three lines in addition to the commonly observed four, corresponding to shifts 1244 ± 10, 1426 ± 8 and 1528 ± 15 cm^{-1}. These may be identified with the lines predicted by Dennison and Adel at 1248, 1426 and 1517 cm^{-1}.

I wish to express my appreciation to Dr. C. C. Hatley and Dr. W. M. Nielsen of the Physics Department of Duke University for their interest and assistance in the work.

[3] Dennison, Rev. Mod. Phys. **3**, 280 (1931).
[4] Dickinson, Dillon and Rasetti, Phys. Rev. **34**, 382 (1929).
[5] Dennison and Adel, Phys. Rev. **43**, 716 (1933).
[6] Placzek, Handbuch der Radiologie **VI**, 2, 321 (1934).

Deepest Terms in Ions of the Isoelectronic Sequences Ni I to Kr IX and Pd I to Xe IX

P. GERALD KRUGER AND W. E. SHOUPP, *Department of Physics, University of Illinois*

(Received May 21, 1934)

Radiations corresponding to the energy differences between the terms $3d^{10}\ {}^1S_0$ and $3d^9\,4p\ {}^3P_1^0$, ${}^1P_1^0\ {}^3D_1^\circ$ in Ge V, As VI, Se VII and Br VIII have been found. Also, the corresponding radiations, $4d^{10}\ {}^1S_0 - 4d^9\,5p\ {}^3P_1^0$, ${}^1P_1^0$, ${}^3D_1^0$ in Sb VI, Te VII and I VIII have been observed. A new relation involving displaced frequencies has been used to predict the wave-length of the lines observed and the corresponding lines of Kr IX and Xe IX as yet not observed. A study of the ionization potentials in the sequences shows that it is possible to calculate the ionization potentials of atoms more highly ionized than those reported.

INTRODUCTION

VARIOUS investigators[1] have studied the spectra of elements of the isoelectronic sequence Ni I, Cu II, etc. Except in the case of Ni I the deepest term is a $^1S_0$ due to $3d^{10}$ electrons. Above this term are the $3d^9\,4s\ {}^1D\ {}^3D$ terms and still higher the $3d^9\,4p\ {}^{1,3}(P^0D^0F^0)$ terms are found. Between these terms and the ground state only three combinations are possible. They are $3d^{10}\ {}^1S_0 - 3d^9\,4p\ {}^3P_1^0$, ${}^1P_1^0$, ${}^3D_1^0$. Lines corresponding to these transitions had been found in Ni I, Cu II, Zn III, and Ga IV, but were not known previously in Ge V, As VI, Se VII and Br VIII.

In the isoelectronic sequence Pd I, Ag II, etc., the $4d^{10}\ {}^1S_0$ terms[2] were known for Pd I, Ag II, Cd III, In IV, and Sn V, but were not known previously for Sb VI, Te VII, or I VIII. The present paper presents data which establish the $3d^{10}\ {}^1S_0$ terms of Ge V, As VI, Se VII, Br VIII and the $4d^{10}\ {}^1S_0$ terms of Sb VI, Te VII and I VIII.

[1] Ni I. Russell, Phys. Rev. **34**, 821 (1929).
Cu II. Shenstone, Phys. Rev. **28**, 382 (1927); Lang, Phys. Rev. **31**, 773 (1928); Menzies, Proc. Roy. Soc. **A119**, 249 (1928); Kruger, Phys. Rev. **34**, 1122 (1929).
Zn III. Laporte and Lang, Phys. Rev. **30**, 378 (1927).
Ga IV. Mack, Laporte and Lang, Phys. Rev. **31**, 748 (1928).
Ge V. Mack, Laporte and Lang, Phys. Rev. **31**, 748 (1928).
As VI. Pattabhiramiah and Rao, Zeits. f. Physik **53**, 587 (1929); Mack, Phys. Rev. **37**, 470 (1931).

[2] Pd I. Shenstone, Phys. Rev. **36**, 670 (1930).
Ag II. Shenstone, Phys. Rev. **31**, 321 (1928); McLennan and Smith, Proc. Roy. Soc. Canada **20**, 110 (1926).
Cd III. McLennan, McLay and Crawford, Trans. Roy. Soc. Canada **22**, 45 (1928).
Cd III In IV. Gibbs and White, Phys. Rev. **31**, 776 (1928).
Sn V. Gibbs and White, Proc. Nat. Acad. Sci. **14**, 345 (1928).

EXPERIMENTAL

All spectrograms were taken with a 21 ft. grazing incidence (87°) vacuum spectrograph which was built by the Mann Instrument Company. The arrangement of the apparatus was essentially the same as that previously described[3] except for the spark chamber and electrode holders.

In previous work the temperature of the spectrograph did not remain constant during an exposure of 2–3 hours despite careful thermostating of the spectrograph assembly and the room. This temperature change was caused by heat conducted to the spectrograph from the spark chamber during operation.

A new spark chamber was constructed of two thin concentric copper spheres between which water was circulated. Adjustable water-cooled electrode holders were also constructed, as shown in Fig. 1. A one inch extension of these was permitted by 2 inches of sylphon tubing D placed in the outer wall. A running sleeve C was used to eliminate any side play in the electrode holders since this would cause the electrodes to get out of line when an adjustment of the electrodes was made during an exposure. Such maladjustment would cause the electrodes to become badly angled during a run, a condition which shielded the slit from the light of the spark. The running sleeve was machined carefully to 0.001 inch and a thin silver coating was applied to the surfaces to insure free sliding C.

With the water-cooled spark chamber and electrode holders it was possible to keep the

[3] Kruger, Rev. Sci. Inst. **4**, 128 (1933).

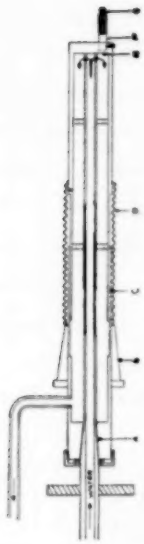

FIG. 1. Assembly of parts for water-cooled electrode holder.

temperature variation of the entire spectrograph to less than $\pm 0.1°C$.

The electrodes were made of 0.25 inch diameter rod F and were inserted into the ends of the electrode holders. The water-cooling stream E then comes within 0.1 inch of the electrode proper.

For best excitation the elements to be excited were made into copper compounds; for example, Cu_2Te, Cu_3As_2, Cu_2Se. These compounds were made by heating in vacuum with an oxyhydrogen flame a mixture of the proper proportions of the elements placed in a quartz tube. Reaction readily takes place leaving sticks of the proper diameter to be used. These sticks G were 0.125 inch in diameter and were pressed into a copper shell and used only in the positive terminal of the spark. Metallic germanium and antimony not compounded with copper were used. Powdered Cu_2Br_2 and Cu_2I_2 were each packed into a copper shell for the excitation of bromine and iodine. The negative terminal electrode was always a pure copper rod.

The length of the vacuum spark varied from 1–2 mm for the various elements. An air-cooled air gap 3 inches long was placed in series with this vacuum gap. The current was supplied by a 4 kenotron bridge set at an output potential of 100 kv. The capacity used was 0.04 mf. The condensers were automatically charged and discharged twice per second, the average spark duration being 0.05 sec.

DATA

Table I gives the intensity, wave-length, wave number and classification of lines observed in Ge V, As VI, Se VII and Br VIII. The wave-lengths were determined by using secondary standard lines[4] of copper. Calculations were made over a range of 5A or less, so that the corrections to be applied to the interpolated wave-lengths rarely exceeded 0.010A.

Ge V[1] $^3D_1^0 - {}^1P_1$ terms have been reported to have a $\Delta\nu$ separation of 1299 cm^{-1} by Mack, Laporte and Lang. The lines involving these terms, as reported in Table I, have a separation of 1298 cm^{-1} which is a satisfactory check for the identification of the lines.

As VI[1] has been reported by Pattabhiramiah and Rao but the present data do not fit their $^3P_1^0$, $^1P_1^0$, $^3D_1^0$ terms, a situation which throws considerable doubt on their classification. Borg and Mack[5] discussed the As VI spectrum at a meeting of the American Physical Society. Their terms[6] with respect to $3d^9\,4s\,{}^3D_3 = 0$ have the following values.

TABLE I. *Lines from transitions into the deepest terms of Ge V, As VI, Se VII and Br VIII.*

Element	Int.	λ	cm^{-1}	Combinations $3d^{10} - 3d^9 4p$
Ge V	5	304.967A	327,904	$^1S_0 - {}^3P_1^0$
	50	295.636	338,254	$^1S_0 - {}^1P_1^0$
	30	294.506	339,552	$^1S_0 - {}^3D_1^0$
As VI	5	232.217	430,632	
	5	226.836	440,847	$^1S_0 - {}^3P_1^0$
	50	221.045	452,397	$^1S_0 - {}^1P_1^0$
	40	219.982	454,583	$^1S_0 - {}^3D_1^0$
Se VII	4	180.220	554,877	
	2	176.781	565,672	$^1S_0 - {}^3P_1^0$
	35	172.920	578,302	$^1S_0 - {}^1P_1^0$
	25	171.965	581,514	$^1S_0 - {}^3D_1^0$
Br VIII	15	139.792	715,349	$^1S_0 - {}^1P_1^0$
	15	138.927	719,802	$^1S_0 - {}^3D_1^0$

[4] Kruger and Cooper, Phys. Rev. **44**, 826 (1933).
[5] Borg and Mack, Phys. Rev. **37**, 470 (1931).
[6] As communicated by letter from Professor Mack to the authors.

$3d^9\,4p\,{}^3D_1^0 = 123{,}390\ \text{cm}^{-1}$,

$3d^9\,4p\,{}^1P_1^0 = 121{,}220$,

$3d^9\,4p\,{}^3P_1^0 = 109{,}710$.

Table II compares the differences between the term values of $3d^9\,4p\,{}^3D_1^0 - {}^1P_1^0 - {}^3P_1^0$ as previously published and the values given by the authors. For Ge V the agreement is good. In the case of As VI the authors' data agree with Borg and Mack's data. However, on account of the greater accuracy of measurement in the region of the spectrum where Mack and his collaborators have taken their data the ${}^3D_1^0$, ${}^1P_1^0$, and ${}^3P_1^0$ term values for Ge V and As VI in Table III correspond to their values.

No data were available on Se VII or Br VIII, so that in these cases it was necessary to rely on intensity relations and predicted $\Delta\nu$ separation from the curves shown in Fig. 2, for the identification of the lines. However, there can be no mistaken identity since the lines given in Table I for Se VII and Br VIII are the only ones which were found on the plates in the predicted region, the intensities are the expected intensities, and the classified lines are the only ones which fit the curves of Fig. 2. It is interesting to note that the ${}^1S_0 - {}^3D_1^0$ transition is almost as strong as the ${}^1S_0 - {}^1P_1^0$ transition and much stronger than ${}^1S_0 - {}^3P_1^0$, a condition which exists throughout the sequence. This means that the coupling is largely *jj* and not L.S.

TABLE II. *Comparison of frequency differences between terms.*

$\Delta\nu$ cm^{-1}	Ge V			As VI			
	Mack, Laporte and Lang	Kruger and Shoupp	Difference in $\Delta\nu$ cm^{-1}	Pattabhiramiah and Rao	Borg and Mack	Kruger and Shoupp	Difference in $\Delta\nu$ cm^{-1}
$3d^9\,4p\,{}^3D_1^0 - 3d^9\,4p\,{}^1P_1^0$	1299	1298	1	1304	2170	2186	16
$3d^9\,4p\,{}^1P_1^0 - 3d^9\,4p\,{}^3P_1^0$	10,400	10,350	50	11,729	11,510	11,550	40
	Te VII			Sb VI			
	Schoepfle published	Schoepfle unpublished	Kruger and Shoupp	Difference $\Delta\nu$ cm^{-1}	Schoepfle published	Schoepfle unpublished	Kruger and Shoupp	Difference $\Delta\nu$ cm^{-1}
$4d^9\,5p\,{}^3D_1^0 - 4d^9\,5p\,{}^1P_1^0$	7247	8556	8530	26	5948	6412	6440	28
$4d^9\,5p\,{}^1P_1^0 - 4d^9\,5p\,{}^3P_1^0$	8842	7533	7502	31	8948	8484	8537	47

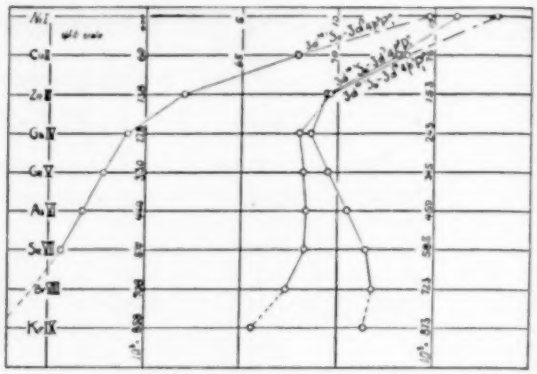

FIG. 2. Displacement of radiated frequencies.

TABLE III. *Term values.*

Element	$3d^{10}\ {}^1S_0$	${}^3P_1^0$	$3d^9\,4p\ {}^1P_1^0$	${}^3D_1^0$
Ge V	753,770	425,915	415,515	414,216
As VI	1,028,800	587,913	576,403	574,233
Se VII	1,341,900	776,228	763,598	760,386
Br VIII	1,692,400	(990,200)	977,051	972,598
Kr IX	(2,080,400)	(1,229,960)	(1,216,790)	(1,211,000)

Table III gives the term values of $3d^{10}\,{}^1S_0$ and $3d^9\,4p\,{}^3P_1^0$, ${}^1P_1^0$, ${}^3D_1^0$. The ${}^1P_1^0$ term values were calculated by assuming $(\nu/R)^{\frac{1}{2}}$ to be a linear function of the atomic number, beyond Ga IV. All other term values have been based on the ${}^1P_1^0$ terms and have been calculated from them by using the data in Table I except for Ge and As as described above.

Fig. 3, a Moseley diagram, shows the relationship between $(\nu/R)^{\frac{1}{2}}$ and atomic number for the sequences.

Table IV gives the new lines of Sb VI, Te VII and I VIII, with their classifications. These wave-lengths were determined in the same way as those in Table I.

Schoepfle[7] has reported the $4d^9\,5p\,{}^3P_1^0$, ${}^1P_1^0$, ${}^3D_1^0$ terms for Sb VI and Te VII, but his published data cannot be fully substantiated by the data in this paper. Schoepfle's ${}^1P_1^0$ terms are incorrectly designated. These data can be made to agree by the classification of the Sb VI line 952.16A as $4d^9\,5s\,{}^3D_2 - 4d^9\,5p\,{}^1P_1^0$ and the Te

[7] Sb VI Te VII. Schoepfle, Phys. Rev. **43**, 742 (1933).

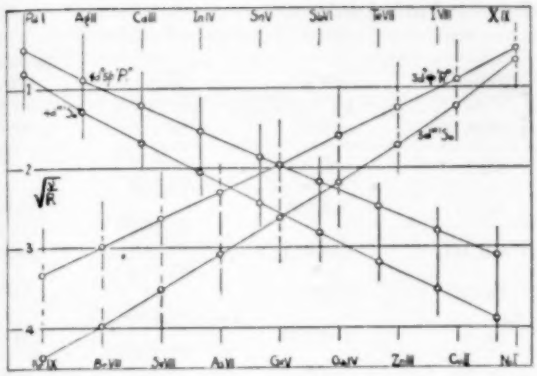

FIG. 3. Moseley diagram.

VII line 845.06A as $4d^9\,5s\,{}^3D_2-4d^9\,5p\,{}^1P_1{}^0$.[8] This gives the Sb VI $^1P_1{}^0$ term the value 107,795 and the Te VII $^1P_1{}^0$ term the value 121,425 on Schoepfle's term scale with $4d^9\,5s\,{}^3D_3=0$. The term difference for these two elements are compared in Table II and again the agreement is satisfactory for the unpublished terms of Schoepfle. As in the case of Ge V and As VI the $^3D_1{}^0$, $^1P_1{}^0$, $^3P_1{}^0$ terms of Sb VI and Te VII listed in Table V correspond with Schoepfle's data.

No data were previously available on I VIII, but again in this case the observed lines have the proper intensity and occur at a wave-length which makes them fit the curves in Fig. 4. The only other iodine line on the plate in this region was at 201.694A which could not be considered since it did not fit the curves in Fig. 4. The relative intensities of the lines in this sequence are analogous to those in the sequence Ni I, Cu II, etc., and check the assigned classification in all cases.

TABLE IV. *Lines from transitions into the deepest terms of Sb VI, Te VII and I VIII.*

Element	Int.	λ	ν cm^{-1}	Combinations $4d^{10}-4d^9\,5p$
Sb VI	15	292.405A	341,991	
	5	291.991	342,476	$^1S_0-{}^3P_1{}^0$
	75	284.890	351,013	$^1S_0-{}^1P_1{}^0$
	60	279.757	357,453	$^1S_0-{}^3D_1{}^0$
Te VII	5	243.880	410,038	
	5	242.248	412,800	
	2	237.541	420,980	
	2	236.460	422,905	$^1S_0-{}^3P_1{}^0$
	40	232.338	430,407	$^1S_0-{}^1P_1{}^0$
	35	227.823	438,937	$^1S_0-{}^3D_1{}^0$
I VIII	5	201.694	495,801	
	1	196.553	508,769	$^1S_0-{}^3P_1{}^0$
	50	194.152	515,060	$^1S_0-{}^1P_1{}^0$
	40	190.158	525,878	$^1S_0-{}^3D_1{}^0$

[8] From Dr. Schoepfle's data as communicated to the authors by him.

TABLE V. *Term values.*

Element	$4d^{10}\,{}^1S_0$	$4d^9\,5p\,{}^3P_1{}^0$	$4d^9\,5p\,{}^1P_1{}^0$	$4d^9\,5p\,{}^3D_1{}^0$
Sb VI	868,140	525,611	517,127	510,715
Te VII	1,106,860	683,986	676,453	667,897
I VIII	1,370,370	861,601	855,310	844,492
Xe IX	(1,659,250)	(1,059,225)	(1,054,440)	(1,041,140)

Table V gives the term values of $4d^{10}\,{}^1S_0$ and $4d^9\,5p\,{}^3P_1{}^0$, $^1P_1{}^0$, $^3D_1{}^0$. These values were calculated in the same way as those of Table III.

Figs. 2 and 4 show a new relationship between displaced frequencies in an isoelectronic sequence. Gibbs and his collaborators have shown that there is a linear displacement toward larger values in the frequency of multiplets from terms due to $3d^9\,4s$ and $3d^9\,4p$ and similar electron configurations. In the present case, where radiation which involves terms due to $3d^{10}$ and $3d^9\,4p$ and similar electron configurations, the displacement is not linear. Table VI gives the wave numbers of lines represented by $3d^{10}\,{}^1S_0$ $3d^9\,4p\,{}^1P_1$ in the isoelectronic sequence Ni I, Cu II, etc., and for $4d^{10}\,{}^1S_0-4d^9\,5p\,{}^1P_1{}^0$ in the sequence Pd I, Ag II, etc., together with the first and second differences between these values. It is observed that the second differences are

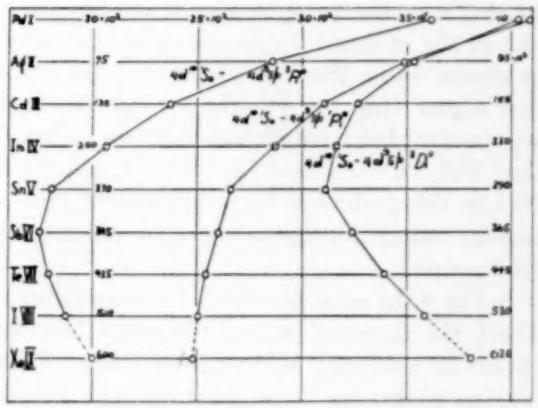

FIG. 4. Displacement of radiated frequencies.

TABLE VI. *Radiated frequencies with first and second differences.*

Elements of sequence	$3d^{10}\,{}^1S_0 - 3d^9\,4p\,{}^1P_1$ cm^{-1}	First difference cm^{-1}	Second difference cm^{-1}	Elements of sequence	$4d^{10}\,{}^1S_0 - 4d^9\,5p\,{}^1P_1$ cm^{-1}	First difference cm^{-1}	Second difference cm^{-1}
Ni I	18,254			Pd I	40,839		
		55,339				49,052	
Cu II	73,593		18,659	Ag II	89,891		7142
		73,998				56,194	
Zn III	147,591		14,488	Cd III	146,085		6423
		88,486				62,617	
Ga IV	236,077		13,691	In IV	208,702		5271
		102,177				67,888	
Ge V	338,254		11,966	Sn V	276,590		6519
		114,143				74,407	
As VI	452,397		11,762	Sb VI	351,013		4987
		125,905				79,394	
Se VII	578,302		11,142	Te VII	430,407		5259
		137,047				84,653	
Br VIII	715,349		(11,200)	I VIII	515,060		(5100)
		(148,247)				(89,753)	
Kr IX	(863,600)			Xe IX	(604,813)		

essentially constant and particularly so after the fifth or sixth stage of ionization has been reached.

From these data the curves in Figs. 2 and 4 were constructed. In Fig. 2, for example, 78,000 cm^{-1} are added to 60,000 cm^{-1}, the value of a point on the scale for Cu II, to get 138,000 cm^{-1} the value of the corresponding point for Zn III. Then 12,000 cm^{-1}, the approximate value of the second differences in Table VI for this sequence, is added to 78,000 cm^{-1} to give 90,000 cm^{-1}, the value added to 138,000 cm^{-1} to get the corresponding point on the graph for Ga IV. Next 12,000 cm^{-1} are added to 90,000 cm^{-1} which gives 102,000 cm^{-1}, the number to be added to 228,000 cm^{-1} in order to obtain the corresponding value 330,000 cm^{-1} for the point on the graph for Ge V. In this way the scale in Fig. 2 is obtained. A plot of the radiated frequencies gives the curves as shown. From them it is seen that, for ionization higher than Ga IV, the second differences are constant but have slightly different values for ${}^1S_0 - {}^3P_1{}^0$, ${}^1S_0 - {}^1P_1{}^0$ and ${}^1S_0 - {}^3D_1{}^0$. The scale for Ni I on this graph has been shifted 6000 cm^{-1} to smaller values for convenience in plotting the Ni I points.

In Fig. 4 the same procedure has been followed. There the constant second difference has been chosen as 5000 cm^{-1} so that after adding 55,000 cm^{-1} to 20,000 cm^{-1} (the point on the Pd I axis) to get 75,000 cm^{-1} for the point on the Ag II axis, 5000 cm^{-1} are added to 55,000 cm^{-1} to give 60,000 cm^{-1} the numbers to be added to 75,000 cm^{-1} to get the value 135,000 cm^{-1} for Cd III, etc. In this case the actual second differences are not as constant as those for Ni I, Cu II, etc., but are varying so slowly that it is possible to extrapolate the curves accurately to predict the corresponding radiation in Xe IX. Such an extrapolation has been made for both Xe IX and Kr IX and these values are included in all tables and curves. A study of the data in Table VI indicates that the extrapolated values should not be in error by more than ± 400 cm^{-1}, a variation which is in agreement with the check obtained between predicted and observed values during the process of following the observed lines through the sequences.

Tables VII and VIII give the ionization potentials for the isoelectronic sequence Ni I, Cu II, etc., and Pd I, Ag II, etc., and the first and second differences between the ionization potentials. Again it has been found that the second differences are essentially constant. From these data it is possible to derive an empirical formula from which the ionization potentials can be calculated. It is

$$I_n = I_1 + (n-1)(D_1 + [(n-2)/2]D_2),$$

where I_n is the ionization potential and n is stage of excitation which takes on the values one for Ni I or Pd I, two for Cu II or Ag II, etc.

TABLE VII. *Ionization potentials in the isoelectronic sequence Ni I, Cu II, etc.*

Element	$3d^{10}\,{}^1S_0$ cm^{-1}	Ionization potential in volts	First difference in volts	Second difference in volts	Ionization potential as calc. fr. formula
Ni I	46,850	5.8			4.4 v.
			14.4		
Cu II	163,634	20.2		4.9	19.5
			19.3		
Zn III	320,000	39.5		5.0	39.3
			24.3		
Ga IV	517,000	63.8		4.9	63.8
			29.2		
Ge V	753,770	93.0		4.7	93.0
			33.9		
As VI	1,028,800	126.9		4.7	126.9
			38.6		
Se VII	1,341,900	165.5		4.7	165.5
			43.3		
Br VIII	1,692,400	208.8		(4.5)	208.8
			(47.8)		
Kr IX	(2,080,400)	(256.6)			256.8

$$I_n = I_1 + (n-1)(D_1 + [(n-2)/2]D_2)$$
$$I_1 = 4.4;\quad D_1 = 15.1;\quad D_2 = 4.7$$

TABLE VIII. *Ionization potentials in the isoelectronic sequence Pd I, Ag II, etc.*

Element	$4d^{10}\,{}^1S_0$ cm^{-1}	Ionization potential in volts	First difference in volts	Second difference in volts	Ionization potential as calc. fr. formula
Pd I	67,236	8.3			8.1 v.
			13.6		
Ag II	177,164	21.9		3.5	21.5
			16.1		
Cd III	308,318	38.0		3.7	38.1
			19.8		
In IV	468,214	57.8		3.1	57.9
			22.9		
Sn V	654,527	80.7		3.5	80.9
			26.4		
Sb VI	868,140	107.1		3.0	107.1
			29.4		
Te VII	1,106,860	136.5		3.2	136.5
			32.6		
I VIII	1,370,370	169.1		3.0	169.1
			35.6		
Xe IX	(1,659,250)	(204.7)			204.9

$$I_n = I_1 + (n-1)(D_1 + [(n-2)/2]D_2)$$
$$I_1 = 8.1;\quad D_1 = 13.4;\quad D_2 = 3.2$$

I_1 corresponds roughly to the ionization potential of the first member of the sequence and has a value of 4.4 e.v. for the Ni I sequence and 8.1 e.v. for the Pd I sequence.

D_1 is approximately the first, first difference. It has a value of 15.1 for the Ni I sequence and 13.4 for the Pd I sequence.

D_2 is the value of the constant second difference and has been chosen as 4.7 for the Ni I sequence and 3.2 for the Pd I sequence.

The last columns of Tables VII and VIII give the values of ionization potentials as calculated from the above formula. The agreement with the experimental values is surprisingly good and is best for high stages of ionization. For this reason it seems that the calculation of ionization potentials for ions from Kr IX to Ag XX and Xe IX to Tb XX should not be in error by more than a few percent.

It is hoped that the extrapolation of the formula can be checked by the completion of the work now in progress on Rb X, Sr XI, Cs X and Ba XI.

It is to be regretted that the lack of a vacuum spectrograph which covers the range 600A to 2000A makes it impossible for the authors to obtain data involving the $d^9p - d^9s$ terms in these sequences. It is hoped that another laboratory having the proper facilities will undertake that study.

Note added in proof:

The following is a list of known As VI levels from Borg and Mack's data which they have asked the authors to add to this paper. The last digit of the term values has been rounded to the nearest zero.

$3d^9\,4s$	$^3D_3$	0 cm^{-1}	$3d^9\,4p$	$^3F_3$	112,620 cm^{-1}?
	$^3D_2$	2,050		$^3P_0$	112,880 ?
	$^3D_1$	5,690		$^3D_2$	118,280
	$^1D_2$	9,050		$^3D_3$	118,290
$3d^9\,4p$	$^3P_2$	104,250		$^1F_3$	120,620
	$^3F_3$	108,730		$^1P_1$	121,220
	$^3P_1$	109,710		$^3D_1$	123,390
	$^3F_4$	111,890		$^1D_2$	124,380

Quadrupole Lines in the *K*-Series of Ruthenium

E. WILHELMY,* *Ryerson Physical Laboratory, University of Chicago*

(Received May 22, 1934)

The Ru $K\beta_4(K-N_{IV}N_V)$ and $K\beta_5(K-M_{IV}M_V)$ lines have been observed with a double crystal spectrometer. The wave-lengths are 559.74 and 566.68 X.U., respectively. $K\beta_5$ appears to be a doublet, the weaker component lying at the long wave-length side. The doublet separation of 0.15 X.U. is within the experimental error in accordance with the $M_{IV}-M_V$ difference. The width of the single components of $K\beta_5$ is smaller than the width of $K\alpha_1$, i.e., <11 volts. $K\beta_4$ is considerably broader, 28 volts. The intensity ratios are $K\beta_4 : K\alpha_1 = 1 : 160$, $K\beta_5 : K\alpha_1 = 1 : 400$. Also a very faint line $K\beta_6$ has been observed the intensity of which is 1 : 2000 of the intensity of $K\alpha_1$. The wave-length of $K\beta_6$ is 558 X.U. It cannot be explained by single electron transitions between known Ru levels.

INTRODUCTION

IN recent years several investigators have reported the observation of very weak lines in the *K*-series of many elements.[1] Two of these new lines, $K\beta_4$ and $K\beta_5$, have been interpreted as quadrupole lines originating in the transitions $K-N_{IV}N_V$ and $K-M_{IV}M_V$. Mo $K\beta_4$ has been differently interpreted by Duane[2] and by DuMond and A. Hoyt.[3] Finding a rather broad line which they called the δ-band they regarded this radiation as being due to conductivity electrons falling into the *K*-level. Duane suggested an additional $K-O$ transition. The width of the δ-band has been estimated by DuMond and Hoyt to be about 16 volts. Carlsson[4] using the photographic method gives a half-width of 7 volts. No data have been published about the width of the $K\beta_5$ line. The only remark about the shape of this line was made by P. A. Ross[5] who found $K\beta_5$ in Pd wider than in Mo and Rh and unsymmetrical.

After the present investigation was finished Ingelstam and Ray[6] published the observation of Ru $K\beta_4$, $K\beta_5$, $K\beta_6$, $K\beta_7$ and η. It is the measurement of the natural width and intensities of some of these lines observed by a double crystal spectrometer that is reported in the present paper.

APPARATUS

The type of double crystal spectrometer which was used in this investigation has been described by Allison and Williams, the specific instrument by Allison.[7] A small part of the surface of the calcite crystals was selected which gave the best resolving power (checked by the measurement of the width of Ru $K\alpha_1$, smallest value 20″). The ionization chamber of the spectrometer was filled with methyl bromide. The electrometer was of the Compton type and operated at a sensitivity of 1000 mm/volt.

Because the lines to be observed are extremely faint, a very constant source of x-rays was required. A high power x-ray tube as described by Dershem[8] was provided with a ruthenium target and connected with a special high tension outfit. This outfit consisted in a high tension transformer, a kenotron and a condenser (0.1μf) in a half-wave rectification scheme. The primary power was produced by a 540 cycle 5 kva generator driven by an 8.5 hp. synchronous motor. The voltage was measured by an electrostatic

* Fellow of the Rockefeller Foundation.

[1] A. Leide, Dissert. Lund (1925) and Compt. Rend. **180**, 1202 (1925); A. Larsson, Phil. Mag. (7), **3**, 1136 (1927); S. Idei, Scient. Rep. Tokohu Imp. Univ. **19**, 641 (1930); H. Beuthe, Zeits. f. Physik **60**, 603 (1930); I. W. M. DuMond and A. Hoyt, Phys. Rev. **38**, 839 (1931); Y. Cauchois, Compt. Rend. **194**, 1479 (1932); P. A. Ross, Phys. Rev. **39**, 536 (1932); **39**, 798 (1932). W. Duane, Proc. Nat. Acad. Sci. **18**, 63 (1932); P. A. Ross and P. Kirkpatrick, Phys. Rev. **43**, 1036 (1933); E. Carlsson, Zeits. f. Physik **80**, 604 (1933); **84**, 119 (1933); E. Carlsson Ingelstam, Zeits. f. Physik **87**, 283 (1934); E. C'son Ingelstam and B. B. Ray, Zeits. f. Physik **88**, 218 (1934).

[2] W. Duane, Proc. Nat. Acad. Sci. **18**, 63 (1932).

[3] I. W. M. DuMond and A. Hoyt, Phys. Rev. **38**, 839 (1931).

[4] E. Carlsson, Zeits. f. Physik **80**, 604 (1933).

[5] P. A. Ross, Phys. Rev. **39**, 536 (1932).

[6] E. C'son Ingelstam and B. B. Ray, Zeits. f. Physik **88**, 218 (1934).

[7] Allison and Williams, J. O. S. A. and R. S. I. **18**, 473 (1929); S. K. Allison, Phys. Rev. **41**, 1 (1932).

[8] E. Dershem, Phys. Rev. (1934). In print.

high tension voltmeter. The filament current was smoothed by a stabilizer. By these means both current and high tension could be kept constant within a small fraction of a percent. The final readings were taken at 42.5 kv and 10 m.a.

Results

Fig. 1 represents a rocking curve which shows Ru $K\beta_2$ with $K\beta_4$ at its short wave-length side. The solid points are measurements, the dotted

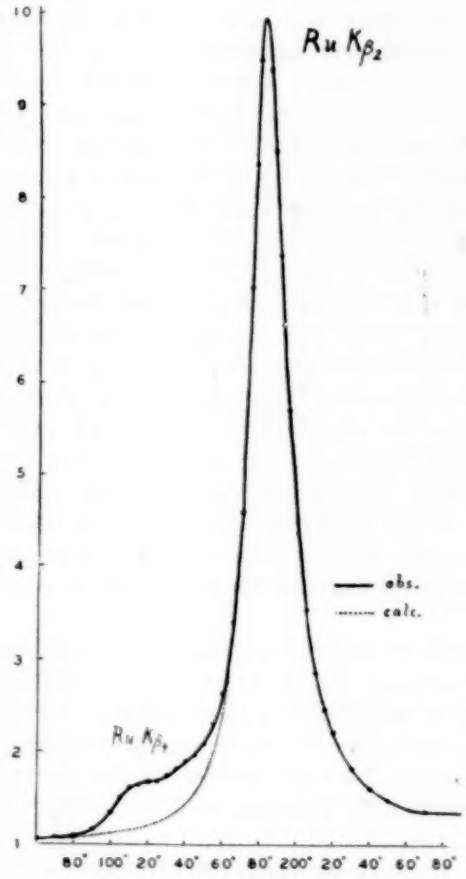

FIG. 1. Ru $K\beta_4$ and $K\beta_2$.

curve was computed by A. Hoyt's[9] equation $y=a/[1+(x/w)^2]$, where y is the ordinate corresponding to a distance x along the abscissa from the center of the line; a is the peak ordinate, w the half-width at half-maximum. This equation fits very well the observed shape of x-ray lines in this wave-length region.

[9] A. Hoyt, Phys. Rev. **40**, 477 (1932).

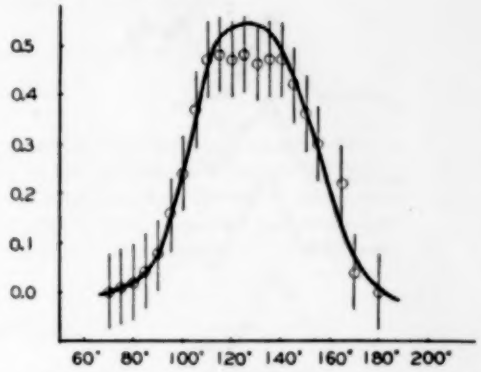

FIG. 2. Ru $K\beta_4$. The vertical lines represent the limits of error.

Plotting the difference between the two curves against Bragg's angle one obtains $K\beta_4$ isolated, Fig. 2. Five rocking curves of this line gave full widths at half-maximum of 56, 51, 36, 56, 47 seconds with an average value of 49.2 seconds or 0.71 X.U. or 28 ± 8 volts. This is almost twice the width which has been found for Mo $K\beta_4$ by DuMond and Hoyt.[3]

The wave-length of $K\beta_4$ was measured in reference to $K\beta_1$ and $K\beta_2$. The values are given in Table I.

TABLE I. *Wave-lengths and ν/R values of ruthenium K lines.*

	λ_W	$\lambda_{\text{Ing. and Ray}}$	ν/R_W	$\nu/R_{\text{I. and R.}}$	$\nu/R_{\text{calc.}}$
$K\beta_4$	559.74 X.U.	559.53 X.U.	1628.0	1628.63	1628.9
$K\beta_2$	566.68	566.55	1608.04	1608.45	1608.45
$K\beta_3$	566.83	—	1607.73	—	1608.14
$K\beta_4$	558	558			

The intensity of Ru $K\beta_4$ (area of curves) is 1/9 of the intensity of $K\beta_2$. From Williams[10] measurements of the relative intensities of the Ru K-lines one finds the ratio $K\beta_4 : K\alpha_1 = 1/160$.

Fig. 3 represents the rocking curves of $K\beta_3$. This line appears not only to be unsymmetrical but also to consist of two components, the weaker one lying at the long wave-length side. The separation of the components amounts to about 10 seconds or 0.15 X.U. whereas the term difference $M_{IV}-M_V$ leads to 0.12 X.U. The resolving power being 9300 the agreement is as good as one can expect. The wave-lengths of the lines are given in Table I. The relative in-

[10] J. H. Williams, Phys. Rev. **44**, 146 (1933).

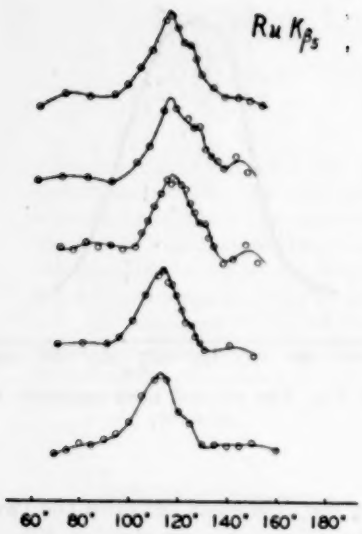

FIG. 3. Ru $K\beta_5$.

tensities of the components can be calculated from the statistical weights of M_V and M_{IV}. The j-values being 5/2 and 3/2, respectively, the intensity ratio is expected to be 3/2, which is consistent with the observation. The intensity of both lines together is 1/400 of $K\alpha_1$'s intensity. Supposing the relative intensities are 3 : 2 one gets for the single lines the ratios 1/670 and 1/1000 of $K\alpha_1$.

The width of both $K\beta_5$ components together is 19 seconds or 0.28 X.U. or 11 ($\pm$1.4) volts. The widths of $K\beta_2$ and $K\alpha_1$ are 24 seconds, 0.35 X.U., 14 volts and 20.5 seconds, 0.30 X.U., 11 volts. Consequently the single components of $K\beta_5$ must be narrower than $K\alpha_1$ i.e., 11 volts. They are the sharpest lines found so far in the ruthenium K-series. It might be mentioned that one gets very nearly the observed curve of $K\beta_5$ if one assumes the intensity as being 3/2, the wave-length difference 0.12 X.U. and the width 14 seconds or 8 volts for each component.

A very faint line was found about midway between $K\beta_5$ and $K\beta_1$ at 558 X.U. This line, $K\beta_6$, has also been found by Ingelstam and Ray.[11] Its intensity amounts to 1/5–1/4 of the $K\beta_5$ doublet or 1/2000 of $K\alpha_1$.

DISCUSSION

The interpretation of $K\beta_4$ and $K\beta_5$ as being quadrupole transitions $K-N_{IV}N_V$ and $K-M_{IV}M_V$, respectively, is very well proved by the agreement between the observed and the calculated frequencies. Furthermore the doublet structure which has been found in the case of $K\beta_5$ corresponds quantitatively to the level diagram. The small width of the $K\beta_5$ lines can be explained classically by the small damping of quadrupole radiation. In the quantum theory it means that the lifetime of the state is a long one.

Now the question rises why $K\beta_4$ is so broad. Relative measurements of the width of lines in the L-series of Mo, Pd, Ag by Jönsson[12] have shown that $L\beta_2$ ($L_{III}-N_V$) is much broader than $L\alpha_1$ ($L_{III}-M_V$). Thus the large width is a general property of lines with the N_V level as final state in these elements. This might be due to the fact that in the elements Y (39) to Rh (45) the electron population of the $N_{IV,V}$ level is incomplete. Also an influence of the potential field of the crystal might be exerted upon the outer x-ray levels of these elements (de Kronig[13]).

No single electron transition can account for $K\beta_6$.

I wish to express my thanks to Professors A. H. Compton and S. K. Allison for the opportunity of working as a guest in Ryerson Physical Laboratory and for many helpful criticisms and suggestions. I am also indebted to the Rockefeller Foundation for granting me a fellowship.

[11] E. C'son Ingelstam and B. B. Ray, Zeits. f. Physik **88**, 218 (1934).
[12] A. Jönsson, Zeits. f. Physik **46**, 383 (1928).
[13] L. de Kronig, Zeits. f. Physik **70**, 317 (1931).

Magnetic Properties of Rare Earth Salts

E. H. WILLIAMS, *Department of Physics, University of Illinois*

(Received May 28, 1934)

Measurements of the paramagnetic susceptibility of certain rare earth salts as a function of temperature yield the surprising result that the plot of the reciprocal of the susceptibility, $1/\chi$, against the absolute temperature, T, consists of a broken line. However, when very careful drying was made, the locus, in the case of $Gd_2(SO_4)_3 \cdot 8H_2O$, became a single straight line passing through the origin. The broken line phenomenon was observed for Gd Cl_3, Nd $Cl_3 \cdot 6H_2O$ and $Gd_2(SO_4)_3 \cdot 8H_2O$.

MAGNETIC susceptibility measurements are subject to many errors as is evident from the results obtained for the same substance by different observers. Not only do the inherent errors due to calibration of the apparatus and observations enter in but also the purity of the substance. It has been shown that slight impurities have a marked effect on the magnetic properties of substances and it is this factor, no doubt, that causes many of the discrepancies.

The author recently, in measuring the magnetic susceptibility of some rare earth salts, observed a phenomenon that is not only interesting in itself but may account for some of the discrepancies in the values of the magnetic susceptibilities of paramagnetic substances. It was found that when the substances were prepared in the usual way the plot of the reciprocal of the susceptibility, $1/\chi$, against the absolute temperature, T, gave a broken line in the case of a number of rare earth salts.

The first substance in which this unexpected result was observed was Gd Cl_3. A very large number of observations of the value of χ were made between room temperature and a temperature of 92°K. When $1/\chi$ was plotted against T two distinct straight lines were obtained (see Fig. 1). A third straight line appeared to exist in the neighborhood of room temperature but this was not so well defined. This broken line will give for Δ, in the relation $\chi = \text{const}/(T-\Delta)$, different values depending on the temperature at which the calculation is made. Starting at lower temperatures the first straight line extends from about 92°K to 168°K. The value of Δ for this range is -1 for the curve drawn but the error due to extrapolation and observation may easily be ± 1. The portion of the curve from 168°K to 255°K gives a straight line for which Δ is 24 ± 2. A second sample of Gd Cl_3 gave results in close agreement with the above.

It was suggested by Professor J. H. Van Vleck that the magnetic susceptibility of $Gd_2(SO_4)_3 \cdot 8H_2O$ be determined as a check on results obtained. Careful measurements have been made on this substance at very low temperatures in the Leiden laboratories and it has been found to follow Curie's law almost perfectly.

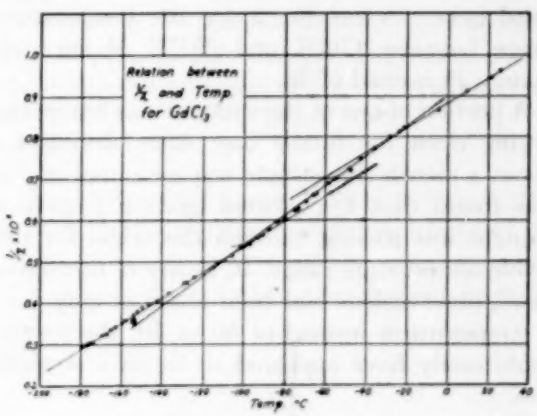

FIG. 1.

Three samples of $Gd_2(SO_4)_3 \cdot 8H_2O$ were prepared. After the crystals had grown to a good size they were dried in an oven at between 100°C and 110°C for 16 or 17 hours. They were then measured for magnetic susceptibility and the results, in all three cases, obtained by plotting $1/\chi$ against T, were very similar to those obtained for Gd Cl_3. The result for one of the samples is shown in Fig. 2. In each case the value of Δ for that portion of the curve lying between 92°K and 170°K was 0 ± 1. For the

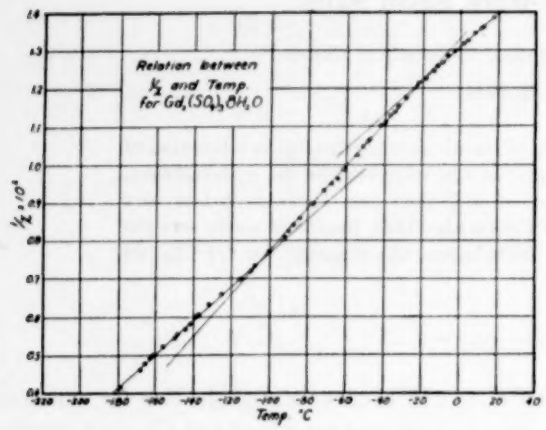

FIG. 2.

portion from 170°K to 255°K the value of Δ was 36 ± 3.

Three more samples of $Gd_2(SO_4)_3\cdot 8H_2O$ were now prepared by a somewhat different process and again dried 16 or 17 hours in the drying oven. Two of these samples gave results almost identical with those of the previous three but the third gave a value for Δ for the temperature range between 170°K and 255°K of approximately 20 instead of 36.

A portion of one of the samples was left in the drying oven for future use. After drying for about a month this sample was measured and it was found that $1/\chi$ plotted against T gave a straight line passing through the origin for the whole temperature range. If, in any of the above cases, observations had been made at only 6 or 7 temperatures instead of 60 or 70, the results could easily have appeared to lie on a straight line.

The question naturally arose as to the quantity of water in the two samples—the one giving a broken line and the other a straight line. Does excessive drying reduce the water in the hydrate *to* $8H_2O$ or *below* $8H_2O$? Careful analysis showed the former to be the case. Whether the water was occluded between the crystals or was present as a higher hydrate, or both, is difficult to say.

The variation of χ with temperature was studied by Freed[1] for hydrated samarium sulphate. He found that "experimental results show that Sm^{+++} does not have a constant Curie 'constant'." Freed attributed the variation to a mixture of two or more electronic isomers whose relative concentration varies with the temperature. In the present case where the change is quite abrupt it does not seem possible to apply this explanation for the change in Δ. Thus far it has not been possible to make magnetic measurements of thoroughly dried $GdCl_3$. This will be done as soon as a new sample can be prepared. It will be interesting to see whether a straight line will be found in this case. One sample only of $NdCl_3\cdot 6H_2O$ was measured and this gave results similar to the hydrous gadolinium sulphate.

It is difficult to explain how the presence of water can cause the sudden break in the rate of change of magnetic susceptibility found in the above substances in the neighborhood of 170°K. In the case of each of the samples of $Gd_2(SO_4)_3\cdot 8H_2O$ the effective Bohr magneton number for that portion of the plot below 170°K is in the neighborhood of 8, the values of four of the samples being 8.14, 8.18, 8.15, and 8.21. These values agree very well with those of Cabrera and Meyer quoted by Van Vleck.[2] Above 170°K the effective Bohr magneton number depends on the dryness of the sample. In calculating the effective Bohr magneton number the values of the susceptibilities of SO_4 and H_2O per mole were taken the same as those used by Freed, namely, -37×0^{-6} for SO_4 and -13×10^{-6} for H_2O and the molar Bohr magneton number value used was 5580.

In conclusion the author wishes to acknowledge his indebtedness to Professor B. S. Hopkins and Dr. L. L. Quill who have prepared all the rare earth substances and made the chemical analysis.

[1] Freed, J. Am. Chem. Soc. **52**, 2702 (1930).
[2] J. H. Van Vleck, *Electrical and Magnetic Susceptibilities*, p. 243.

Non-Orthogonal Wave Functions and Ferromagnetism

D. R. INGLIS, *Ohio State University*

(Received* May 21, 1934)

Close consideration of the influence of non-orthogonality of the electronic wave functions in a crystal shows that because of the large number of terms arising from the possible permutations of electrons, the usual procedure involving the neglect of most of the terms arising from this lack of orthogonality may be seriously in error. The dependence of the relative energies of the states of low and high multiplicity on this factor is discussed and exemplified in the cases of some simple molecular models.

INTRODUCTION

ALL treatments[1] of the problem of the existence of ferromagnetism from the atomic point of view have been guilty of the convenient but otherwise unjustified neglect of the lack of orthogonality of the electronic wave functions of two neighboring atoms in a crystal. The terms in question are negligible in the limit of extreme dilation. Though suggestive, it is not entirely satisfactory to explain only the weak ferromagnetism of an ideally distended crystal (and no more has been done), because ferromagnetism does not exist in the opposite extreme of high concentration,[2] due to the electrons' zero-point energy.

It is here suggested that the neglected terms have probably much more influence on the result of the first-order calculation than do the terms which have been given as a "criterion for ferromagnetism." The influence of the neglected terms is expected to appear not only in the existence of ferromagnetism and the magnitude of the "exchange coupling," but perhaps also in saturation and paramagnetic magneton numbers. It is further suggested that a consistent manner of neglecting non-orthogonality does not lead to the usual exchange integral as the criterion, but rather shows, as one should expect, that the inter-nuclear terms would have no influence on the orientation of the electron spins.

I

In calculating the first-order energies, the terms due to non-orthogonality may not be tacitly neglected because of their enormous number, arising from the large number of permutations of the electron coordinates in even a small crystal.

This may be seen by examining the elements of the secular determinant. It is derived from the Hamiltonian

$$H=-\sum_{\alpha}\Delta^{\alpha}+\sum_{\alpha<\beta}V_{\alpha\beta}+\sum_{ab}V_{a}{}^{b}+\sum_{a<b}V^{ab},$$

where

$$\Delta^{a}=(h^{2}/8\pi^{2}m)(\partial^{2}/\partial x_{a}{}^{2}+\partial^{2}/\partial y_{a}{}^{2}+\partial^{2}/\partial z_{a}{}^{2}),$$

Greek letters refer to the atomic cores, Roman letters to electrons and the V's to mutual electrostatic energies of two particles. This in the wave equation

$$(H-NE_{0}-\epsilon)\sum_{m_{\alpha}m_{\beta}\cdots}c_{m_{\alpha}m_{\beta}\ldots m_{\nu}}\sum_{P}(-)^{P}P\psi_{m_{\alpha}}{}^{a}\psi_{m_{\beta}}{}^{b}\cdots\psi_{m_{\nu}}{}^{n}=0,$$

where permutation operator P acts on the atomic coordinates α, $\beta\cdots\nu$ and P in the exponent is the order of P, and where $\psi_{m_{\alpha}}{}^{a}=\psi_{\alpha}{}^{a}\delta(m_{s_{a}}/\sigma_{a})=\psi(x_{a}{}^{a}y_{a}{}^{a}z_{a}{}^{a})\delta(m_{s_{a}}/\sigma_{a})$ satisfies the atomic wave equation $(\Delta^{a}-V_{a}{}^{a}+E_{0})\psi_{m_{a}}{}^{a}=0$, gives for the first order energies ϵ of the states having the spin

---

* From Mexico City, as a Letter to the Editor.

[1] W. Heisenberg, Zeits. f. Physik **49**, 619 (1928); *Sommerfeld Festschrift* 114; D. R. Inglis, Phys. Rev. **42**, 442 (1932); J. C. Slater, Phys. Rev. **35**, 509 (1930); F. Bloch, Zeits. f. Physik **61**, 206 (1930); **74**, 295 (1932); H. Bethe, Zeits. f. Physik **71**, 205 (1931); D. R. Inglis, Phys. Rev. **45**, 128 (1934) (Abstract—further details to appear soon).

[2] F. Bloch, Zeits. f. Physik **57**, 545 (1930).

projection $M=\Sigma m_\theta$ the crystalline secular determinant:

$$\left|\{\sum_P(-)^P\sum_{\alpha\cdots}\int\bar{\psi}^{\alpha}{}_{m_\alpha}\cdots\bar{\psi}^{\nu}{}_{m_\nu}(\sum_{\alpha<\beta}V_{\alpha\beta}-\epsilon+\sum_{\alpha,\beta}V_\alpha{}^b-\sum_\alpha V_{P\alpha}{}^a+\sum_{a<b}V^{ab})P\psi_{m_\alpha}{}^a\cdots\psi_{m_\nu}{}^\nu\}\right|=0. \quad (1)$$

The determinant is here written with only one sample element. The rows are characterized by choices of $m_\alpha\cdots m_\nu$ and the columns by choices of $m_\alpha'\cdots m_\nu'$ each m_θ being $\pm\frac{1}{2}$ and subject to the condition $\Sigma m_\theta=M$. (Volume elements $dx^k dy^k dz^k$ are unwritten.)

Here, as in molecules but contrary to the case in many atomic problems, the electronic wave functions are not orthogonal. The integral

$$S=\int\bar{\psi}_\kappa{}^k\psi_\lambda{}^k$$

is less than one but distinctly greater than zero. (Here and hereafter, λ is a neighbor of κ.)

A term of (1) is in general large if the set $m_\alpha\cdots m_\nu$ differs from $m_\alpha'\cdots m_\nu'$ not at all (diagonal term), or by the interchange of the sign of $m_\gamma m_\delta$ of a pair of neighbors $\gamma\delta$, whereas a term is small if the sets differ by interchanges of many pairs of neighbors, or of a distant pair. Excepting the case $M=n/2$, even the largest non-diagonal terms of the determinant are of the order of nz times as numerous as the diagonal terms.

Even if we neglect that complication, and examine only a diagonal term, we see that we are not justified in tacitly neglecting non-orthogonality. In a diagonal term of (1), with $m_\alpha'\cdots m_\nu'=m_\alpha\cdots m_\nu$ we find in making the summation over P that the multiplier of $(\Sigma V_{\alpha\beta}-\epsilon)$ has as first term 1 due to the identical permutation $P=1$. Added to this are $nZ/2$ terms due to permutations which differ from $P=1$ only by exchange of two neighbors $\gamma\delta$ ($Z=$number of neighbors of each atom). For such a permutation, the integration (and the accompanying summation over spins σ) gives $-S^2$ if $m_\gamma=m_\delta$, or 0 if $m_\gamma=-m_\delta$. The fraction of pairs of m's which are equal to each other is

$$f(n_+)=[n_+(n_+-1)+n_-(n_--1)]/n(n-1),$$

where n_+ is the number of $m_\theta=+\frac{1}{2}$ and n_- is the number of $m_\theta=-\frac{1}{2}$ so that $\frac{1}{2}n_+-\frac{1}{2}n_-=M$. Hence we get as the term in S^2: $-\frac{1}{2}nZf(n_+)S^2$. By a similar process, neglecting overlapping except that of wave functions of nearest neighbors, we get the approximate expression for a diagonal term of (1):

$$(\sum_{\alpha<\beta}V_{\alpha\beta}-\epsilon)\{1-(n/2)f(n_+)zS^2+\tfrac{1}{4}n(n-2)[f(n_+)z]^2S^4-\cdots\} \quad (2.1)$$

$$+\sum_{\alpha\neq k}n\left\{\int\bar{\psi}_\alpha{}^kV_\alpha{}^k\psi_\alpha{}^k-f(n_+)zS\int\bar{\psi}_\alpha{}^kV_\alpha{}^k\psi_\lambda{}^k\right\}\{1-\tfrac{1}{2}(n-2)f(n_+)zS^2+\cdots\} \quad (2.2)$$

$$+\tfrac{1}{2}nz\left\{\int\bar{\psi}_\alpha{}^k\bar{\psi}_\lambda{}^lV^{kl}\psi_\alpha{}^k\psi_\lambda{}^l-f(n_+)\int\bar{\psi}_\alpha{}^k\bar{\psi}_\lambda{}^lV^{kl}\psi_\lambda{}^k\psi_\alpha{}^l\right\}\{1-(\tfrac{1}{2}(n-4)z+1)f(n_+)zS^2+\cdots\}. \quad (2.3)$$

The calculations which have as yet been made[1] tacitly neglect terms in S^2, considering them small in comparison with the terms without S. In actual crystals, S is of the order of magnitude of $1/10$. Taking $n=10^5$, $z=10$, we see that the S^2 term, the second term in the first line of (2), amounts to over 10^3 times as much as the first term, and the terms in S^4, 10^7 times as much as the first term. Even if S were only 10^{-3} (probably making the Curie point below 10°K), the higher terms would hardly be negligible compared to the first. The ratios of the three series in (2) demands investigation, ere we may claim to have explained the order of magnitude of the Weiss "internal field" from the atomic viewpoint. The alternation of signs leaves the possibility that the higher powers of S may prove to be negligible.

II

In our problem, it is important to know how the energies ϵ (or their centers of gravity) vary with n_+ and n_- (that is, with M). Thus, in the usual "approximation," the nature of the multiplier of $f(n_+)$ in (2) [and in the non-diagonal terms] appears as the "criterion for ferromagnetism." This multiplier is

$$\tfrac{1}{2}nzS^2(\sum V_{\alpha\beta}-\epsilon)+nzS\int \bar{\psi}_\epsilon{}^k \sum_{\alpha\neq k} V_\alpha{}^k\psi_\lambda{}^k+\sum_{k>l}\int \bar{\psi}_\epsilon{}^k\bar{\psi}_\lambda{}^l V^{kl}\psi_\lambda{}^k\psi_\epsilon{}^l, \tag{3.1}$$

which takes a form similar to an "exchange integral":

$$\tfrac{1}{2}nz\int \bar{\psi}_\epsilon{}^k\bar{\psi}_\lambda{}^l\{(\sum V_{\alpha\beta}-\epsilon)+2V_{\lambda k}+V^{kl}\}\psi_\lambda{}^k\psi_\epsilon{}^l \tag{3.2}$$

if we neglect integrals of electronic potentials involving more than two neighboring atoms.

It has been customary to carry along, rather inconsistently, only one term in S^2, namely, the term $V_{\epsilon\lambda}$ in (3.2), neglecting $(\frac{1}{2}nz-1)$ equal terms $V_{\alpha\beta}$ and ϵ. This has given the "exchange integral" familiar from the problem of the hydrogen molecule:

$$\int \bar{\psi}_\epsilon{}^k\bar{\psi}_\lambda{}^l(V_{\epsilon\lambda}+2V_\lambda{}^k+V^{kl})\psi_\lambda{}^k\psi_\epsilon{}^l. \tag{3.3}$$

It is more consistent to neglect $V_{\epsilon\lambda}$ as well. We thus have the revised "exchange integral":

$$\int \bar{\psi}_\epsilon{}^k\bar{\psi}_\lambda{}^l(2V_\lambda{}^k+e^2/r_{kl})\psi_\lambda{}^k\psi_\epsilon{}^l, \tag{3.4}$$

of which only a positive value may lead to a ferromagnetic result in this convenient "approximation." Here ferromagnetism should arise from the tendency of the Pauli exclusion principle to rarefy the charge distribution of states of high multiplicity in the space between adjacent nuclei. If this detracts less from the integrated negative energy $2V_\lambda{}^k$ than from the positive energy e^2/r_{kl}, the states of high multiplicity should have low energy and there should be ferromagnetism. It is thus more satisfactory that the mutual energy $V_{\epsilon\lambda}$ of the fixed nuclei does not enter (3.4).

III

Pending a satisfactory solution of the secular problem for the crystal, we may get some indication of the nature of the effects of non-orthogonality by the study of the effects in molecules, and their tendencies as we increase the number of atoms. We shall confine our comparison to three molecules composed of equidistant and similar atoms and one outer s-electron per atom: a diatomic molecule, a triatomic molecule forming an equilateral triangle, and a tetratomic molecule which forms an equilateral tetrahedron. In these cases, the possible permutations of the electrons are few enough that we may neglect higher powers of S in comparison with low powers.

In molecules, the analog of ferromagnetism is a state of high multiplicity with lower energy than has each state of low multiplicity. The familiar solution[3] for the singlet and triplet energies, ${}^1\epsilon=\epsilon_+$ and ${}^3\epsilon=\epsilon_-$, of the hydrogenic molecule

$$\epsilon_\pm=\int \bar{\psi}_\alpha{}^a\bar{\psi}_\beta{}^b(V_{\alpha\beta}+V_\beta{}^a+V_\alpha{}^b+V^{ab})(\psi_\alpha{}^a\psi_\beta{}^b\pm\psi_\beta{}^a\psi_\alpha{}^b)/(1\pm S^2) \tag{4}$$

gives, to the degree of accuracy S^2, the triplet-singlet separation:

$${}^3\epsilon-{}^1\epsilon=-2\left\{\int \bar{\psi}_\alpha{}^a\bar{\psi}_\beta{}^b(2V_\beta{}^a+V^{ab})\psi_\beta{}^a\psi_\alpha{}^b-S^2\int \bar{\psi}_\alpha{}^a\bar{\psi}_\beta{}^b(2V_\beta{}^a+V^{ab})\psi_\alpha{}^a\psi_\beta{}^b\right\}. \tag{5}$$

[3] Heitler and London, Zeits. f. Physik **44**, 455 (1927).

Neglecting S^2 in the denominator of (4), the singlet-triplet separation is measured by the exchange integral (3.3). Taking into account the S^2 terms, the separation is measured by (5), which lacks $V_{\alpha\beta}$, but contains instead a correction term $-2S^2\int\bar{\psi}_\alpha{}^a\psi_\alpha{}^a V_\beta{}^a - S^2\int\bar{\psi}_\alpha{}^a\psi_\alpha{}^a V^{ab}\bar{\psi}_\beta{}^b\psi_\beta{}^b$ which is essentially positive (favoring ferromagnetism), and for H_2 approximately equal to the lacking $V_{\alpha\beta}$ term. In the equilateral triatomic molecule, the energy difference between the quartet and the coincident doublets is

$$ {}^4\epsilon - {}^2\epsilon = -3\Big\{\int\bar{\psi}_\alpha{}^a\bar{\psi}_\beta{}^b(2V_\beta{}^a+V^{ab})\psi_\beta{}^a\psi_\alpha{}^b - 3S^2\int\bar{\psi}_\alpha{}^a\bar{\psi}_\beta{}^b(2V_\beta{}^a+V^{ab})\psi_\alpha{}^a\psi_\beta{}^b $$
$$ +2S\int\bar{\psi}_\alpha{}^a\bar{\psi}_\beta{}^b(V_\alpha{}^b+V_\beta{}^a+V^{ab})\psi_\alpha{}^a\psi_\gamma{}^b\Big\}. \quad (6) $$

Here we have neglected terms in the third power of the overlapping. In the regular tetratomic molecule, the corresponding energy differences are

$$ \left.\begin{aligned} &{}^5\epsilon - {}^3\epsilon = -12K, \qquad {}^3\epsilon - {}^1\epsilon = -6K, \\ K = &\int\bar{\psi}_\alpha{}^a\bar{\psi}_\beta{}^b(2V_\beta{}^a+V^{ab})\psi_\beta{}^a\psi_\alpha{}^b - 6S^2\int\bar{\psi}_\alpha{}^a\bar{\psi}_\beta{}^b(2V_\beta{}^a+V^{ab})\psi_\alpha{}^a\psi_\beta{}^b \\ &+4S\int\bar{\psi}_\alpha{}^a\bar{\psi}_\beta{}^b(V_\alpha{}^b+V_\beta{}^a+V^{ab})\psi_\alpha{}^a\psi_\gamma{}^b. \end{aligned}\right\} \quad (7) $$

There are three triplet states with equal energy, and likewise two singlets.

[*Note:* Suffice it merely to outline the derivation of these results. The calculation has been organized for more general cases by Slater.[4] For the three-electron case he gives expressions for the energies which simplify immediately for our equilateral molecule to

$$ {}^4\epsilon = \{(abc|H|abc) - 3(abc|H|bac)\}(1+3S^2), $$
$$ {}^2\epsilon = (abc|H|abc). $$

In the four-electron case, the quintet is had as the diagonal element for his state I (reference 4, page 1125). The singlets fall together because the symmetry in our tetratomic molecule makes $P=Q=R$. Among the states D, E, and F, the non-diagonal elements are zero and the diagonal elements are equal, so the triplets coincide and are ${}^3\epsilon = (D|H|D)$. It happens also that the energy sum rule for the states with $M_S=0$, 1, and 2, holds to the degree of approximation S^2, and determines the energies, once the degeneracy has been established.

$$ {}^5\epsilon = \{(abcd|H|abcd) - 6(abcd|H|abdc)\}(1+6S^2), $$
$$ {}^3\epsilon = \{(abcd|H|abcd) - 2(abcd|H|abcd)\}(1+2S^2), $$
$$ {}^1\epsilon = (abcd|H|abcd).] $$

The low-multiplicity energies are of interest in the question of saturated valence. The degeneracy of like multiplicities is the analog of a sharp distribution replacing Heisenberg's " Gaussian distribution " or the Bloch-Bethe spreading.

Comparison of (5), (6), and (7) shows that the "criterion for ferromagnetism" depends increasingly on the terms in S^2 as the number of atoms in the molecule increases. This fact, as well as the above examination of Eq. (2), makes it seem very probable that the lack of orthogonality is very important in so large a molecule as a crystal. The integrals arising from the lack of orthogonality are such as to decrease the energy of the states of high multiplicity, so this seems in the molecular analog to be a tendency toward "ferromagnetism."

[4] J. C. Slater, Phys. Rev. **38**, 1109 (1931).

Magnetic Properties of Iron-Cobalt Single Crystals*

J. W. SHIH, *Sloane Physics Laboratory, Yale University*

(Received May 25, 1934)

Single crystals of Fe–Co alloys were obtained from recrystallized pure ingots and their components of magnetization parallel to magnetic forces applied along axes of symmetry were measured by a pendulum magnetometer. It was found that the direction for easiest magnetization changes from <100> to <111> as the amount of cobalt in the alloy increases. This transition occurs at about 42 percent Co. This result contradicts Fowler and Powell's view concerning the dependence of direction of magnetization upon crystal structure. Some magnetic properties of polycrystalline alloys are explained. Akulov's theory for the magnetization curve of a single crystal was applied to a specimen with 70 percent Co. The agreement between theory and experiment is good in this case.

IN his theory on the deviation of the direction of magnetization from that of the magnetic field Powell[1] assumes that the interaction between each electron and the atom to which it belongs can be represented by a field G fixed in the crystal. G can have its equivalent maxima in a number of possible directions which are simply related to the crystal structure. By this means the deviation effect can be described both in cubic and non-cubic crystals. Later he and Fowler[2] carried this theory one step further. If the axes of the atomic angular momenta are arranged as required by Powell's theory, then the direction of easiest magnetization will be of the form <100> in iron and of the form <111> in nickel. This is the experimental finding. On this view the direction of easiest magnetization of a substance depends primarily only upon the structure. For instance, any ferromagnetic substance of body-centered cubic structure would be expected to have <100> as the easiest direction.

In order to prove or disprove Fowler and Powell's prediction it is necessary to investigate the magnetic properties of crystals having the same structure as iron, nickel or cobalt but otherwise differing as much as possible. Besides iron-nickel single crystals which have been recently studied by Lichtenberger,[3] iron-cobalt alloys lend themselves to such investigation. The iron-cobalt series has three different structures[4] at room temperature, namely, body-centered cubic lattice from 0 to 78 percent cobalt, face-centered cubic lattice from 78 to 95 percent cobalt, and hexagonal (close-packed) lattice from 95 to 100 percent cobalt. So over the widest range they are of the same structure as iron.

Furthermore, iron-cobalt alloys have some peculiar properties. Over a considerable range of composition they have higher saturation magnetization[5] than either constituent and have large magnetostriction.[6] Alloys of around 50 percent cobalt are easily magnetizable and have high electric conductivity. This shows that some of the iron-cobalt alloys are, in themselves, very interesting ferromagnetic substances.

Very pure iron was obtained from P. P. Cioffi of the Bell Telephone Laboratories, New York and pure cobalt was supplied by the Harshaw Chemical Company, Cleveland, Ohio. The cobalt is found to be 99.37 percent pure and its predominant impurities are iron, manganese and sulphur. Alloys were made in magnesia crucibles in vacuum by means of an induction furnace the coil of which can be gradually raised so that the metal solidifies slowly from the bottom upward. The ingot (50 to 70 grams) obtained in this way contains a large number of small single crystals. In order to make the crystals bigger and more

* Part of a dissertation presented to the faculty of the Graduate School of Yale University in candidacy for the degree of Doctor of Philosophy.

[1] F. C. Powell, Proc. Roy Soc. **A130**, 167 (1930).

[2] R. H. Fowler and F. C. Powell, Proc. Camb. Phil. Soc. **27**, 280 (1931).

[3] F. Lichtenberger, Ann. d. Physik [5], **15**, 45 (1932).

[4] R. Ruer and K. Kaneko, Ferrum **2**, 33 (1911); H. Masumoto, Sci. Rep. Tohoku Imp. Univ. **15**, 449 (1926); T. Kasé, ibid. **16**, 491 (1927).

[5] P. Weiss, Trans. Faraday Soc. London **8**, 149 (1912); H. Masumoto, Sci. Rep. Tohoku Imp. Univ. **18**, 195 (1930); G. W. Elmen, J. Frank. Inst. **207**, 583 (1929); A. Kussmann, B. Scharnow and A. Schulze, Zeits. f. techn. Physik **13**, 449 (1932).

[6] S. R. Williams, Rev. Sci. Inst. **3**, 675 (1932); Y. Masiyama, Sci. Rep. Tohoku Imp. Univ. **21**, 394 (1932).

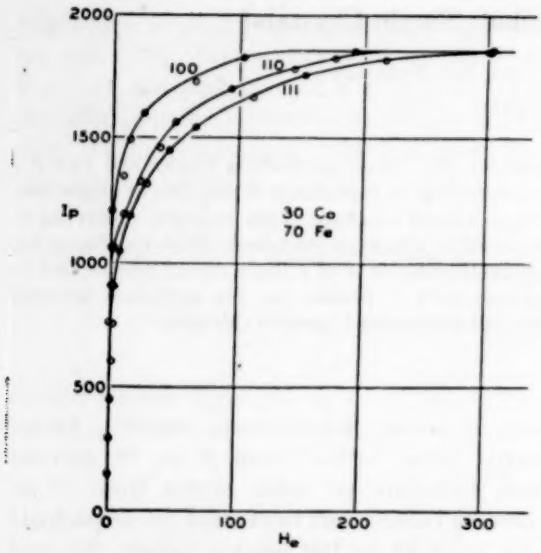

FIG. 1. I_p—*vs.*—H_e for 30 percent Co.

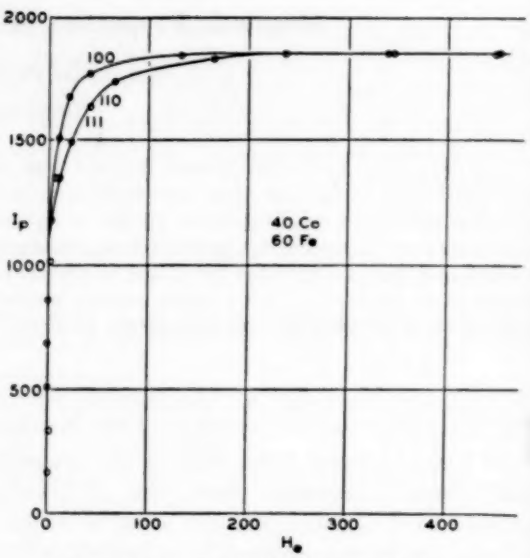

FIG. 2. I_p—*vs.*—H_e for 40 percent Co.

perfect the ingot was annealed in a resistance furnace in an atmosphere of hydrogen for several hours. The annealing temperature was not higher than 50°C above the allotropic transformation point (above which the alloys have a face-centered cubic structure) and the rate of cooling was about 4 or 5°C per minute.

The recrystallized ingot was etched with nitric acid in alcohol as usual and the etch plane is of the form {100}. In order to cut a specimen in a certain crystallographic plane the orientation of the selected crystal was determined by means of a goniometer with a Gauss eyepiece. An oblate spheroid with its axis of rotation parallel to a <110> direction was carefully prepared by means of a new and accurate method.[7] It was then annealed in hydrogen for two hours at a temperature about 50°C below its transformation point. The final step before deciding that a spheroid was fit for magnetic measurements was to take a Laue photograph to determine its crystal axes. The results of the x-ray analysis and some other constants of the specimen are given in Table I. In this table, N denotes the demagnetizing factor for the equatorial plane computed from the formula

$$N=2\pi\left[\frac{(1-e^2)^{\frac{1}{2}}}{e^3}\sin^{-1}e-\frac{1-e^2}{e^2}\right],$$

where e is the eccentricity of the generating ellipse, α the angle between the axis of rotation of the spheroid and one of the four-fold crystal axes and β the angle between this axis and a {001} plane which contains the said four-fold axis. (α is 45° and β is 0° for a perfectly cut specimen.) The crystals are more or less imperfect as shown by the irregularity of Laue spots. This may be due to alloying or to mechanical disturbance during the process of shaping. Since we are interested in the general features of the magnetization curve these small imperfections have been ignored.

For magnetic measurement a pendulum magnetometer[7] was constructed. It is especially suitable for small crystal specimens and has some advantages over Weiss's torsion magnetometers. The results of measurement are plotted in Figs. 1

TABLE I. *Constants of specimens.*

Percent Co by synthesis	Assumed $\alpha-\gamma$ Temp.	Vol. cm³	Thickness cm	Diameter cm	N	α	β
30	950°C	.001114	.024	0.299	0.718	45°	7°
40	970°C	.001535	.025	0.350	0.635*	40°	0
50	960°C	.00180	.0238	0.360	0.601	45°	0
70	860°C	.001559	.0244	0.343	0.644	40°	0

* Calculated value is 0.646 but 0.635 is the highest value which fits the data.

[7] L. W. McKeehan, Rev. Sci. Inst. (Aug.) (1934).

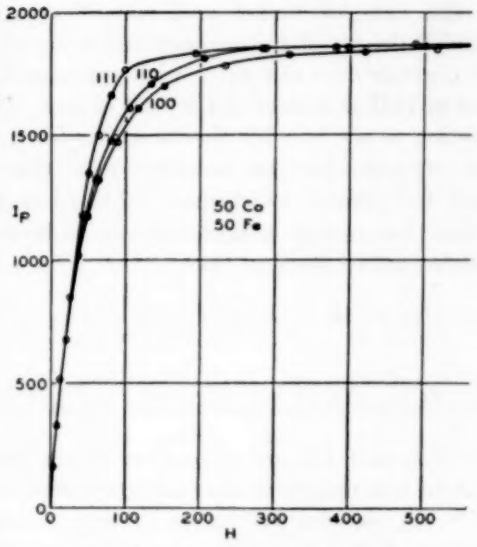

FIG. 3. I_p—vs.—H, for 50 percent Co.

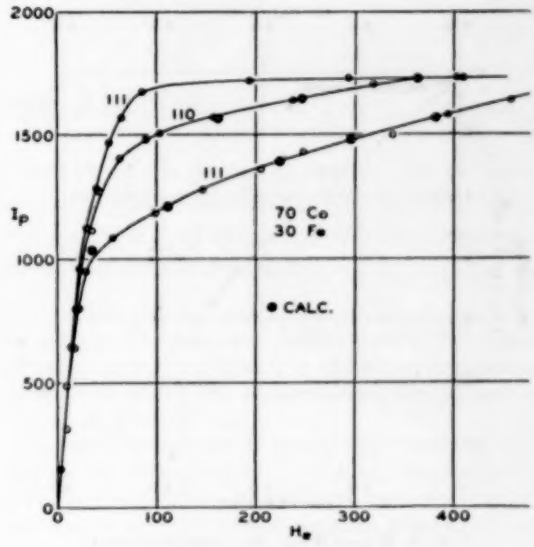

FIG. 4. I_p—vs.—H_e for 70 percent Co.

to 4. In these figures I_p denotes the component of magnetization parallel to the applied magnetic field and H_e the field corrected for the demagnetizing effect. H_e is hardly to be distinguished from 0 up to a considerable value of I_p. The probable error in the absolute measurement is about 1.6 percent of which about 1 percent is due to the error in weighing the specimen. Relative measurements on a single specimen are more precise.

We see that the direction of easiest magnetization depends upon the amount of cobalt in the alloy. The alloys we measured are all of body-centered cubic lattice but those of 30 and 40 percent Co have <100> those of 50 and 70 percent Co have <111> as the easiest direction. This indicates that the direction for easiest magnetization does not depend merely upon the crystal structure and does depend upon the kind of atoms of which the crystal consists, contradicting Powell and Fowler's prediction.

The shift of the direction of easiest magnetization in our alloys is similar to that already found in the iron-nickel system by Lichtenberger.[3] From 33 to 100 percent nickel Fe-Ni alloys are of face-centered cubic lattice. The direction for easiest magnetization changes in this range from <100> as in iron to <111> as in nickel, the transition occurring at about 71 percent nickel. Lichtenberger was not able to fix this point very accurately.

The magnetic energy input per unit volume is represented by the area included between an $I-H$ curve and the I-axis up to any value of I. Part of this is stored and part is dissipated in hysteresis. Since in our case the hysteresis effect is negligibly small the energy difference for magnetization along different symmetry axes may be taken as the area included between the two $I-H$ curves under consideration. These energy differences are given in Table II.

TABLE II. *Energy differences.*

Percent Co	$W_{111}-W_{100}$ erg. cm^{-3}	$W_{110}-W_{100}$ erg. cm^{-3}
30	0.38×10^6	0.24×10^6
40	0.11 "	0.11 "
50	−0.37 "	−0.17 "
70	−1.41 "	−1.05 "

Fig. 5 shows how the composition for $W_{111}-W_{100}=0$ is graphically obtained.[5] We see that the curve cuts the concentration axis at about 42 percent Co. This agrees well with the findings[5] that the polycrystalline alloy with about 40 percent cobalt has maximum initial permea-

[5] The point for iron is derived from measurements by K. Honda and S. Kaya, Sci. Rep. Tohoku Imp. Univ. 15, 721 (1926).

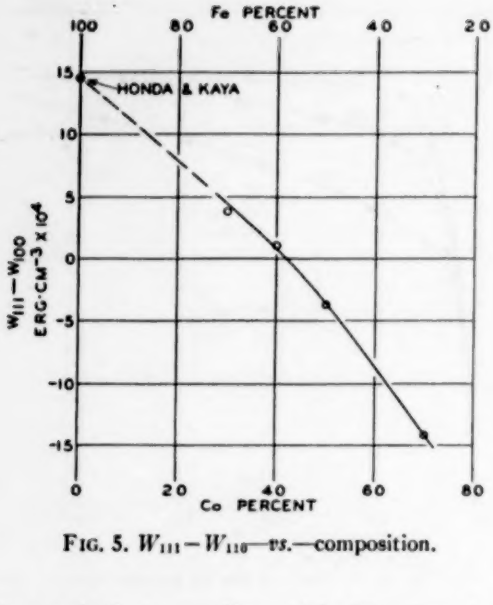

FIG. 5. $W_{111}-W_{110}$ *vs.*—composition.

bility and that an alloy with 50 percent has maximum intrinsic induction in low field. Alloys in this range of composition will be expected to contain elementary crystals which are easily magnetized in all directions. In a comparative high field this effect will be relatively less important so that the magnetization-concentration curve becomes flatter for higher applied field intensities.

Although our maximum magnetizing field is not very high the magnetization is seen to attain nearly to the saturation value. The 30, 40 and 50 percent alloys have practically the same saturation value (I_∞). Weiss[5] and Masumoto[5] found a maximum I_∞ for 34 percent Co alloy while Elmen[5] places the maximum at 50 percent. Recently Kussmann, Scharnow and Schulze[5] obtained about the same limiting magnetization over the range from 30.9 to 52.4 percent Co and maximum electric conductivity at around 50 percent Co instead of at 60 percent as found by Elmen. Kussmann and his co-workers conclude that in the alloy with 50 percent Co the atoms are more or less in an ordered state so that the metallic compound FeCo may be said to exist. Weiss much earlier proposed the existence of a compound Fe_2Co, and Elmen suggests $FeCo_2$. The formula FeCo corresponds to 48 percent Co by weight. Our results on the direction of magnetization apparently support Kussmann's view.

In the case of nickel and cobalt[9] crystals Akulov's[10] theory of the magnetization curve of single crystals does not agree with experimental results so well as it does in the case of iron. It is interesting to see how his theory works for iron-cobalt crystals. Let us consider first the 70 percent Co crystal which has $<111>$ as the direction for easiest magnetization. Following Akulov's method we find that

$$H_{110}=H_{111}+(2K/I_\infty)(I_{110}/I_\infty)[2-3(I_{110}/I_\infty)^2]$$

and

$$H_{100}=H_{111}+(2K/I_\infty)(I_{100}/I_\infty)[1-3(I_{100}/I_\infty)^2],$$

where H_{hkl} and I_{hkl} are, respectively, the magnetic field and magnetization along the direction $<hkl>$. I_∞ is the saturation value of magnetization, K is a material constant which may be computed from the equation $W_{111}-W_{100}=2K/3$. $W_{111}-W_{100}$ is here found to be -1.41×10^5 ergs·cm^{-3}. Hence K is equal to -2.13×10^5 ergs·cm^{-3}. By assigning different values to I_{hkl}, we can compute corresponding values of H_{hkl}. These pairs of I, H, values are represented by the black circles in Fig. 4. The good agreement between theory and experiment is to be expected because Akulov's theory should apply only in cases where there is no hysteresis. This is nearly true in the present case, the maximum hysteresis work per cycle (not accurately measurable) being estimated to be less than 7×10^3 ergs·cm^{-3} for the hardest specimen, that with 70 percent Co. The theory is less satisfactory for an alloy with 40 percent Co where two of the three $I-H$ curves for different axes are indistinguishable. No single value of K can account for such behavior.

In conclusion, the author wishes to express his thanks to Professor L. W. McKeehan for suggesting this problem and for his advice and encouragement during the investigation. He is also indebted to Professor W. E. Milligan of the Hammond Laboratory for making chemical analysis of cobalt, and to the China Foundation, Peiping, China for their financial help in 1932 and 1933.

[9] F. Bitter, Phys. Rev. **38**, 528 (1931).
[10] N. Akulov, Zeits. f. Physik **67**, 794 (1931); **69**, 78 (1931).

LETTERS TO THE EDITOR

Prompt publication of brief reports of important discoveries in physics may be secured by addressing them to this department. Closing dates for this department are, for the first issue of the month, the twentieth of the preceding month; for the second issue, the fifth of the month. The Board of Editors does not hold itself responsible for the opinions expressed by the correspondents.

On the Photoelectric Effect for the *L*-Shell

We have calculated the absorption coefficient τ_{L_1} for the L_1 ($2S_{\frac{1}{2}}$) shell for the case of quantum energies $h\nu > mc^2$, by a method recently applied[1] to find τ_k. The formula obtained for τ_{L_1}/τ_k is valid to within a fractional error of α/ϵ. A qualitative approximation is given by

$$\tau_{L_1}/\tau_k \sim w_1^2/(\alpha N_0)^2_k \sim 1/N^2$$

which becomes, when α is negligible

$$\tau_{L_1}/\tau_k = 1/8.$$

For Pb ($Z=82$) and $\lambda = 4.7$ X.U., we find from the more exact equation

$$\tau_{L_1}/\tau_k = 0.20.$$

w_1 is the constant occurring in the normalized radial wave functions for L_1.

$(\alpha N_0)_k$ is α times the constant of normalization for the radial functions of the K state.

$$N^2 = 2(1+\rho_1); \quad \rho_1^2 = 1-\alpha^2.$$

Thus, as might have been expected from the calculations of Hulme[2] on internal conversion for the limit $\lambda \to 0$, there is no great change in the ratio of τ_{L_1}/τ_k due to relativistic effects.

If the absorption by the L_2, L_3, $M \cdots$ shells is inappreciable, and a rough estimate seems to indicate that this is so, the total photoelectric absorption per atom is theoretically given by

$$\tau = 1.3 \times 10^{-24} \text{ cm}^2$$

or about 10 percent of the total absorption observed.

HARVEY HALL
WILLIAM RARITA

Columbia University,
June 9, 1934.

[1] Harvey Hall, Phys. Rev. **45**, 620 (1934). The same notation is used in this note.
[2] Hulme, Proc. Roy. Soc. **A138**, 643 (1932).

Measurement of Flicker Effect

Recent observations on the flicker effect in diodes by R. C. Meyer have indicated a different trend to the effect than that observed by J. B. Johnson[1] or predicted by Shottky.[2] The measurements were made in a carefully constructed diode using a tungsten filament 4 cm long and a collector 1 cm long with guard rings 2 cm long on either side. The tube was connected to a high vacuum system through a charcoal trap which was kept at liquid air temperatures during measurements. The pressure was kept constant at 10^{-7} mm.

An aperiodic shot circuit was used in connection with a very sharply tuned heterodyne analyzer. The overall band width of the amplifier was 2 cycles per second so that accurate measurements could be made down to 10 cycles per second.

A representative plot of the frequency variation of the fluctuation voltage is shown in Fig. 1. V^2 observed is

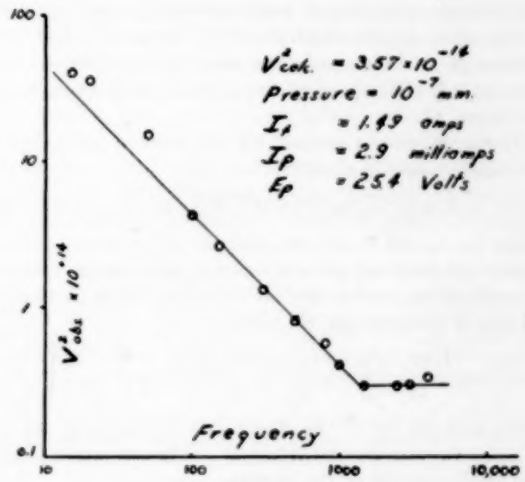

FIG. 1.

plotted in mean square volts per cycle band. It can be seen that the slope is approximately -1 rather than -2 as observed by J. B. Johnson. With the tube used approximately this slope was always obtained, although under different conditions it was sometimes somewhat less than -1.

It was found that this slope existed when the space current was limited by space charge. With increase in emission current, reduction of the shot effect to as low as 1/300 of the calculated value was observed. If the filament temperature was increased sufficiently the fluctuation voltage rose again to values greater than the calculated value.

[1] J. B. Johnson, Phys. Rev. **26**, 71 (1925).
[2] W. Shottky, Phys. Rev. **28**, 74 (1926).

This was presumably due to the effect of positive ions emitted by the filament acting on the space charge sheath surrounding the filament.

These measurements are being extended by one of us using thoriated and oxide as well as tungsten filaments.

R. C. MEYER
E. A. JOHNSON[3]

Massachusetts Institute of Technology,
June 18, 1934.

[3] Round Hill Research Division, Department of Electrical Engineering.

Reflection Coefficient of Electrons[1]

In an attempt to interpret their experimental results upon the degree of ionization of potassium atoms on a hot tungsten filament the authors have suggested[2] that the results could be explained by assuming that the ratio $(1-r_+)/(1-r_a)$,—where r_+ and r_a are the reflection coefficients of positive ions and atoms, respectively,—is about 2. They were not aware at that time that Taylor and Langmuir[3] had proved definitely that the reflection coefficient of caesium atoms from tungsten is equal to zero to within less than one percent. Since it seems very likely that the reflection coefficient of potassium atoms is also zero, it becomes necessary to seek a different interpretation for one of the experimental observations in the note; namely the absence of an intercept in the plot, $\log \nu_+/\nu_a$ *versus* $1/T$. The purpose of the present note is to set forth a new interpretation.

The equilibrium constant[4] for the thermal ionization of potassium vapor is given by

$$K=\bar{\nu}_+\bar{\nu}_\epsilon/\bar{\nu}_a=(\omega_+\omega_\epsilon/\omega_a)(2\pi m_\epsilon kT/h^2)^{\frac{3}{2}}\exp\left[-I_\epsilon/kT\right], \quad (1)$$

where $\bar{\nu}_+$, $\bar{\nu}_a$ and $\bar{\nu}_\epsilon$ are, respectively, the number of ions, atoms and electrons per cm³ in an equilibrium mixture. If we replace the number per cm³ of each kind of particle by its rate of evaporation, we have

$$\frac{\nu_+\nu_\epsilon}{\nu_a}=\frac{(1-r_+)(1-r_\epsilon)}{(1-r_a)}\frac{\omega_+\omega_\epsilon}{\omega_a}\frac{2\pi m_\epsilon k^2}{h^3}T^2\exp\left[-\frac{I_\epsilon}{kT}\right]. \quad (2)$$

Upon multiplying by the charge ϵ of the electron, putting r_a equal to zero, and introducing numerical values for the statistical weights of the particles, we obtain

$$\nu_+ i/\nu_a=(1-r_+)(1-r_\epsilon)(2\pi m_\epsilon k^2\epsilon/h^3)T^2\exp\left[-I_\epsilon/kT\right], \quad (3)$$

in which i is the saturation electron current per cm² at zero field. The emission of electrons from tungsten may be represented by the empirical equation

$$i=A'T^2\exp\left[-\phi_0\epsilon/kT\right]. \quad (4)$$

Substituting for i in (3) and replacing $2\pi m_\epsilon k^2\epsilon/h^3$ by A, we have

$$\nu_+/\nu_a=(1-r_+)(1-r_\epsilon)(A/A')\exp\left[-(I-\phi_0)\epsilon/kT\right]. \quad (5)$$

If $\log \nu_+/\nu_a$ is plotted against $1/T$ the intercept is equal to $\log(1-r_+)(1-r_\epsilon)A/A'$. Since A/A' may be obtained from thermionic data, the product $(1-r_+)(1-r_\epsilon)$ may be calculated from the experimental value of the intercept. Both r_+ and r_ϵ must lie between zero and unity; consequently maximum limits can be set to their values. On the basis of the very small intercept, $\log(1-r_+)(1-r_\epsilon)A/A'$, which we have obtained in recent experiments it appears that the maximum value of r_+ (or r_ϵ) is of the order 0.1.

Becker and Brattain[5] in a recent paper in the *Physical Review* discuss in considerable detail the question of thermionic emission of electrons from metals. They conclude that it is unlikely that r_ϵ should ever exceed 0.1. The measurement of the degree of ionization of potassium vapor on a tungsten wire appears to furnish experimental evidence in favor of their conclusion.

If in Eq. (1) we express $\bar{\nu}_\epsilon$ by

$$\bar{\nu}_\epsilon=\omega_\epsilon(2\pi m_\epsilon kT/h^2)^{\frac{3}{2}}\exp\left[-\phi_\epsilon\epsilon/kT\right], \quad (6)$$

where ϕ_ϵ is the work function at the temperature T, we obtain

$$\bar{\nu}_+/\bar{\nu}_a=(\omega_+/\omega_a)\exp\left[-(I-\phi)\epsilon/kT\right] \quad (7)$$

and

$$\frac{\nu_+}{\nu_a}=\frac{(1-r_+)}{(1-r_a)}\frac{\omega_+}{\omega_a}\exp\left[-\frac{(I-\phi)\epsilon}{kT}\right]. \quad (8)$$

If we consider the reflection coefficients to be very small or zero, then it is evident that there is a factor which cancels the ratio of statistical weights, ω_+/ω_a in Eq. (8). Such a factor probably is the temperature coefficient α of the work function (discussed by Becker and Brattain[5]). We may write with them

$$\phi=\phi_0+\alpha T, \quad (9)$$

where

$$\exp\left[-\alpha\epsilon/k\right]=\omega_+/\omega_a=\tfrac{1}{2}. \quad (10)$$

M. J. COPLEY
T. E. PHIPPS

Department of Chemistry,
University of Illinois,
Urbana, Illinois,
June 19, 1934.

[1] Since the present note was written a Letter to the Editor has appeared (A. L. Reimann, Phys. Rev. **45**, 898 (1934)) discussing one of the points emphasized herein.
[2] Copley and Phipps, Phys. Rev. **45**, 344 (1934).
[3] Taylor and Langmuir, Phys. Rev. **44**, 423 (1933).
[4] Fowler, *Statistical Mechanics*, p. 281, Cambridge Press, (1929).
[5] Becker and Brattain, Phys. Rev. **45**, 694 (1934).

Hopfield's Rydberg Series and the Ionization Potential and Heat of Dissociation of N_2*

Recent work has made it very probable that the heat of dissociation of N_2, long in dispute, is close to 7.4 volts.[1, 2, 3] Herzberg and Sponer[2] give 7.34 ± 0.02 volts.[4] This value is based on a careful consideration of emission bands and predissociation phenomena studied by Kaplan, Vegard, Coster and Brons, Van der Ziel, and others.

* *Added in proof:* Cf. also, H. Beutler, Naturwiss. **20**, 759 (1932).
[1] Cf. J. Kaplan, Phys. Rev. **45**, 898 (1934).
[2] G. Herzberg and H. Sponer, Zeits. f. physik. Chemie **B26**, 1(?), 1934. The writer is indebted to Dr. Herzberg for the opportunity to see this article in proof.
[3a] W. W. Lozier, Phys. Rev. **44**, 575 (1933).
[3b] Lozier, Phys. Rev. **45**, 840 (1934).
[4] A possible difficulty with a value 7.4 volts for $D(N_2)$ is that it requires D of the A' state of N_2^+ to be about 3.1

From electron impact data, Lozier[3] gets 8.62 ± 0.02 volts for an energy of dissociation of N_2^+; as he has pointed out, the products of dissociation at this energy can hardly be unexcited ($^4S+^3P$). If the N^+ is assumed excited to ^1D(1.89 volts), one obtains 6.73 volts for the heat of dissociation $D(N_2^+)$ into unexcited atom and ion; but dissociation into $^1D+^4S$ seems unlikely.[5] If the N is assumed excited to ^3D(2.37 volts), $D(N_2^+)$ comes out 6.25 volts. Other possibilities are too improbable.[3] The value 6.25 volts combined with the ionization potential 15.65 ±0.02 volts for N_2 determined by Tate, Smith and Vaughan,[6] gives 7.42 volts for $D(N_2)$, in good agreement with the above spectroscopic value.[4]

It seems desirable to call attention at this time to a Rydberg series of N_2 absorption bands reported some time ago by Hopfield.[7] Hopfield's data closely fit the Rydberg formula $\nu=151{,}240-R/(m-0.092)^2$, with $m=3$, 4, 5, 6, 7, $\cdots$. The limit ($\nu=151{,}240=18.67$ volts) must be identified, as Hopfield pointed out, with the ionization of N_2 to form an excited state of N_2^+. There can now be practically no doubt that this state is the well-known A', $^2\Sigma^+_u$ state of N_2^+, which is 3.156 volts above the $^2\Sigma^+_g$, probably normal, state of N_2^+. (The $^2\Pi_u$ state of N_2^+ is probably only a little above the $^2\Sigma^+_g$, but its exact location is uncertain, and there is a bare possibility that it might be the normal state.)

If $^2\Sigma_g^+$ is the normal state of N_2^+, then the minimum ionization potential of N_2 must be $18.67-3.156=15.51$ volts. This value is in good enough agreement with the value 15.65 of Tate, Smith and Vaughan so that we may safely accept the above interpretation. The fact that it is a little *lower* than that of Tate, Smith and Vaughan, tends to eliminate the possibility that $^2\Pi_u$ can be below $^2\Sigma_g^+$, since the Tate-Smith-Vaughan value must belong to the minimum potential, whether the latter be $^2\Sigma_g^+$ or $^2\Pi_u$. That the Hopfield potential 18.67 volts really belongs to $A'\,^2\Sigma_u^+$, not to some other neighboring spectroscopically not yet known state, is quite sure on theoretical grounds, since the electron configuration theory gives no possibility of such an additional state.

The occurrence of a Rydberg series of single bands is most reasonably interpreted on the supposition that each band is a (0,0) band, other possible bands being very much weaker. According to the Franck-Condon principle, this would mean that r_e is nearly the same for the various excited N_2 electron states (upper levels of the Hopfield bands), and for the N_2^+ state to which the limit of the series corresponds, as for the normal state of N_2. This is in agreement with the conclusion that the limit of the series is $^2\Sigma_u^+$ of N_2^+, since the latter has $r_e=1.07$A, while the normal state of N_2 has $r_e=1.09$A. That the entire set of N_2 electron states converging to $^2\Sigma_u^+$ of N_2^+ have about the same r_e as $^2\Sigma_u^+$ of N_2^+ is to be expected,[8] since all these states are nothing but N_2^+ ($^2\Sigma_u^+$) plus an electron in an excited orbit much larger than the N_2^+ core and so unable to affect appreciably the strength of the N–N bond. Similar relations are known in the Rydberg series of H_2 and He_2.

For a definite determination of the nature of the excited electron orbits in the Rydberg series states, we must await further data; the selection rules, however, require them to be of $_g$ type. For $m=3$, the types σ_g4s and σ_g3d are perhaps the most probable; σ_g3s and σ_g3p would have larger quantum defects than the observed defect 0.092 (this, however, becomes 1.092 if σ_g4s is correct; in that case one more member of the Rydberg series must exist at longer wave-lengths, in a region difficult to analyze because of the presence of many bands, according to a private communication from Dr. Hopfield). The large molecular orbitals σ_g4s, σ_g3d, etc., should not differ much from atomic orbitals $4s$, $3d\sigma$, etc., as we can see by approximately constructing them by adding two $4s$ or two $3d\sigma$ orbitals, one for each N atom, and noting that the distance between the two N nuclei is small compared with the dimensions of the $4s$ or $3d\sigma$ orbital. Similar atom-like molecular orbitals are known in the high excited states of He_2 and H_2, and should occur quite generally. Types such as Π_g3p and Π_g3d, although at first sight plausible, would probably give unstable states of N_2, as one sees after noting that their approximate construction requires *subtraction* of $3p\Pi$ or $3d\Pi$ atomic orbitals of two nearly coincident atoms, then normalizing.

The foregoing interpretation of Hopfield's Rydberg series makes it very probable that the correct value of the ionization potential of N_2 lies within the limits 15.51–15.52 volts. Combining this with Lozier's value of 6.25 volts for $D(N_2^+)$, we get $15.51+(6.25\pm0.02)-14.48=7.28\pm0.02$ volts for $D(N_2)$, in close agreement with the value 7.34 ±0.02 given by Herzberg and Sponer. Or conversely, from the H.S. value 7.34 for $D(N_2)$ one gets $14.48+7.34-15.51=6.31$ volts for $D(N_2^+)$; and $6.31-3.156=3.15$ volts for D of the A', $^2\Sigma_u^+$ state[4] of N_2^+. As rounded values for $D(N_2)$ and $D(N_2^+)$ we may then probably now accept with considerable confidence 7.3 volts and 6.3 volts.

---

volts,[3b] whereas Birge estimates it to be 3.67 ± 0.1 volts by a not very long extrapolation from the A' vibrational levels measured by Herzberg. Herzberg and Sponer,[3] however, accept without discussion the lowered value of D for the A' state; their value of $D(N_2)$ gives 3.17 volts for the A' state, if 15.65 volts[6] is used for the ionization potential of N_2.

[5] That the products of dissociation are $^4S+^1D$, as Lozier at first assumed (reference 3a) seems improbable, since this would require that the N_2^+ which is excited by electron impact and then at once dissociates in Lozier's work is some *quartet* state of N_2^+. It seems unlikely that such a state would be predominantly produced by electron impact from N_2 (state $^1\Sigma$), especially since this would necessarily involve simultaneous removal of one N_2 electron and removal of another.

[6] J. T. Tate, P. T. Smith and A. L. Vaughan, Phys. Rev. **43**, 1054A (1933).

[7] J. J. Hopfield, Phys. Rev. **36**, 789A (1930). Hopfield also reported an emission Rydberg series, appearing on the same photograph as the absorption series, and converging to the same limit. In conversation, however, Dr. Hopfield states that the reality of the emission series is doubtful. The absorption series, however, consists of a beautifully clear set of narrow bands, according to a reproduction which Dr. Hopfield has very kindly shown the writer. Dr. Hopfield informs me that there seems now to be no possibility that the bands belong to anything but N_2, although he first attributed them to He_2 (Phys. Rev. **35**, 1133 (1930)). Dr. Hopfield tells me that he intends to publish a more complete account of the bands shortly.

Using $D(O_2)$ and thermochemical data,[3a] we then have 5.25 volts as the best value for $D(NO)$.

ROBERT S. MULLIKEN

Ryerson Physical Laboratory,
University of Chicago,
June 27, 1934.

Properties of Evaporated Films of Aluminum over Chromium

Following the proposal by the author[1] that large astronomical mirrors be coated with metallic films by the evaporation process, considerable work has been done toward the development of the most suitable films for this use.[2, 3, 4] In coating the Crossley 36 inch reflector of the Lick Observatory,[4] aluminum was considered to be the best coating for astronomical purposes, for although its hardness is not great, it has excellent tenacity, untarnishability and reflectivity.

A film has been developed in this laboratory which greatly excels pure aluminum in the first of the above properties, and is comparable to it in the remaining three. The glass is first prepared by careful chemical cleaning, and is then bombarded with ions[5] in the vacuum chamber. A thin film of pure chromium is first evaporated upon the glass, and this is immediately covered by an aluminum film sufficient to make the two films opaque. A method of dissolving chromium placed directly upon glass has been found, and hence such films can be removed, if desired, without injury to the glass surface.

When first deposited this chromium-aluminum film can be scratched fairly easily, but it is hardened instantly by washing in water, alcohol, or even by condensed breath-moisture. The resulting hardness is astonishing; rubbing with a blunt steel instrument, or even with steel-wool affects the film only slightly. A test for resistance to abrasion was made by rubbing a small area of the film 500 times with cheesecloth and with wadded cotton as hard as the hand could rub. A slight increase in scattered light was noticed, but no appreciable decrease in reflectivity could be observed. It was also found that pure aluminum films are considerably harder after washing with water, but even after the water treatment, they are not as hard as the unwashed chromium-aluminum films. A hardened pure aluminum film which had satisfactorily withstood the "adhesive-tape test"[6] was completely removed from the glass after 50 hard rubs with cheesecloth or with wadded cotton. A chromium-aluminum sample was coated with a layer of kerosene soot onto which was dropped sand and grit, and the mirror was then cleaned with alcohol and water. This was repeated twenty times, with the result that only the faintest surface scratches could be detected. The same test with a hardened pure aluminum film showed a comparable scratching of the surface at the end of four times. These tests were performed upon Corning borosilicate glass.

The tenacity of the chromium-aluminum film is such that nothing has yet been found that will strip it from the glass, although several kinds of tape and glue have been tried.

The aluminum layer can be removed with KOH without removing the underlying chromium. Immersion for a few hours in a concentrated salt solution will likewise remove and dissolve the aluminum. Two samples have been immersed in water and in ethyl alcohol for 10 days without any deterioration of the film. This means that in laboratory use repeated cleaning with alcohol and water can be safely undertaken. Fumes of burning sulphur, of H_2S and of H_2O_2 have no apparent effect upon the films.

The reflectivity of both washed and unwashed films of chromium-aluminum has been measured from λ6000 to λ2900, and although it varies slightly among samples, it is as good as that reported by Williams and Sabine[3] for pure aluminum; *viz.*, 90 percent at λ6000 to 80 percent at λ3000, and very slightly less than that reported by Pettit.[6] The aluminum layer is sufficiently thick to act as the sole reflector, and hence might be expected to reflect as well as pure aluminum.

ROBLEY C. WILLIAMS

Department of Physics,
Cornell University,
June 29, 1934.

[1] Williams, Phys. Rev. **41**, 255 (1932).
[2] Edwards, Phys. Rev. **43**, 205 (1933).
[3] Williams and Sabine, Astrophys. J. **77**, 316 (1933).
[4] Strong, Pub. Ast. Soc. Pac. **46**, 18 (1934).
[5] This well-known "clean-up" process for metals has been successfully employed by Strong in cleaning glass.
[6] Pettit, Pub. Ast. Soc. Pac. **46**, 27 (1934).

A Partial Interpretation of the Raman and Infrared Spectra of Benzene

By using the formulas for the normal frequencies of vibration recently published[1] I have been able to assign the Raman-active and infrared-active fundamentals of benzene to definite modes of vibration of the regular plane hexagon model for this molecule. In addition I have found what seems to be a clear-cut case of quantum-mechanical resonance between a fundamental and a combination level.

The selection of the lines to be ascribed to fundamentals has been discussed by others and the choice which I have made was in part based on these previous investigations. There should be seven Raman-active fundamentals and four infrared-active fundamentals, with the nine remaining fundamentals completely inactive. There are four bands in the fundamental region of the infrared which nearly all observers have estimated to be considerably stronger than the other bands. I have chosen these, which lie near 660, 1040, 1480 and 3080 cm^{-1}, as fundamentals. The ten strongest lines in the Raman spectrum, as observed by nearly all investigators, are at 605, 849, 991, 1178, 1584, 1605, 2947, 3047, 3060 and 3184 cm^{-1}. The lines at 991 and 3060 cm^{-1} have been previously ascribed to the symmetrical expansions of the molecule (ν_1 and ν_2 of Fig. 3, reference 1). The other nine active fundamental frequencies are functions of only three force constants besides those determined from ν_1 and ν_2. I therefore tried varying these three force constants until the calculated frequencies

[1] E. Bright Wilson, Jr., Phys. Rev. **45**, 706 (1934).

agreed most closely with the observed lines. It was possible in this way to get sufficiently close agreement to enable each of the fundamentals to be assigned to one of the theoretical modes of vibration discussed in reference 1. Table I gives this assignment.

TABLE I. *Assignment of fundamental frequencies.*

Raman active		Infrared active
$\nu_1 = 991$ cm^{-1}	$\nu_7 = 3047$	$\nu_{11} = 1040$ cm^{-1}
$\nu_2 = 3060$	$\nu_8 = (1584–1605)$	$\nu_{18} = 660$
$\nu_6 = 605$	$\nu_9 = 849$	$\nu_{19} = 1480$
	$\nu_{10} = 1178$	$\nu_{20} = 3080$

This assignment is also in accord with the observed polarization of the Raman lines. The remaining lines and bands, which are nearly all much weaker than those assigned to fundamentals in Table I, are to be considered as overtones and combinations from this viewpoint.

I believe that the doublet at 1600 cm^{-1} in the Raman spectrum is to be explained on the basis of quantum-mechanical resonance between ν_8 and $\nu_1+\nu_6$. The latter sum falls at 1596 cm^{-1}, which is between the members of the doublet. Furthermore, the symmetry of these two levels is the same, so that resonance between them is not forbidden for symmetry reasons. If such resonance occurred two moderately strong lines should occur, as observed, instead of one strong fundamental and one weak combination frequency. Further evidence for this explanation is provided by the Raman spectra of benzene derivatives. In nearly all of these a single line occurs near 1600 cm^{-1}; in none of them is a doublet reported. This is in harmony with the fact that the accidental degeneracy $\nu_1+\nu_6 \sim \nu_8$ is not nearly so close as in benzene.

The suggestion which has several times been made that the spectra of benzene are not compatible with hexagonal symmetry does not appear to be justified since it is based on the supposed coincidence of certain Raman lines with certain infrared bands which I do not believe have been measured with sufficient precision to establish a result so contrary to all the other evidence.

This work is being continued in order to obtain the values of the force constants which give the best fit with experiment, so that a reasonably accurate estimation of the inactive fundamental frequencies may be made, from which it should be possible to make assignments for the other lines and bands as combinations and overtones. Such an assignment would strengthen the provisional interpretation of the fundamentals given here.

I wish to express my appreciation for the criticism and suggestions which I have received from Professors Richard Badger and Linus Pauling in connection with this paper.

E. BRIGHT WILSON, JR.

Gates Chemical Laboratory,
California Institute of Technology,
Pasadena, California,
June 29, 1934.